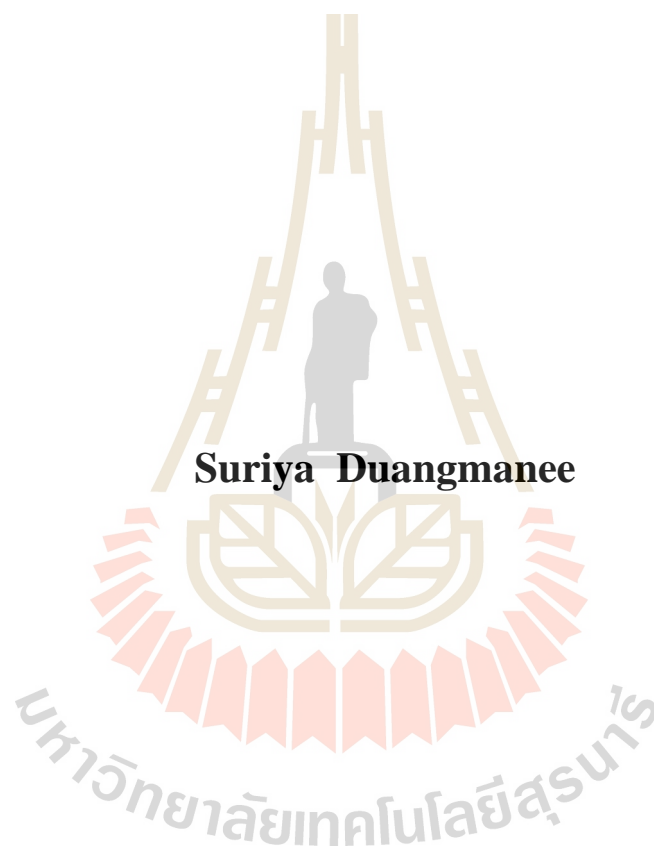


**STUDY OF FLUORESCENCE RESONANCE ENERGY
TRANSFER OF DONOR – ACCEPTOR
DYE CONFINED IN ZEOLITE L**



**A Thesis Submitted in Partial Fulfillment of the Requirements for the
Degree of Doctor of Philosophy in Chemistry
Suranaree University of Technology
Academic Year 2018**

การศึกษาการถ่ายโอนพลังงานเรโซแนนซ์ฟลูออเรสเซนซ์ของดีเอ็นเอตัวรับ
และตัวให้ที่ถูกกักขังในซีไอไลต์แอล



นายสุรียา ดวงมณี

วิทยานิพนธ์นี้เป็นส่วนหนึ่งของการศึกษาตามหลักสูตรปริญญาวิทยาศาสตรดุษฎีบัณฑิต
สาขาวิชาเคมี
มหาวิทยาลัยเทคโนโลยีสุรนารี
ปีการศึกษา 2561

STUDY OF FLUORESCENCE RESONANCE ENERGY

TRANSFER OF DONOR – ACCEPTOR

DYE CONFINED IN ZEOLITE L

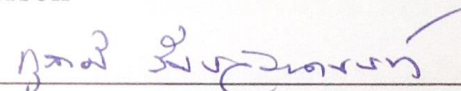
Suranaree University of Technology has approved this thesis submitted in partial fulfillment of the requirements for the Degree of Doctor of Philosophy.

Thesis Examining Committee



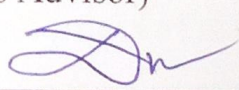
(Dr. Sakesit Chumnarnsilapa)

Chairperson



(Asst. Prof. Dr. Kunwadee Rangriwatananon)

Member (Thesis Advisor)



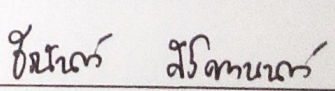
(Assoc. Prof. Dr. Siriporn Jungsuttiwong)

Member



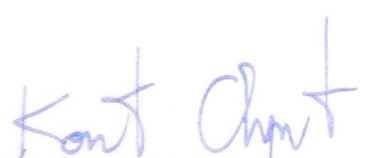
(Asst. Prof. Dr. Wilaiporn Insuwan)

Member



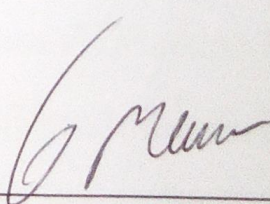
(Asst. Prof. Dr. Theeranun Siritanon)

Member



(Assoc. Prof. Ft. Lt. Dr. Kontorn Chamniprasart)

Vice Rector for Academic Affairs
and Internationalization



(Assoc. Prof. Dr. Worawat Meevasana)

Dean of Institute of Science

สุริยา ดวงมณี : การศึกษาการถ่ายโอนพลังงานเรโซแนนซ์ฟลูออเรสเซนซ์ของสีย้อม

ตัวรับและตัวให้ที่ถูกลักขังในซีโอไลต์แอล (STUDY OF FLUORESCENCE

RESONANCE ENERGY TRANSFER OF DONOR – ACCEPTOR DYE CONFINED

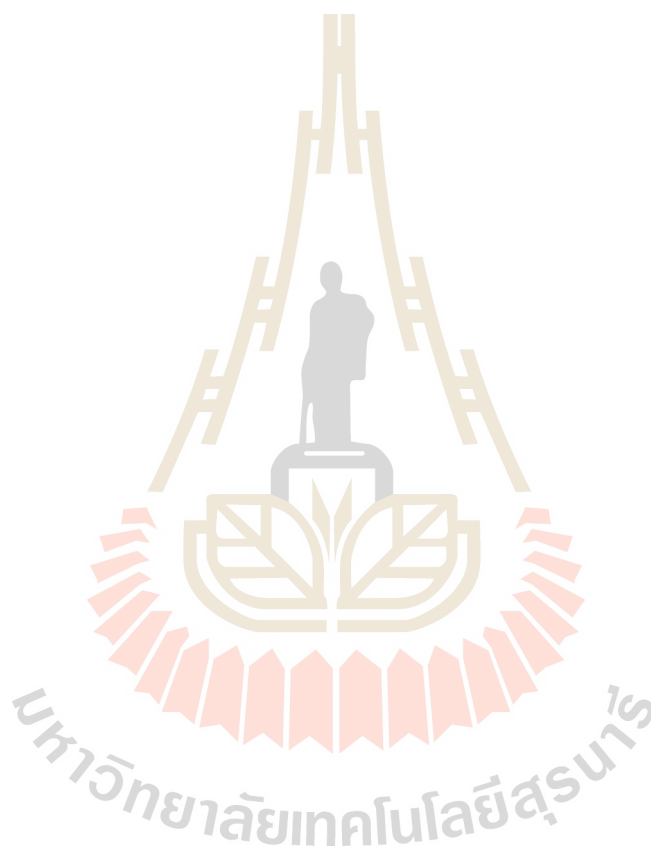
IN ZEOLITE L). อาจารย์ที่ปรึกษา : ผู้ช่วยศาสตราจารย์ ดร.กฤตวิ รัมย์วัฒนานนท์,

143 หน้า

วิทยานิพนธ์นี้มุ่งเน้นการเตรียมสีย้อม ซีโอไลต์แอลคอมโพสิตโดยการกักขังสีย้อมเรืองแสงในโพรงของซีโอไลต์แอล ซึ่งสีย้อมต่าง ๆ ที่นำมาศึกษานั้นมีช่วงการเรืองแสงที่แตกต่างกันเช่น ช่วงสีฟ้า สีเขียว สีส้มและสีแดง ได้นำมาใช้สำหรับ สีย้อม ซีโอไลต์แอลคอมโพสิต การศึกษาไอโซเทอร์มการดูดซับของสีย้อมชนิดประจวบ พบว่ามีความเข้ากันกับโมเดลของ แลงเมียร์ และปริมาณทางอุณหพลศาสตร์บ่งชี้ว่าการดูดซับสีย้อมบนซีโอไลต์แอล นั้นเกิดได้เองเป็นธรรมชาติ ปฏิกริยาเป็นแบบดูดความร้อน นอกจากนี้การเตรียมสีย้อมให้เข้าไปกักขังในซีโอไลต์แอลสามารถเตรียมโดยการแลกเปลี่ยนแคตไอออนและวิธีแก๊สเฟส (การแพร่ผ่านด้วยความร้อน) ด้วยข้อจำกัดในการใส่สีย้อมโดยวิธีแลกเปลี่ยนแคตไอออน จึงได้พัฒนาวิธีแก๊สเฟสเพื่อปรับปรุงข้อจำกัดนั้น โดยสามารถใช้ได้ทั้งสีย้อมประจวบ เช่น อะครีดินไฮโดรคลอไรด์ (AC) อะคริฟลาวีนไฮโดรคลอไรด์ (AF) เฮมิซยานีน (Hemi) ไทโอนีน (Th) และสีที่เป็นกลาง ไทโออินดิโก (Thio) ซึ่งถูกกักขังด้วยซีโอไลต์แอลชนิด โพแทสเซียม (K-LTL) และ โพรโตเนตซีโอไลต์แอล (H-LTL) วิธีแก๊สเฟสที่ใช้ปริมาณของสีย้อมที่มีความน่าจะเป็นในการใส่ (p) ที่แตกต่างกัน คือ 0.1 0.25 0.5 และ 1.0 ซึ่งการเตรียมสีย้อม ซีโอไลต์แอลคอมโพสิตประสบความสำเร็จโดยที่ $p = 0.25$ มีความเหมาะสมที่สุด เนื่องจากเกิดการรวมตัวของสีย้อมน้อยและไม่ลดคุณสมบัติการเรืองแสงในซีโอไลต์

สำหรับการศึกษาถ่ายโอนพลังงานฟลูออเรสเซนซ์เรโซแนนซ์ (FRET) ในสังเคราะห์ ตัวให้-ตัวรับ-ซีโอไลต์แอล ได้ใช้สีย้อมสองชนิดใส่เข้าไปในโพรงของซีโอไลต์แอล ซึ่งเป็นตัวรับและตัวให้ในระบบ เช่น AC_Hemi AC_AF และ AF_Th ลำดับของวิธีการใส่นั้นคือวิธีการแลกเปลี่ยนแคตไอออน - แก๊สเฟส (i-g) แก๊สเฟส- การแลกเปลี่ยนไอออน (g-i) แก๊สเฟส- แก๊สเฟส (g-g) หรือ / และการแลกเปลี่ยนแคตไอออน _ แก๊สเฟส (i-g) ผลลัพธ์ของแต่ละระบบมีประสิทธิภาพการดับสูงในซีโอไลต์ชนิดโพแทสเซียม (K-LTL) ซึ่งก็คือ AC (g) _AF (i) KLTL (72.2%) AC (i) _Hemi

(g) (65.9%) และ AF (i)_Thio (g) (52.6%) ซึ่งแสดงให้เห็นว่าวิธีการในการใส่สี่ข้อมแต่ละชนิดเข้าไปในซีโอดีแอลส่งผลต่อประสิทธิภาพการการส่งถ่ายพลังงานในระบบ FRET และวิธีนี้สามารถนำไปใช้กับวัสดุเสาอากาศและปรับปรุงอุปกรณ์ทางแสงให้มีประสิทธิภาพยิ่งขึ้นได้



สาขาวิชาเคมี

ปีการศึกษา 2561

ลายมือชื่อนักศึกษา ศิวา ออมณ์

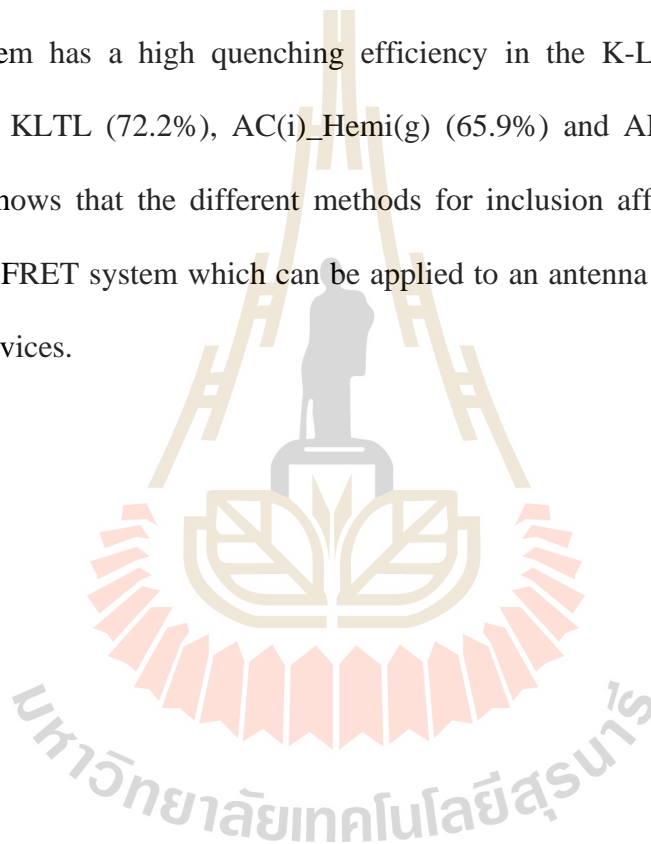
ลายมือชื่ออาจารย์ที่ปรึกษา ดร.วิ อังคนอก

SURIYA DUANGMANEE : STUDY OF FLUORESCENCE
RESONANCE ENERGY TRANSFER OF DONOR – ACCEPTOR DYE
CONFINED IN ZEOLITE L. THESIS ADVISOR : ASST. PROF.
KUNWADEE RANGSRIWATANANON, Ph.D. 143 PP.

ZEOLITE L/ DYE/ DYE-ZEOLITE L/ FLUORESCENCE/ ANTENNA SYSTEM/
THERMAL DIFFUSION/ GAS PHASE METHOD

This thesis focuses on preparation of dye_zeolite L composite with luminescence dyes inclusion into zeolite L. The different dyes with different emission regions such as blue, green, orange and red were used for dye_zeolite L composite. The study of adsorption isotherms of cationic dyes shows that the isotherms are fit well to the Langmuir model. In addition, the thermodynamic quantities indicate that the adsorptions of the dyes on zeolite L are spontaneous, endothermic and highly disordered. In addition, the inclusion of organic dye into zeolite L was prepared using cation exchange and gas phase method (thermal diffusion). According to the limitation for inclusion of dye via cation exchange, gas phase methods are used for improvement. Cationic dyes such as acridine hydrochloride (AC), acriflavine hydrochloride (AF), hemicyanine iodide (Hemi) and thionine acetate (Th) and a neutral dye of thioindigo (Thio) are encapsulated onto K-LTL and H-LTL zeolite by the gas phase method in which the amount of the dye with different occupation probabilities (ρ) of 0.1, 0.25, 0.5 and 1.0 were used. The successful inclusion of the dye into zeolite with the occupation probability at 0.25 is most suitable for preparation of the dye_zeolite due to the interruption of the dye aggregation and the quenching emission of the dye in the zeolite.

For study of the fluorescence resonance energy transfer (FRET), in the synthesis of donor-acceptor-zeolite L two dyes were used into the channel of zeolite L, in which a donor-acceptor such as Acridine - Hemicyanine (AC_Hemi), Acridine - Acriflavine (AC_AF) and Acriflavine - Thioindigo (AF_Thio). The sequence of the method to insert the dyes is cation exchange – gas phase (i -g), gas phase - cation exchange (g – i), gas phase - gas phase (g – g) or/and cation exchange_ gas phase (i – g). The result of each system has a high quenching efficiency in the K-LTL zeolite, which is AC(g)_AF(i) KLTL (72.2%), AC(i)_Hemi(g) (65.9%) and AF(i)_Thio(g) (52.6%). This result shows that the different methods for inclusion affect on the quenching efficiency of FRET system which can be applied to an antenna material and improve the optical devices.



School of Chemistry

Student's Signature

Academic Year 2018

Advisor's Signature

ACKNOWLEDGEMENTS

This success of my thesis work comes from the help of many people. I would like to express the deepest gratitude to all those. First of all, I would like to thank my thesis advisor, Asst. Prof. Dr. Kunwadee Rangriwatananon for her patience, invaluable supervision, continuous guidance and encouragement towards the completion of this research. I also wish to thank all my thesis committee members Assoc. Prof. Dr. Siriporn Jungstittiwong, Dr. Wilaiporn Insuwan and Asst. Prof. Dr. Theranun Siritanon for their available, suggestion and criticism. My thanks go to all lecturers in the School of Chemistry for their suggestions and encouragement.

I would like to tanks all of staffs at the Center of Science and Technological Equipment for their service and helpful suggestion. I wish to thank Zeolite's group and all of my friends at Suranaree University of Technology for their kindness and help.

Finally, I would like to thank my family for understanding and support throughout the long time of my study.

Suriya Duangmanee

CONTENTS

	Page
ABSTRACT IN THAI.....	I
ABSTRACT IN ENGLISH.....	III
ACKNOWLEDGEMENT.....	V
CONTENTS.....	VI
LIST OF TABLES.....	X
LIST OF FIGURES.....	XIII
LIST OF ABBREVIATIONS.....	XXI
CHAPTER	
I INTRODUCTION.....	1
1.1 Significance of study	1
1.2 Research objectives.....	2
1.3 Scope and limitations of the study.....	3
II LITERATURE REVIEW.....	5
2.1 Zeolite L (LTL Zeolite).....	5
2.2 Dyes.....	9
2.2.1 Insertion of dyes into the channels of zeolite L.....	11
2.2.2 Consecutive Insertion of Different Molecules.....	13
2.3 Dye-zeolite L material.....	14
2.3.1 Pigment.....	14

CONTENTS (Continued)

	Page
2.3.2 Solar cells sensitized by dye loaded zeolite LTL antenna.....	14
2.3.3 Luminescent solar concentrators (LSC).....	16
2.4 Fluorescence resonance energy transfer (FRET).....	17
2.5 Adsorption.....	21
2.5.1 Langmuir’s isotherm.....	21
2.5.2 Freundlich isotherm.....	23
2.6 References.....	25
III SYNTHESIS OF ZEOLITE L AND ADSORPTION	
ISOTHERM OF CATIONIC DYES.....	29
3.1 Abstract.....	29
3.2 Zeolite L.....	30
3.3 Experimental Section.....	31
3.3.1 Materials and Chemicals.....	31
3.3.2 Zeolite L Synthesis.....	31
3.3.3 Characterization.....	32
3.3.4 Adsorption isotherm studies.....	33
3.4 Result and discussion.....	34
3.4.1 Zeolite L Synthesis.....	34
3.4.2 Adsorption isotherms of cationic dyes.....	39
3.4.2.1 Adsorption isotherm of Acridine (AC).....	41

CONTENTS (Continued)

	Page
3.4.2.2 Adsorption isotherm of Afriflavine (AF).....	45
3.4.2.3 Adsorption isotherm of Hemicyanine (Hemi).....	47
3.4.2.4 Adsorption isotherm of Thionine (Th).....	49
3.5 Conclusion	51
3.6 References.....	51
IV INSERTION OF SINGLE CATIONIC AND NEUTRAL DYE ON H-LTL AND K-LTL ZEOLITE.....	54
4.1 Abstract.....	54
4.2 Introduction.....	55
4.3 Materials and method	57
4.3.1 Synthesis of zeolite LTL.....	57
4.3.2 Dyes-loaded on zeolite LTL.....	59
4.4 Results and discussion.....	62
4.4.1 Synthesis of LTL zeolite.....	62
4.4.2 Dye insertion onto zeolite L.....	64
4.4.2.1 Acridine hydrochloride (AC) on to zeolite (AC_LTL)	64
4.4.2.2 Acriflavine hydrochloride (AF) on to zeolite (AF_LTL).....	71

CONTENTS (Continued)

	Page
4.4.2.3 Hemicyanine Iodide (Hemi) on to zeolite (Hemi_LTL).....	78
4.4.2.4 Thioindigo (Thio) on to zeolite (Thio_LTL).....	87
4.4.2.5 Cyaninine (Cy) on to zeolite (Cy_LTL).....	91
4.4.2.6 Thionine Acetate (Th) on to zeolite (Th_LTL).....	98
4.5 Conclusions.....	100
4.6 References.....	101
V FLUORESCENCE RESONANCE ENERGY TRANSFER FROM THE DONOR -ACCEPTER OF ORGANIC DYE ONTO ZEOLITE LTL.....	106
5.1 Abstract.....	106
5.2 Introduction.....	107
5.3. Material and Method.....	109
5.3.1 Synthesis of zeolite LTL.....	109
5.3.2 Dyes-loaded on zeolite LTL.....	109
5.4 Results and discussions.....	111
5.4.1 Fluorescence resonance energy transfer (FRET) experiments.....	111

CONTENTS (Continued)

	Page
5.4.1.1 Acridine (AC)-Hemicyanine (hemi) Zeolite L system (AC_Hemi-LTL).....	113
5.4.1.2 Acridine (AC)- Acriflavine (AF) Zeolite L system (AC_AF -LTL).....	119
5.4.1.3 Acriflavine (AF) – Thioindigo (Thio) Zeolite L system (AF_Thio -LTL).....	124
5.4.2 The energy transfer with confocal microscope.....	127
5.5 Conclusion.....	129
5.6 References.....	130
VI CONCLUSIONS.....	132
APPENDIX.....	135
CURRICULUM VITAE.....	143

LIST OF TABLES

Table	Page
2.1 Cationic and some special dyes.....	10
2.2 Neutral dyes.....	11
3.1 Chemical composition of K-LTL and H-LTL with round shape (r) and cylindrical shape (cy).....	38
3.2 Parameters for adsorption of AC on K-LTL and H-LTL.....	43
3.3 Thermodynamic parameters for adsorption of AC on K-LTL and H-LTL.....	44
3.4 Parameters for adsorption of AF on K-LTL and H-LTL.....	45
3.5 Thermodynamic parameters for adsorption of AF on K-LTL and H-LTL.....	46
3.6 Parameters for adsorption of Hemi on K-LTL and H-LTL.....	47
3.7 Thermodynamic parameters for adsorption of Hemi on K-LTL and H-LTL.....	48
3.8 Parameters for adsorption of Th on K-LTL and H-LTL.....	49
3.9 Thermodynamic parameters for adsorption of Th on K-LTL and H-LTL.....	50
4.1 The amount of dyes in the K and H-LTL after loading with gas phase and cation exchange method.....	70
4.2 The amount of AF dyes content in the K and H-LTL after loading.....	78

LIST OF TABLES (Continued)

Table		Page
4.3	The amount of Hemi dyes in the K-LTL and H-LTL after loading.....	86
4.4	The amount of Thio dye on the K-LTL and H-LTL zeolite.....	90
4.5	The amount of Cy dye on the K and H-LTL zeolite.....	96
5.1	Calculated overlap integral, quantum yield, Förster distance and quenching efficiency for the donor–acceptor pairs of AC_Hemi K-LTL.....	116
5.2	Calculated overlap integral, quantum yield, Förster distance and quenching efficiency for the donor–acceptor pairs of AC_Hemi H-LTL.....	117
5.3	Calculated overlap integral, quantum yield, Förster distance and quenching efficiency for the donor–acceptor pairs of AC_AF_K-LTL.....	121
5.4	Calculated overlap integral, quantum yield, Förster distance and quenching efficiency for the donor–acceptor pairs of AC_AF H-LTL.....	123
5.5	Calculated overlap integral, quantum yield, Förster distance and quenching efficiency for the donor–acceptor pairs of AF_Thio_K-LTL.....	126
6.1	Thermodynamic parameters for adsorption of dyes on K-LTL.....	132
6.2	Thermodynamic parameters for adsorption of dyes on H-LTL.....	133

LIST OF FIGURES

Figure	Page
2.1 Structure of zeolite L.....	6
2.2 Structure of zeolite L and framework.....	7
2.3 Insertion of two difference dyes into the zeolite framework.....	13
2.4 Principle of dye sensitized solar cells.....	15
2.5 Principle of operation of a LSC based on a thin dye-doped polymer film.....	17
2.6 Principle of fluorescence resonance energy transfer (FRET).....	18
2.7 Spectral overlap of the donor and acceptor required for FRE.....	18
2.8 Jablonski diagram of FRET process.....	19
3.1 The simulated XRD powder pattern of LTL.....	34
3.2 XRD patterns of K-LTL zeolite product in different morphologies.....	35
3.3 SEM image of zeolite L with different morphologies.....	36
3.4 NH ₃ -TPD adsorption pattern of K-LTL and H-LTL.....	38
3.5 Adsorption isotherms of Ac on K-LTL.....	41
3.6 Linear plot of Langmuir isotherm of AC on K-LTL and H-LTL at 303, 313 and 323 K.....	42
4.1 The morphology of zeolite.....	62
4.3 XRD patterns of K-LTL and H-LTL zeolite with round shape.....	63

LIST OF FIGURES (Continued)

Figure	Page
4.4 The absorption spectra of Ac in water and 0.1 HCl solution.....	65
4.5 The emission spectrum of AC in water and 0.91 HCl solution.....	65
4.6 Diffuse reflectance spectra of Ac in K-LTL and H-LTL.....	66
4.7 Emission spectra of Ac on K-LTL and H-LTL zeolite.....	67
4.8 Emission spectra of AC with different loadings onto K-LTL zeolite by gas phase method.....	68
4.9 Emission spectra of AC with different loadings onto H-LTL zeolite by gas phase method.....	69
4.10 The absorption spectra of AF in solution.....	71
4.11 The emission spectrum of AF in water and 0.01 M HCl solution.....	72
4.12 The diffuse reflectance and emission spectra of AF on K-and H-LTL zeolite.....	74
4.13 Diffuse reflectance spectra of AF in K-LTL and H-LTL zeolite.....	75
4.14 The emission spectra of AF in K-LTL with different occupation probabilities.....	76
4.15 The emission spectra of AF_H-LTL zeolite with different occupation probabilities.....	77
4.16 The absorption spectra of hemicyanine in various solvents.....	79

LIST OF FIGURES (Continued)

Figure	Page
4.17 Emission spectra of Hemi in different solvents.....	80
4.18 Diffuse reflectance spectra of AF in K-LTL and H-LTL.....	81
4.19 The emission spectra of Hemi in K-LTL and H-LTL zeolite.....	81
4.20 Diffuse reflectance spectra of hemi in K-LTL and H-LTL zeolite.....	83
4.21 The emission spectra of Hemi_K-LTL zeolite with various occupation probabilities.....	84
4.22 The emission spectra of Hemi_H-LTL zeolite with various occupation probabilities.....	84
4.23 The absorption spectra of Thio in various solvents.....	87
4.24 Emission spectra of Thio in different solvents.....	88
4.25 Diffuse reflectance spectra of Thio confined in K-LTL and H-LTL zeolite.....	89
4.26 The emission spectra of Thio in K-LTL zeolite with various occupation probabilities.....	90
4.27 The absorption spectra of Cy in 0.01 HCl and water solvents.....	91
4.28 Diffuse reflectance spectra of Cy confined in K-LTL and H-LTL zeolite prepared by the cation exchange method.....	93

LIST OF FIGURES (Continued)

Figure	Page
4.29	The emission spectra of Cy on K-LTL and H-LTL zeolite prepared by ion exchange.....94
4.30	Diffuse reflectance spectra of Cy confined in K-LTL and H-LTL zeolite prepared by gas phase method.....95
4.31	The emission spectra of Cy on K-LTL and H-LTL zeolite.....97
4.32	The absorption spectra of Th in water and methanol solvents.....98
4.33	Diffuse reflectance spectra of Cy confined in K-LTL and H-LTL zeolite.....99
4.34	The emission spectra of Th_K-LTL and Th_H-LTL zeolite.....99
5.1	The donor - acceptor molecule for FRET study.....108
5.2	Insertion of two different dyes into the zeolite framework.....109
5.3	Energy transfer experiment, absorption and emission spectra of Ac and Hemi dissolved in aqueous solution.....114
5.4	The emission spectra of AC – K-LTL prepare by the ion exchange and gas phase method and emission spectra of AC and Hemi in the system of AC_Hemi K-LTL for energy transfer experiment.....115
5.5	The emission spectra of AC – H-LTL prepare by the ion exchange and gas phase method and emission spectra of AC and Hemi in the system of AC_Hemi H-LTL for energy transfer experiment.....117

LIST OF FIGURES (Continued)

Figure	Page
5.6	Absorption and emission spectra of Ac and hemi dissolved in aqueous solution for the energy transfer experiment.....119
5.7	The emission spectra of AC – K-LTL prepare by the ion exchange and gas phase method and emission spectra of AC and Hemi in the system of AC_AF K-LTL for energy transfer experiment.....120
5.8	The emission spectra of AC – H-LTL prepare by the ion exchange and gas phase method and emission spectra of AC and Hemi in the system of AC_AF H-LTL for energy transfer experiment.....122
5.9	Energy transfer experiment, absorption and emission spectra of AF and Thio dissolved in aqueous solution.....124
5.10	The emission spectra of AF – K-LTL prepare by the ion exchange and gas phase method and emission spectra of AF and Thio in the system of AF_Thio K-LTL for energy transfer experiment.....125
5.11	Microscopy images of AC_AF K-LTL system and AC_Hemi K-LTL system.....128

LIST OF ABBREVIATIONS

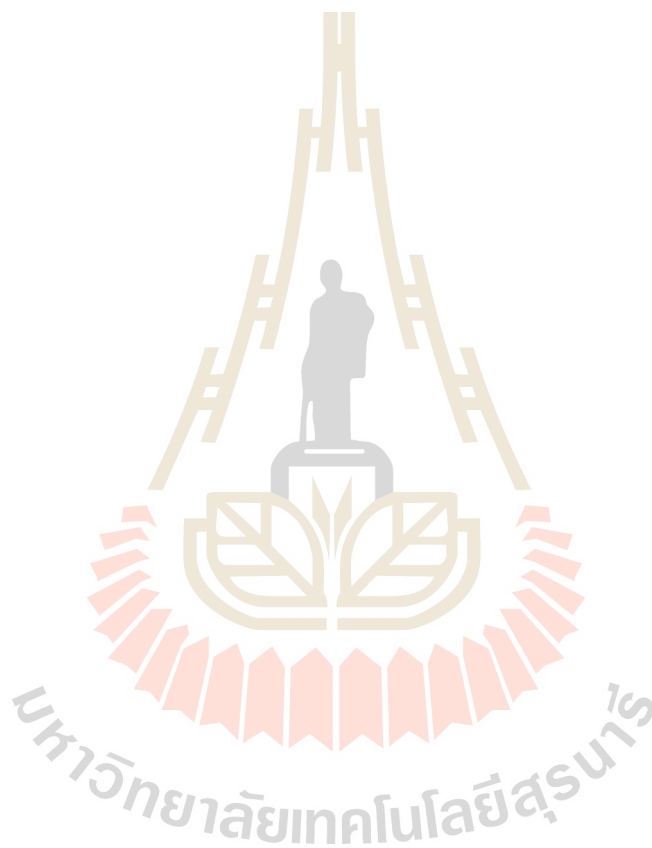
cm^{-1}	wavenumber (per centimeter)
C_0 and C_e	concentrations of dyes in solution at initial and equilibrium, respectively
d_z	diameter of the crystal in nanometer
FT-IR	Fourier transform infrared
FRET	Fluorescence resonance energy transfer
g	gram
K_L	Langmuir constant
L	optical path length
LSC	luminescenced solar concentrators
LTL	Linde Type L, Zeolite L
M	Molar
mL	milliliter
mM	millimolar
Mz	molar mass of pure potassium zeolite K-LTL (2883 g/mol)
M_D	molar mass of the dye.
nm	nanometer
n_{D+}	number of molecules intercalated
n_s	number of sites available in zeolite LTL
ρ_z	density of the zeolite crystal
q_e	amount of dye adsorbed at equilibrium

LIST OF ABBREVIATIONS (Continued)

q_m	maximum adsorption monolayer capacity
R	ideal gas constant
R^2	R-squared
SEM	Scanning electron microscopy
T	temperature
V	volume of the solution.
W_z	amount of zeolite LTL in grams
ΔG°	change in standard Gibbs free energy
ΔH°	change in standard enthalpy
ΔS°	change in standard entropy
Θ_{max}	maximum loading
μm	micrometer
XRF	X-ray Fluorescence spectrometer
TPD	Temperature Programmed Desorption
AC	Acridine Hydrochloride
AF	Acriflavine Hydrochloride
Cy	Cyanine iodide
Thio	Thioindigo
Th	Thionine Acetate
Hemi	Hemicyanine
Å	Angstrom

LIST OF ABBREVIATIONS (Continued)

ρ	occupation probability of dyes molecule
λ_{abs}	absorption maximum wavelength
λ_{emis}	emission maximum wavelength



CHAPTER I

INTRODUCTION

1.1 Significance of study

Zeolite L with well-ordered pores and crystal can be applied in various applications. The structural and chemical properties, size and morphology of crystal can play the important role on their efficiencies in the applications. Unlike other sorbents, zeolites have specific pore shape and size which can suitably be used for the distinction and controlling the access of molecules with different sizes, shapes and polarities. Control of the morphology and size of the zeolite crystals allowed them to be filled with a variety of guest species such as metal complexes, organic dyes, contaminants or clusters. The shape and the size of zeolite crystal are used for different studies. A large crystal (1-3 μm in cylindrical) is useful for studying the optical and photophysical properties of dye-composites on single crystals. A disc-shaped morphology and small crystals are used in photonic antenna system. Furthermore, zeolite L can be useful for catalyst supports and host for composite material. The supramolecular organization of the dye molecules accommodated by zeolite L channels exhibits interesting optical properties. Only dye molecules of appropriate size are arranged with their long molecular axis along the one-dimensional channels and they cannot glide past each other because the channels are too narrow. This allows the filling of specific parts of the nanocrystals. Insertion of different dye molecules can be applied

as an antenna system via fluorescence resonance energy transfer (FRET).

This work focuses on how to insert and optimize dyes molecules onto the zeolite L and the fluorescence resonance energy transfer (FRET) of the prepared dyes-zeolite with difference in preparations including computational study. In addition, the adsorption study of dyes onto zeolite providing the information on the interaction of dye and zeolite that plays a determining role on artificial photonic antenna system will be considered.

1.2 Research objectives

1.2.1 To synthesize and characterize the physical and chemical properties of the pure zeolites L.

1.2.2 To investigate the different methods (ion exchange and gas phase) to insert a single dye and two dyes (acriflavine hydrochloride, acridine hydrochloride, hemicyanine, 1,1'-diethyl-2,2'-cyanine iodide, thionine and thioindigo) on zeolite H-LTL and K-LTL.

1.2.3 To study the adsorption of some single dye-zeolite L systems from 1.2.2

1.2.4 To characterize the photophysical properties of single dye-zeolite L and two dyes-zeolite L systems from 1.2.2

1.2.5 To study the photonic artificial antenna systems with long wavelength (red region).

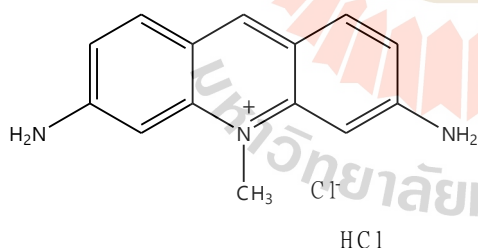
1.3 Scope and limitations of the study

1.3.1 The products of zeolite L with cylinder and disc shape will be synthesized and their physical and chemical properties will be characterized by XRD, SEM, and the particle size distribution techniques.

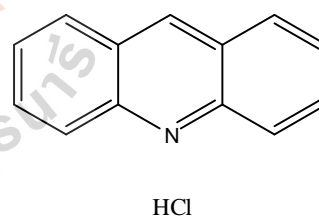
1.3.2 A single dye or two dyes of acriflavine hydrochloride, acridine hydrochloride, hemicyanine, 1,1'-diethyl-2,2'-cyanine iodide, thionine and thioindigo will be inserted onto zeolites (H-LTL and K-LTL) by ion exchange and gas phase methods.

1.3.3 The photophysical properties will be determined by UV-VIS and fluorescence technique.

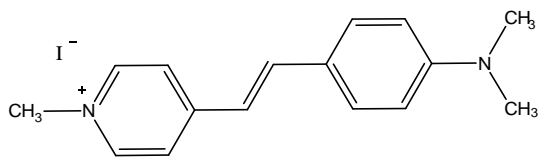
1.3.4 The adsorption isotherms of some single dye onto zeolite L by ion exchange method will be studied and the adsorption thermodynamic parameters will be determined.



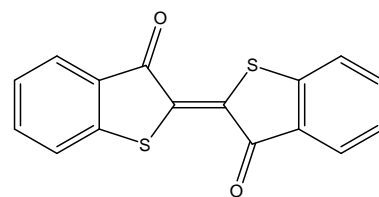
Acriflavine hydrochloride



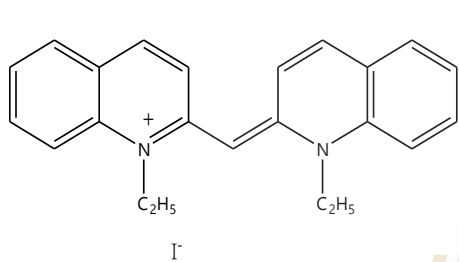
Acridine hydrochloride



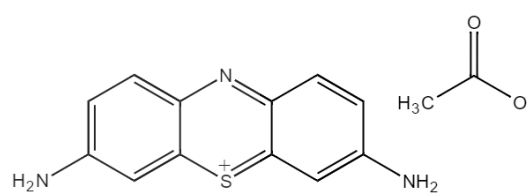
trans-4-[4-(Dimethylamino)styryl]-1-methylpyridinium



Thioindigo



1,1'-Diethyl-2,2'-cyanine iodide



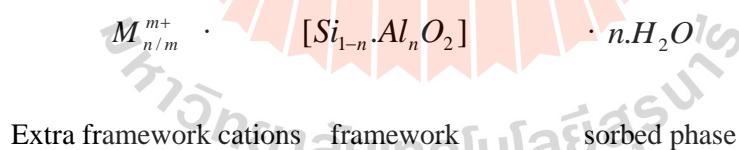
3,7-Diamino-5-phenothiazinium acetate

CHAPTER II

LITERATURE REVIEW

2.1 Zeolite L (LTL Zeolite)

Zeolites are microporous crystalline aluminosilicates, composed of TO_4 tetrahedra ($T = Si, Al$) with O atoms connecting neighboring tetrahedra. For a completely siliceous structure, combination of TO_4 ($T = Si$) units in this fashion leads to silica (SiO_2), which is an uncharged solid (Calzaferri et al., 2003; Hennessy et al., 1999; Treacy et al., 2007). Upon incorporation of Al into the silica framework, the +3 charge on the Al makes the framework negatively charged and requires the presence of extra framework cations (inorganic and organic cations can satisfy this requirement) within the structure to keep the overall framework neutral. The zeolite composition can be best described as having three components:



The extra framework cations are ion exchangeable and give rise to the rich ion-exchange chemistry of these materials. The novelty of zeolites stems from their microporosity which is a result of the topology of the framework (Thomson, 2004). Zeolite L was first described in 1968. It is hexagonal with unit cell dimensions of $a = 18.4 \text{ \AA}$ and $c = 7.5 \text{ \AA}$ and with space group P6/mmm (Insuwan et al., 2012). The structure of zeolite L is illustrated in Figure 2.1. The primary building units of classical

zeolites are TO_4 tetrahedra where T is equal to Al or Si, Figure 1(A). Connecting them by means of oxygen bridges, one obtains a secondary building unit. In the present case, the cancrinite cage is shown in Figure 1(B)-(D). Cancrinite cages are stacked into columns along the c -axis as shown in Figure 1(E), and these columns are connected in the a,b -plane, Figure 2.1(F) and Figure 2.2 resulting in the system of 1D parallel channels characteristic for zeolite L. The units form columns in the c -direction, which are connected by oxygen bridges and thus give rise to 12-membered rings with a free diameter of 7.1 \AA (Figure 2.1). As a consequence, zeolite L consists of one dimensional channels, running through the whole crystal, with a largest free diameter of about 12.6 \AA and a unit cell length of 7.5 \AA . The main channels are linked via non-planar 8-rings, which form an additional two dimensional channel system with about 1.5 \AA ring openings (Megelski et al., 2001).

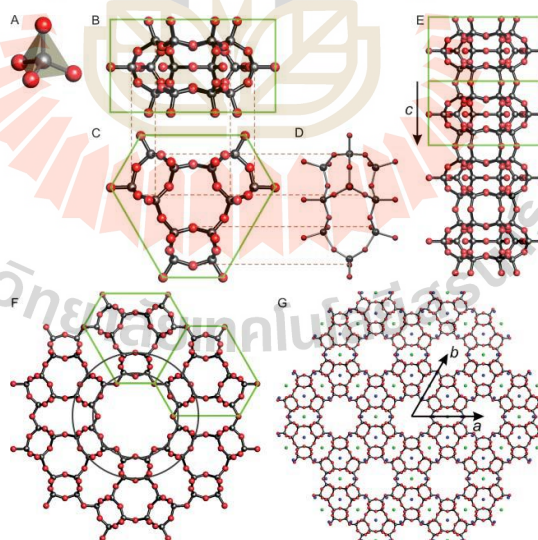


Figure 2.1 Structure of zeolite L. (A) Primary building unit, TO_4 tetrahedron. (B)–(D) Secondary building unit, cancrinite cage. (E) Stacking the cages along the c -axis of the crystal. (F) Top view of a 1 channel; cancrinite cages are connected in a plane perpendicular to the c -axis (a,b -plane) (Calzaferri et al., 2003).

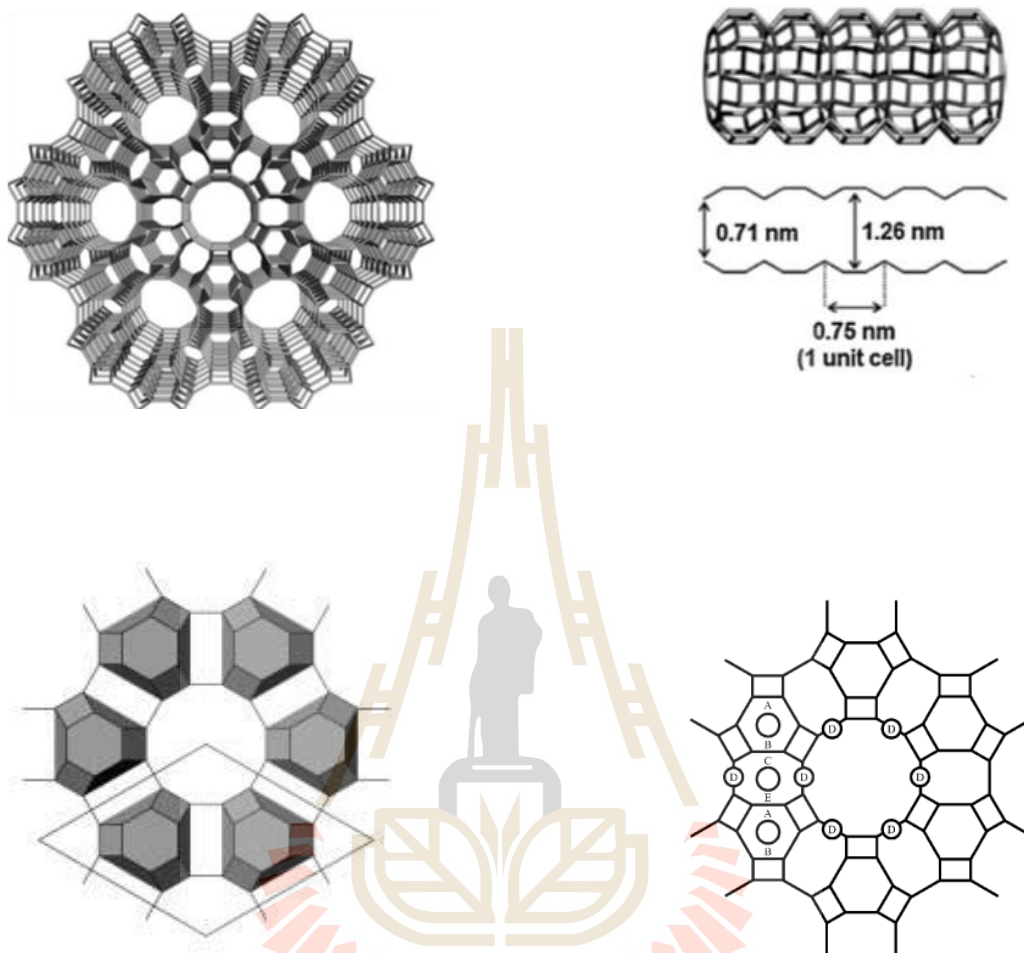


Figure 2.2 Upper: structure of zeolite L and framework side view of a main channel. Lower: the cancrinite cages highlighted as polyhedra and the different cation site positions A to E (Zhou et al., 2013).

In zeolite L, five positions are found for the extra-frame work. Cation A is in the center of the D6R-unit; B is in the center of the ϵ -cage; C lies midway between the centers of two adjacent ϵ -cavities and D is inside the main channel near the wall of the 8-ring. Dehydrated zeolite L shows an additional cation site located midway between two adjacent sites A and is indicated as E. Only the cations in site D are exchangeable

at room temperature (Hashimoto et al., 2001). In addition, they also calculated the number of parallel channels in the crystal as follows (Devaux et al., 2009) :

$$n_{ch} = \frac{\pi(\frac{d_z}{2})^2}{|a|^2(\sin(60))} = \frac{\pi}{2\sqrt{3}}(\frac{d_z}{|a|})^2 \quad (2.1)$$

where d_z is the diameter of the crystal in nanometer and $|a|$ is the length of the primitive vector. Using the values of zeolite LTL the equation can be simplified to

$$n_{ch} = 0.267 (d_z)^2 \quad (2.2)$$

A zeolite LTL crystal of 600 nm in diameter gives rise to about 96,000 parallel channels. The number of unit cells (in mol) in m_z grams of zeolite LTL can be calculated as follows.

$$n_{u.c.} = \frac{m_z}{M_z} \quad (2.3)$$

where m_z is the molar mass of a unit cells, $M_z = 2883$ g/mol for pure potassium zeolite LTL. 10 mg of pure potassium zeolite L contains 3.47×10^{-6} mol unit cells.

Synthesis of LTL Zeolite

LTL zeolite can be synthesized by hydrothermal process and Si/Al ratio of synthetic LTL zeolite is varied from 3-6. Gels with the molar compositions $2.62K_2O: Al_2O_3: 10.00 SiO_2:160H_2O$ has yielded a pure phase of highly crystalline zeolite L where the shape of the crystals can be varied from cylindrical to clam shapes. The size of the crystals increased as a function of the H_2O and SiO_2 contents, while it decreased with increasing the K_2O content. However, regardless of the size, altering the Al_2O_3

content did not change the shape of the crystals (cylindrical shape) (Insuwan et al., 2012).

Alexandra, I. et al. (2013) used zeolite growth modifiers (ZGMs) of zeolite L (LTL type) crystallization method to selectively control the growth of zeolite crystals, which used extensively in a wide range of industrial applications (Lupulescu et al., 2013). This method cooperatively tunes crystal properties, such as morphology and surface architecture, through the use of inexpensive, commercially available chemicals with specificity for binding to crystallographic surfaces and mediating anisotropic growth.

2.2 Dyes

Fluorescence dye as a guest of host zeolite L that can be incorporated in their channels are cationic and neutral molecules. Table 1 and 2 show the cationic and neutral dye molecules which have been explored to date.

Table 2.1 Cationic and some special dyes.

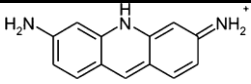
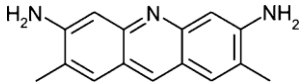
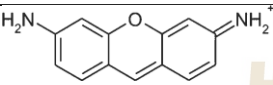
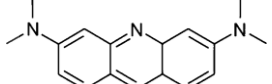
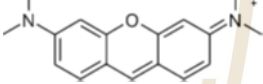
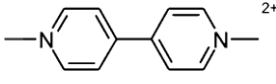
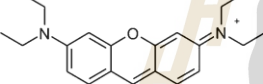
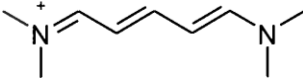
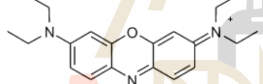
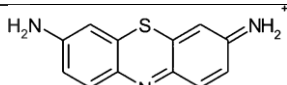
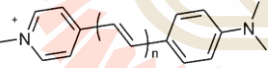
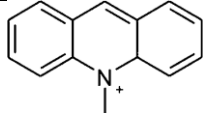
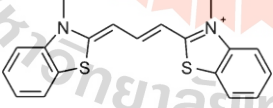
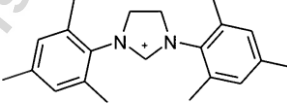
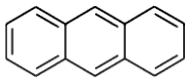
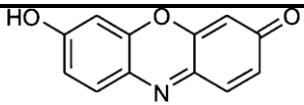
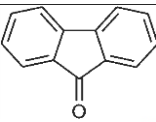
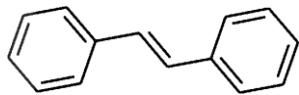
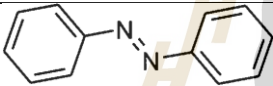
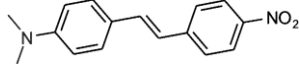
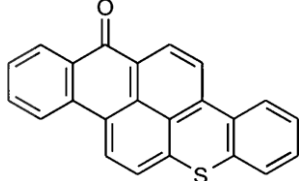
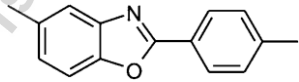
Name/ abbreviation	Structural formula	Name/ abbreviation	Structural formula
Proflavine ⁺		AY	
Py ⁺		AQ	
PyGY ⁺		MV2 ⁺	
PyB ⁺		BDP ⁺	
Ox ⁺		Th ⁺	
DSM ⁺ (n = 1)		MeAcr ⁺	
PC20 ⁺		BTMPI ⁺	

Table 2.2 Neutral dyes.

Name/ abbreviation	Structural formula	Name/ abbreviation	Structural formula
Anthracene		ResH	
Fluorenone		Stilbene	
Azobenzene		DANS	
PR 149		Hostasol Red	
Isoviolanthron		PBOX	

2.2.1 Insertion of dyes into the channels of zeolite L

Normally, cationic dye can be incorporated within the channel of zeolite L by means of ion exchange. Neutral dye can be inserted to the channel by mean of gas phase (Hennessy et al., 1999; Pauchard et al., 2000). The three types of dye molecules

that can be inserted into the channels of zeolite L are (i) molecules that are small enough to fit into a unit cell such as methyl viologen (MV^{2+}) (Hennessy et al., 1999), azobenzene and stilbene, (ii) molecules with the sizes which are hard to guess their position and orientation in the channel such as oxonine, pyronine, and thionine (Gigli et al., 2015; Pauchard et al., 2000), (iii) Molecules which are so large, have no other choice but to align along the c-axis such as xanthene (Fois et al., 2012). Because of their length, the molecules can align along the cylindrical axis of the channels of zeolite L, resulting in high stability and also high luminescence quantum yield. In this study, Acriflavine hydrochloride, acridine hydrochloride, trans-4-[4-(Dimethyl amino) styryl]-1-methylpyridinium iodide, thionine and thioindigo are interesting. The loading, or occupation probability, ρ of a dye-zeolite LTL material is defined as follows (Devaux et al., 2009);

$$\rho = \frac{\text{number of occupied sites}}{\text{total amount of sites}} \quad (2.4)$$

From Eq. (4), one gets the following expression to calculate the loading, if the weight m_z and m_D are zeolite and dye in grams;

$$\rho = \frac{m_D}{M_D} \left(\frac{M_Z n_s}{m_z} \right) \quad (2.5)$$

where M_D is the molar mass of the dye. ρ ranges from 0 for an empty zeolite to 1 for a full one. The dye concentration of a dye-zeolite material $c(\rho)$, can be expressed as a function of loading (Devaux et al., 2009);

$$c(\rho) = \frac{p_z \rho}{M_Z n_s} \quad (2.6)$$

where p_z is the density of the zeolite crystal; M_z is the molar mass of one unit cell; n_s is the number of unit cells that form one site, and $c(p)$ is expressed in units of mol/L.

Inserting the values for potassium zeolite LTL ($\rho_z = 2.17 \text{ g/cm}^3$, $M_z = 2883 \text{ g/mol}$), one obtains

$$c(\rho) = 0.752 \frac{\rho}{n_s} \quad (2.7)$$

2.2.2 Consecutive Insertion of Different Molecules

The fact that appropriately chosen dyes cannot glide past each other because the channels are too narrow is the underlying principle for preparing photonic antenna systems as illustrated in Figure 2.3.

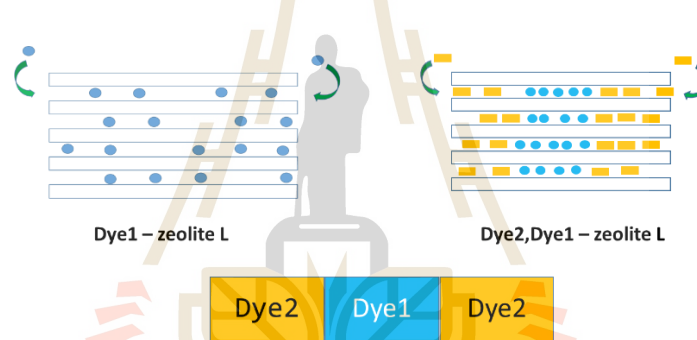


Figure 2.3 Insertion of two different dyes into the zeolite framework.

The first step results in a material named dye1-zeolite L. After removing the dyes which might eventually be adsorbed at the outer surface, a second dye, dye2 is inserted. Conditions must be chosen such that dye1 has no chance to exit the channels at the beginning of this second step. Once a dye2 molecule has entered each channel from both sides, the dye1 molecules have no chance to escape. In fact, they are pushed deeper into the channels by the incoming dye2 species, and form the dye2, dye1-zeolite L material. The same procedure is repeated for dye3. The resulting material is the dye3,dye2, dye1-zeolite L material. Different insertion methods can be combined. Dye1, for example, can be a cationic dye that is inserted by cation exchange, dye2 can

be a neutral dye, inserted from the gas phase (Pauchard et al., 2000). Structures with more than three different dyes can be prepared but this is still to be explored.

2.3 Dye-zeolite L material

2.3.1 Pigment

Pigments are defined as colorants that are insoluble in the application medium, implying that they retain a particulate (or crystal) structure throughout the coloration process. Pascal Woodtli et al (2018) intercalated indigo molecules into the nanochannels of zeolite L. Thus indigo-ZL can be considered as a pigment, although its light absorption properties are comparable to dissolved indigo monomers. By preventing the formation of indigo aggregates, the absorption spectrum of indigo-ZL in a matrix or on a substrate is highly predictable. The application of indigo-ZL on cotton was tested by roll coating. The light absorption properties of the resulting textile prints showed no significant alteration when compared to the pure indigo-ZL powder (Woodtli et al., 2018).

2.3.2 Solar cells sensitized by dye loaded zeolite LTL antenna

An antenna material which absorbs all light in the right wavelength range and transfers it by radiationless energy transfer to a device like a semiconductor offers a unique possibility of developing dye sensitized solar cells or luminescent solar concentrators. This kind of sensitised solar cell functions by first absorbing light over a broad spectral range in the zeolite antenna material. The excitation energy migrates radiationlessly among the inserted dyes towards the stopcock molecules. From there, Förster energy transfer to the semiconductor takes place across a thin insulating layer.

The injected energy can now be used for driving the charge separation process in the active medium. Finally, the resulting electrical current is collected *via* appropriate contacts. Figure 3 two strategies that can be followed, the one on the left applicable for thin layer silicon cells and the right for organic solar cells where the design must match the short free path lengths of the charge carriers in such devices (Minkowski et al., 2006).

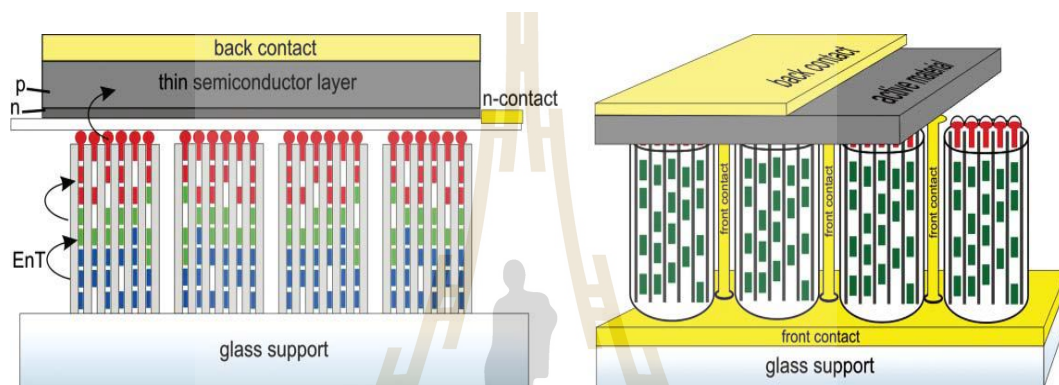


Figure 2.4 Principle of dye sensitized solar cells (Calzaferri et al., 2003).

From Figure 2.4 arranging crystals with their *c*-axes perpendicular to the surface of a semiconductor and a length of 50 nm up to a few hundred nm ranges allows transport of the excitation energy towards the zeolite-semiconductor interface by energy migration. Stopcock molecules are placed only at one channel end to allow energy transfer. The semiconductor layer can be very thin, because the electron-hole pairs form near the surface. The transfer of electrons from antenna to semiconductor is prevented by introducing a thin insulating layer, preferably directly into the stopcock. The scheme on the left shows a principle related *e.g.* to thin layer silicon devices. The scheme on the right is related to organic solar or plastic solar cells. The white area on top of the head is an insulating part directly integrated into the stopcock. The zeolite materials are enlarged with respect to the rest of the device.

2.3.3 Luminescent solar concentrators (LSC)

A LSC concentrates light with an inexpensive polymer-based device into efficient photovoltaic cells (Gfeller et al., 1997; Gfeller et al., 1998). It is a transparent plate containing luminescent chromophores (dyes or phosphores). Light enters the face of the plate, is absorbed, and is subsequently re-emitted at longer wavelength. The luminescent light is trapped by total internal reflection and guided to the edges of the plate, where it can be converted to electricity by a photovoltaic cell. Because the edge area of the plate is much smaller than the face area, the LSC operates as a concentrator of light. Recently, some work has presented that it can be coupled to solar cell as shown in Figure 2.5 (Brühwiler et al., 1998; Iwasaki et al., 2000). A major disadvantage in old LSC is the reflection loss caused by the overlap between the absorption and emission spectra of the chromophores. Self-absorption is the key problem that has to be solved in order to develop commercially viable LSC products (El-Zaria et al., 2005). The conception of an advanced LSC with reduced self-absorption is based on dye-zeolite inclusion compounds (Wang et al., 2010). The channel of zeolite LTL are filled with a large number of donor molecules, which absorb the incident light and subsequently transport the electronic excitation energy to a comparatively small number of acceptor dyes by means of FRET. As the donor molecules are not able to absorb the acceptor luminescence, photons emitted by the acceptor molecules can travel through the LSC with low self-absorption losses.

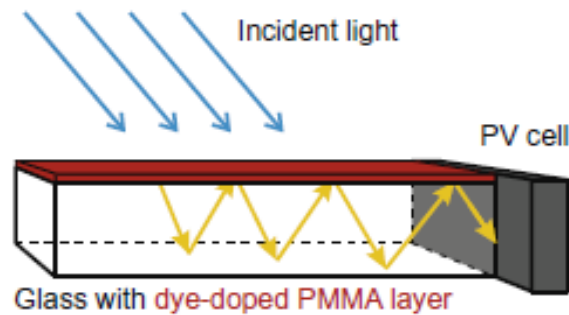


Figure 2.5 Principle of operation of a LSC based on a thin dye-doped polymer film. Re-emitted light is guided toward the edges by total internal reflection (yellow arrows) (Thomas Dienel, 2010)

For optimizing the light-harvesting and FRET efficiency Calzaferri et al. (2011) improve an efficient FRET between donor and acceptor dyes, the donor-to-acceptor ratio (d/a) which high to reduce self-absorption. (Busby et al., 2011; Calzaferri, 2012; Insuwan et al., 2015; Saha et al., 2016). This is an important proof for the feasibility of the high donor-to-acceptor ratios required for the reduction of self-absorption

2.4 Fluorescence resonance energy transfer (FRET)

Fluorescence (Förster) Resonance Energy Transfer (FRET) is the process by which an initially excited donor (D) relaxes to the ground state by transferring its energy to a nearby acceptor (A) in a nonradiative way, i.e. without the emission of a photon (Lakowicz, 2006). The most common term 'Fluorescence' Resonance Energy Transfer is also used for FRET to imply that the acceptor is a fluorophore.

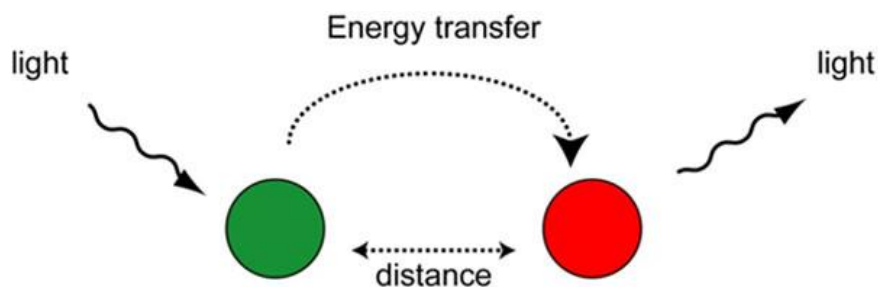


Figure 2.6 Principle of fluorescence resonance energy transfer (FRET).

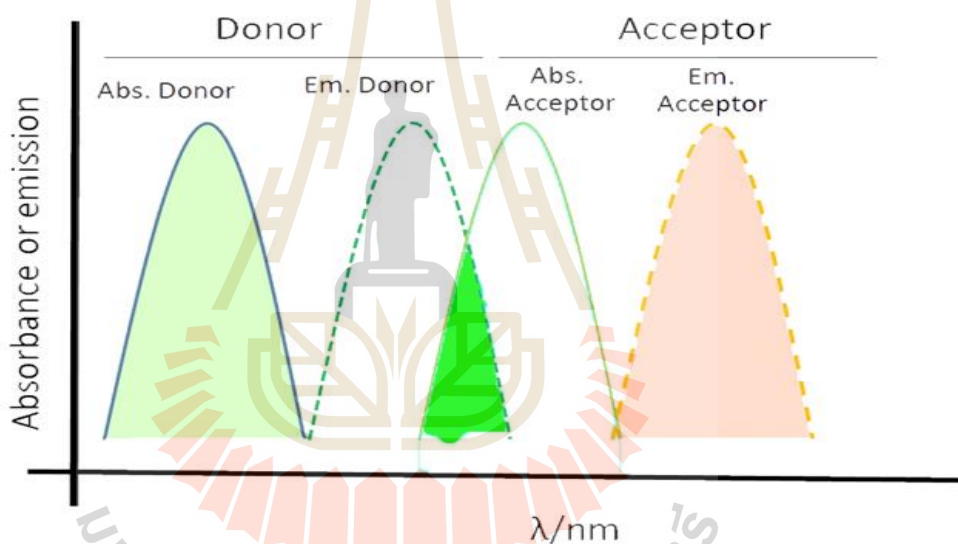


Figure 2.7 Spectral overlap of the donor and acceptor required for FRET.

The Jablonski diagram (Figure 2.8) illustrates the relationship between vibrational energy states, the fluorescent state and resonance energy transfer. In the first step, absorption of light by a donor causes excitation from the ground singlet state (S_0) to a higher state. A very rapid (ps) decay from the S_2 to the lowest vibrational level in this state (S_1) is followed by a slower (ns) return to the S_0 , and the process is accompanied by the emission of a photon. Different energy states are possible for the

excited donor, including spontaneous emission and nonradiative processes. If certain conditions are satisfied. First of all, donor and acceptor molecules must be located in a close proximity like 0-10 nm. In addition to the proximity requirement, the spectral characteristics of donor and acceptor molecules must have significant similarity, i.e., the overlapping area of the emission spectrum of donor and the absorption spectrum of acceptor, must be large enough. Relative orientations of donor and acceptor also play an important role in the efficiency of the resonance energy transfer. Additionally, extinction coefficients of donor and acceptor, refractive index of the medium and lifetime of donor fluorophore are the other factors that affect the energy transfer efficiency and rate.

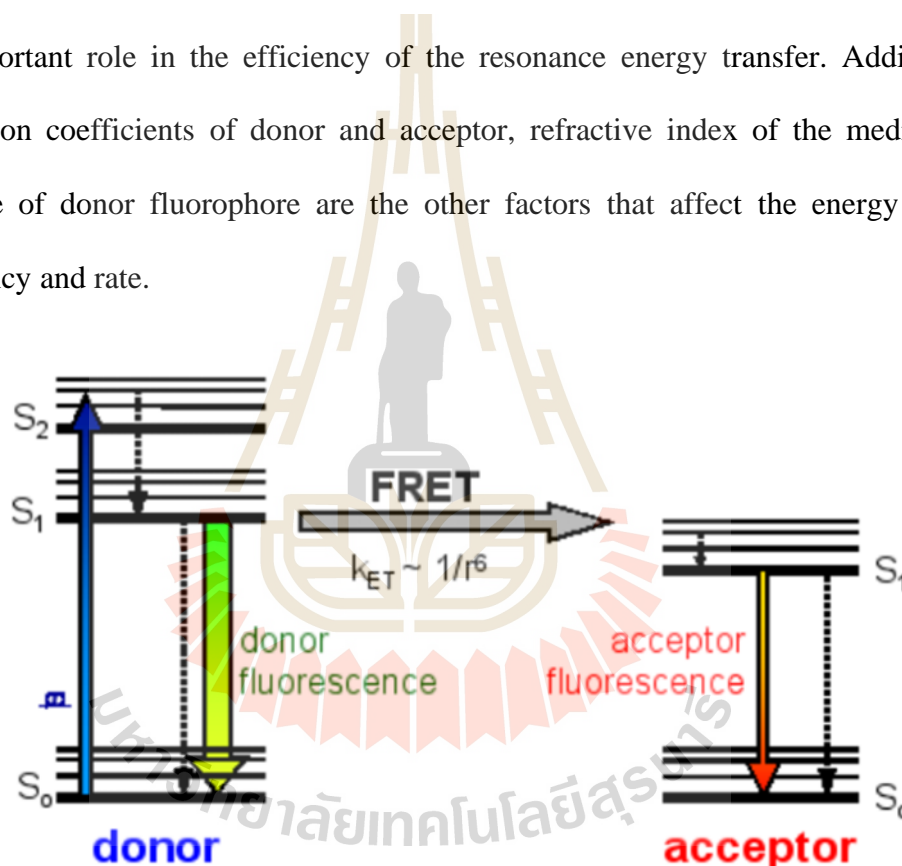


Figure 2.8 Jablonski diagram of FRET process.

The rate of energy transfer depends upon the extent of spectral overlap of the emission spectrum of the donor with the absorption spectrum of the acceptor (Figure 2.8), the quantum yield of the donor, the relative orientation of the donor and acceptor, transition dipoles and the distance between the donor and acceptor molecules. The

energy transfer rate constant k_{ET} from an excited donor (D) to an acceptor (A) can be written as Equation 2.8 in the point dipole approximation.

$$k_{ET} = \left(\frac{9000 \ln 10}{128 \pi^5 N_A n^4 \tau_D} \right) \Phi_D J_{DA} G_{DA} p_D p_A \quad (2.8)$$

where Φ_D and τ_D [s⁻¹] are the fluorescence quantum yield and the intrinsic fluorescence lifetime of the donor, N_A [mol⁻¹] is Avogadro's number, n is the refractive index of the medium, J_{DA} [cm³m⁻¹] is the spectral overlap integral between the normalized donor emission and the acceptor absorption spectra, G_{DA} is the geometrical factor, p_D and p_A are the occupation probabilities of the sites with donors and acceptors.

The most common application of FRET is to measure the distance between two sites of a macromolecule. If there is a single donor and acceptor and if the donor–acceptor distance does not change during the excited–state lifetime, then the donor–acceptor distance can be determined from the efficiency of the energy transfer. The transfer efficiency (E) can be determined by steady–state measurements of the extent of donor quenching due to the acceptor (Lakowicz, 2006).

$$E = 1 - \frac{F_{DA}}{F_D} \quad (2.9)$$

$$E = 1 - \frac{\tau_{DA}}{\tau_D} \quad (2.10)$$

where F is the relative fluorescence intensity in the absence (F_D) and presence (F_{DA}) of the acceptor, and τ is the lifetime (τ_D) in absence and (τ_{DA}) presence of the acceptor.

Fluorescence resonance energy transfer is a key mechanism in organic optoelectronic devices such as organic photovoltaic cells (OPVs) and light-emitting diodes (OLEDs) and widely utilized for a variety applications. For example it has been used as a tool for pH sensor (Ryder et al., 2003). Some researcher applied a quantum-chemical (QM) /Monte Carlo(MC) (Viani et al., 2016) approached over the inhomogeneous distribution of the cationic dyes (Py^+ and Ox^+) obtained from confocal microscopy images on of Py^+ crystals, revealing that increasing inhomogeneity leads to a strong change in the exciton dynamics, reducing the exciton lifetimes and modifying the dimensionality of the transport.

2.5 Adsorption

Adsorption is usually described through isotherms, that is, functions which connect the amount of adsorbate on the adsorbent, with its pressure (if gas) or concentration (if liquid). One can find in literature several models describing process of adsorption, namely Langmuir isotherm and Freundlich isotherm (Hameed et al., 2007).

2.5.1 Langmuir's isotherm

Langmuir's isotherm describing the adsorption of adsorbate (A) onto the surface of the adsorbent (S) requires three assumptions:

- The surface of the adsorbent is in contact with a solution containing an adsorbate which is strongly attracted to the surface
- The surface has a specific number of sites where the solute molecules can be adsorbed.

- The adsorption involves the attachment of only one layer of molecules to the surface, i.e. monolayer adsorption. The chemical reaction for monolayer adsorption.

The chemical reaction for monolayer adsorption can be represented as follows:



Where AS represents a solute molecule bound to a surface site on S. The equilibrium constant K_{ads} for this reaction is given by:

$$K_{ads} = \frac{[AS]}{[A][S]} \quad (2.12)$$

[A] denotes the concentration of A, while the other two terms [S] and [AS] are two-dimensional analogs of concentration and are expressed in units such as mol/cm². The principle of chemical equilibrium holds with these terms. The complete form of the Langmuir isotherm considers Eq. (2.12) in terms of surface coverage θ which is defined as the fraction of the adsorption sites to which a solute molecule has become attached. An expression for the fraction of the surface with unattached sites is therefore (1 - θ). Given these definitions, thus rewrite the term [AS]/[S] as

$$\frac{[AS]}{[S]} = \frac{\theta}{(1 - \theta)} \quad (2.13)$$

Express [A] as C and rewrite Eq. (2.12) as:

$$K_{ads} = \frac{\theta}{C(1 - \theta)} \quad (2.14)$$

Rearranging, that obtain the final form of the Langmuir adsorption isotherm:

$$\Theta = \frac{K_{ads}C}{1 + K_{ads}C} \quad (2.15)$$

If we define Y as the amount of adsorption in units of moles adsorbate per mass adsorbent, and Y_{max} as the maximal adsorption, then:

$$\Theta = \frac{Y}{Y_{max}} \quad (2.16)$$

and the isotherm can be expressed as:

$$\frac{C}{Y} = \frac{1}{K_{ads}Y_{max}} + \frac{C}{Y_{max}} \quad (2.17)$$

Where K_{ads} is the equilibrium constant, C is concentration of solute molecule at equilibrium, Y is the amount of mole of adsorbate per mass of adsorbent and Y_{max} is the maximal adsorption corresponding to complete monolayer coverage on the adsorbent surface.

2.5.2 Freundlich isotherm

Freundlich isotherm is an empirical model used to describe the adsorption in aqueous systems. This is commonly used to describe the adsorption characteristics for the heterogeneous surface, in which it is characterized by the heterogeneity factor $1/n$. Hence, the empirical equation can be written

$$q_e = K_F C_e^{1/n} \quad (2.18)$$

Where q_e is the solid phase adsorbate concentration in equilibrium (mg/g), C_e the equilibrium liquid phase concentration (mg/L), K_F the Freundlich constant (mg/g) (L/mg)^{1/n} and $1/n$ is the heterogeneity factor. A linear form of the Freundlich expression can be obtained by taking logarithms of Eq. (2.19):

$$\ln q_e = \ln K_F + \frac{1}{n} \ln C_e \quad (2.19)$$

Therefore, a plot of $\ln q_e$ versus $\ln C_e$ enables the constant K_F and exponent $1/n$ to be determined.

Adsorption thermodynamic properties

In normally, the enthalpy can be performed by adsorption experiments at different temperatures. The results are used to calculate the equilibrium constant at various temperatures. For calculate the changes of Gibbs free energy, Gibbs-Helmholtz equation (Eq. 2.20) was used to calculate (Rytwo et al., 2003):

$$\left(\frac{\partial}{\partial T} \left(\frac{\Delta G}{T} \right) \right)_P = \frac{-\Delta H}{T^2} \quad (2.20)$$

Where ΔG and ΔH are the difference in Gibbs free energy and enthalpy between the final and the initial state. As at equilibrium, $\Delta G = 0$, from (Eq. 2.15) can relate the equilibrium constant can be related to the standard free energy of the reaction as follows:

$$\Delta G^\circ = -RT \ln K \quad (2.21)$$

By combining (Eq. 2.20) and (Eq. 2.21) the Vant'Hoff equation is obtained:

$$\left(\frac{\partial \ln K}{\partial T} \right)_P = \frac{\Delta H^\circ}{T^2 R} \quad (2.22)$$

Where ΔH° is the enthalpy of the reaction at standard pressure. In addition, ΔH° can be assumed constant over the temperature range of an experiment and a plot of $\ln K$ vs $1/T$ provides a convenient estimate of ΔH . Form the slope of the line which is equal to $-\Delta H^\circ/R$.

2.5 References

- Brühwiler, D., Gfeller, N., and Calzaferri, G. (1998). Resorufin in the Channels of Zeolite L. **The Journal of Physical Chemistry B**. 102: 2923-2929.
- Busby, M., Devaux, A., Blum, C., Subramaniam, V., Calzaferri, G., and De Cola, L. (2011). Interactions of Perylene Bisimide in the One-Dimensional Channels of Zeolite L. **The Journal of Physical Chemistry C**. 115: 5974-5988.
- Calzaferri, G. (2012). Nanochannels: hosts for the supramolecular organization of molecules and complexes. **Langmuir**. 28: 6216-6231.
- Calzaferri, G., Huber, S., Maas, H., and Minkowski, C. (2003). Host-guest antenna materials. **Angewandte Chemie International edition in English**. 42: 3732-3758.
- Devaux, A., and Calzaferri, G. (2009). Manipulation of Energy Transfer Processes in Nanochannels International Journal of Photoenergy (Vol. 2009).
- El-Zaria, M., El-din H. Etaiw, S., and Sh. Ibrahim, M. (2005). Antenna behavior of donor–acceptor dye-loaded novel supramolecular framework hosts (Vol. 19).
- Fois, E., Tabacchi, G., and Calzaferri, G. (2012). Orientation and Order of Xanthene Dyes in the One-Dimensional Channels of Zeolite L: Bridging the Gap between

- Experimental Data and Molecular Behavior. **The Journal of Physical Chemistry C**. 116: 16784-16799.
- Gfeller, N., and Calzaferri, G. (1997). Energy Migration in Dye-Loaded Hexagonal Microporous Crystals. **The Journal of Physical Chemistry B**. 101: 1396-1408.
- Gfeller, N., Megelski, S., and Calzaferri, G. (1998). Transfer of Electronic Excitation Energy between Dye Molecules in the Channels of Zeolite L (Vol. 102).
- Gigli, L., Arletti, R., Vitillo, J.G., Alberto, G., Martra, G., Devaux, A., and Vezzalini, G. (2015). Thionine Dye Confined in Zeolite L: Synthesis Location and Optical Properties. **The Journal of Physical Chemistry C**. 119: 16156-16165.
- Hameed, B.H., Ahmad, A.A., and Aziz, N. (2007). Isotherms, kinetics and thermodynamics of acid dye adsorption on activated palm ash. **Chemical Engineering Journal**. 133: 195-203.
- Hashimoto, S., Hagiri, M., Matsubara, N., and Tobita, S. (2001). Photophysical studies of neutral aromatic species confined in zeolite L: Comparison with cationic dyes. **Physical Chemistry Chemical Physics**. 3: 5043-5051.
- Hennessy, B., Megelski, S., Marcolli, C., Shklover, V., Bärlocher, C., and Calzaferri, G. (1999). Characterization of Methyl Viologen in the Channels of Zeolite L. **The Journal of Physical Chemistry B**. 103: 3340-3351.
- Insuwan, W., Jungstittiwong, S., and Rangsrivatananon, K. (2015). Host–guest composite materials of dyes loaded zeolite LTL for antenna applications. **Journal of Luminescence**. 161: 31-36.
- Insuwan, W., and Kunwadee, R. (2012). Morphology-Controlled Synthesis of Zeolite and Physicochemical Properties. **Engineering Journal**. 16: 1-12.

- Iwasaki, M., Kita, M., Ito, K., Kohno, A., and Fukunishi, K. (2000). Intercalation characteristics of 1,1'-diethyl-2,2'-cyanine and other cationic dyes in synthetic saponite: Orientation in the interlayer (Vol. 48).
- Lakowicz, R. (2006). Energy Transfer. In J. R. Lakowicz (Ed.), *Principles of Fluorescence Spectroscopy* (pp. 443-475). Boston, MA: Springer US.
- Lupulescu, A.I., Kumar, M., and Rimer, J.D. (2013). A facile strategy to design zeolite L crystals with tunable morphology and surface architecture. **Journal of the American Chemical Society**. 135: 6608-6617.
- Megelski, S., and Calzaferri, G. (2001). Tuning the Size and Shape of Zeolite L-Based Inorganic–Organic Host–Guest Composites for Optical Antenna Systems. **Advanced Functional Materials**. 11: 277-286.
- Minkowski, C., Pansu, R., Takano, M., and Calzaferri, G. (2006). Energy Collection, Transport, and Trapping by a Supramolecular Organization of Dyes in Hexagonal Zeolite Nanocrystals. **Advanced Functional Materials**. 16: 273-285.
- Pauchard, M., Devaux, A., and Calzaferri, G. (2000). Dye-Loaded Zeolite L Sandwiches as Artificial Antenna Systems for Light Transport. **Chemistry – A European Journal**. 6: 3456-3470.
- Ryder, A., Power, S., and Glynn, T. (2003). Evaluation of Acridine in Nafion as a Fluorescence-Lifetime-Based pH Sensor (Vol. 57).
- Rytwo, G., and Ruiz-Hitzky, E. (2003). Enthalpies of adsorption of methylene blue and crystal violet to montmorillonite. **Journal of Thermal Analysis and Calorimetry**. 71: 751-759.

- Saha, J., Dey, D., Roy, A.D., Bhattacharjee, D., and Hussain, S.A. (2016). Multi step FRET among three laser dyes Pyrene, Acriflavine and Rhodamine B. **Journal of Luminescence**. 172: 168-174.
- Thomson, K.T. (2004). Handbook of Zeolite Science and Technology Edited by Scott M. Auerbach (University of Massachusetts, Amherst), Kathleen A. Carrado (Argonne National Laboratory), Prabir K. Dutta (The Ohio State University). Marcel Dekker, Inc.: New York, Basel. 2003. xii + 1184 pp. \$235.00. ISBN 0-8247-4020-3. **Journal of the American Chemical Society**. 126: 8858-8859.
- Treacy, M.M.J., and Higgins, J.B. (2007). LTL - Linde Type L. In M. M. J. Treacy and J. B. Higgins (Eds.), Collection of Simulated XRD Powder Patterns for Zeolites (Fifth Edition) (pp. 256-257). Amsterdam: Elsevier Science B.V.
- Viani, L., Minoia, A., Cornil, J., Beljonne, D., Egelhaaf, H.-J., and Gierschner, J. (2016). Resonant Energy Transport in Dye-Filled Monolithic Crystals of Zeolite L: Modeling of Inhomogeneity. **The Journal of Physical Chemistry C**. 120: 27192-27199.
- Wang, Y., Li, H., Feng, Y., Zhang, H., Calzaferri, G., and Ren, T. (2010). Orienting Zeolite L Microcrystals with a Functional Linker. **Angewandte Chemie International Edition**. 49: 1434-1438.
- Woodtli, P., Giger, S., Müller, P., Sägesser, L., Zucchetto, N., Reber, M.J. and Brühwiler, D. (2018). Indigo in the nanochannels of zeolite L: Towards a new type of colorant. **Dyes and Pigments**. 149: 456-461.
- Zhou, X., Wesolowski, T.A., Tabacchi, G., Fois, E., Calzaferri, G., and Devaux, A. (2013). First-principles simulation of the absorption bands of fluorenone in zeolite L. **Physical Chemistry Chemical Physics**. 15: 159-167.

CHAPTER III

SYNTHESIS OF ZEOLITE L AND ADSORPTION ISOTHERM OF CATIONIC DYES

3.1 Abstract

Zeolite L was synthesized with variation of chemical compositions leading to the differences in morphologies and crystal sizes. The morphology varied from ice hockey to cylindrical shapes and the crystal sizes varied from 0.50 - 2.50 μm . The appropriate round shape of zeolite was used for the study of the adsorption isotherm of cationic dye such as acridine (AC), acriflavine (AF), hemicyanine (Hemi) and thionine (Th). The amount of the adsorbed dyes and the interactions between the dyes and zeolite framework were examined by the adsorption isotherms study. The result illustrates that the adsorption isotherms are fit very well with the Langmuir model. In addition, the thermodynamic quantities indicated that the adsorptions of those dyes on zeolite L are spontaneous, endothermic and highly disordered. Moreover, the maximum loading (Θ_{max}) of Hemi is lower than that of the other dyes which corresponds to the steric hindrances of Hemi molecule which is difficult for insertion onto zeolite L.

3.2 Zeolite L

Zeolites with a well-defined structure used as catalysts and molecular sieves are becoming increasingly popular in the field of design and fabrication of advanced functional materials (Wang et al., 2010). Zeolites are the ideal host for achieving supramolecular organization of photoactive species, leading to versatile building blocks for the realization of hierarchically organized multifunctional composite materials. Different zeolites with suitable channel dimensions, such as $\text{AlPO}_4\text{-5}$, zeolite Y and zeolite L as well as mesoporous materials, such as MCM-41 have been successfully adopted as nanosized host matrices for the synthesis of these composites (Calzaferri et al., 2003; Easwaramoorthi et al., 2008; Hennessy et al., 1999; Ihlein et al., 1998). The only few of dye-zeolite are the possible to be applied with fascinating systems such as microlasers, pigments, optical switches, or artificial antenna systems. In this rapidly research, the inclusion of photoactive molecules into one-dimensional channel systems is of paramount relevance for further progress in some of the most challenging fields of nanoscience and nanotechnology. Since the nanometric diameter channels of zeolites may induce an anisotropic arrangement of photoactive molecules, the resulting host-guest materials show outstanding energy transfer capabilities that required for the fabrication of increasingly sophisticated optical devices which might open novel pathways in areas such as solar energy harvesting (Fois et al., 2013). Zeolite L crystals feature strictly parallel channels arranged in a hexagonal symmetry. Their one-dimensional channels can be filled with suitable guests. Geometrical constraints imposed by the host structure lead to supramolecular organization of the guests in the channels (Ban et al., 2007). The supramolecular organization of dyes inside the zeolite L channels is the first stage of organization. It allows light harvesting within the volume

of a dye-loaded zeolite L crystal and allows radiationless energy transport in the channel (Calzaferri, 2012; Devaux et al., 2009; Fois et al., 2013). The cationic dyes as a guest, were used for inclusion onto zeolite L such as acridine (AC), acriflavine (AF), hemicyanine (hemi) and thionine (Th). Those of cationic dyes have the different ranges of luminescence properties which is $\lambda_{em} = 450, 500, 550$ and 620 nm for AC, AF, Hemi and Th, respectively.

Specifically, this chapter focuses on hydrothermal synthesis of zeolite L and the equilibrium isotherms of cationic dyes that is an invaluable tool for the theoretical evaluation and interpretation of thermodynamic parameters, such as heats of adsorption and Gibbs free energy.

3.3 Experimental Section

3.3.1 Materials and Chemicals

The used silica sources are colloidal silica sol (Ludox HS-40 from Dupont, 40% SiO₂), and alumina sources is aluminium hydroxide (CARLO ERBA, 98%) and potassium hydroxide (CARLO ERBA, 85%) is used for alkali metal cations.

3.3.2 Zeolite L Synthesis

Zeolite L crystals were synthesized by a method from the literature (Wilaiporn Insuwan et al., 2012) with a different morphology such as ice hockey, round, cylindrical and clam shape. A 0.59 g of aluminium hydroxide was dissolved in boiling potassium hydroxide solution (1.28 g of potassium hydroxide added to 2.51 g of double distilled water to get a clear solution). This solution was added to 5.52 g of Ludox HS-40 with 4.82 g of double distilled water in a mixer. The clear solution mixture was stirred for 3 minutes to obtain a gel with viscosity and turbidity. The starting gel was

then transferred into a teflon-lined autoclave for crystallization at 180 °C for 2 days without stirring. After crystallization, the Teflon-lined autoclave was cooled in cold water before opening. The product was washed with distilled water until the pH of liquid was close to 7. Finally, the crystalline solid was dried overnight at 80 °C in hot air oven. All materials used in this study were of reagent grade.

NH₄LTL was prepared by ion-exchanging the K-LTL with 0.1 NH₄Cl solution. Ion exchange was carried out at 50 °C for 12 hours. After that the zeolite samples were washed with distilled water and dried at 100 °C for 12 hours. NH₄LTL was calcined at 450 °C for 4 hours to decompose NH₄⁺ ions to NH₃, then NH₄LTL was transformed to H-LTL.

3.3.3 Characterization

The products were analyzed by powder X-ray diffraction (XRD) using a Bruker D2 PHASER radiations scanning from 3-30° at a rate of 0.05°/s with current 30 kV and 10 mA. The chemical compositions were analyzed by energy dispersive X-ray fluorescence (EDXRF, Horiba XGT-5200 X-ray Analytical Microscope) with Rh X-ray tube with a 50 kV and 1 mA. For the examination of LTL morphology, scanning electron microscope (SEM, JEOL JSM-6010LV) at an acceleration voltage of 10-20 kV were used. Acidity strength was determined by ammonium temperature programmed desorption (NH₃-TPD) with a Bel Japan Model BelcatB. The NH₃-TPD spectra were measured using a conventional flow-through reactor connected to a thermal conductivity detector (TCD). The TCD responses were calibrated by a dose containing known amounts of ammonia.

3.3.4 Adsorption isotherm studies

The adsorption was performed by batch experiments. The adsorption of the dyes was performed by shaking 0.1g of the zeolite L (round shape) in 25 mL of the solutions with varied concentrations (10^{-6} - 10^{-5} M) at different temperatures (30, 40 and 50 °C). The samples were collected by separating the zeolites from solution using a centrifuge. The concentration of the dyes was determined spectrophotometrically by measuring absorbance at 355, 450, 485 and 560 nm for λ_{\max} of Ac, AF, Hemi and Th, respectively. The data obtained from the adsorption tests were used to calculate the %w/v of the adsorbent by a mass-balance relationship, which represents the amount of adsorbed dye per the amount of dye adsorbent (Hameed et al., 2007):

$$q_e = \frac{(C_0 - C_e)V}{m} \quad (3.1)$$

where q_e (M/g) is the amount of dye adsorbed at equilibrium. V (L) is the volume of the solution. m (grams) is the mass of the zeolite LTL. C_0 and C_e (M) are concentrations of dyes in solution (M) at initial and equilibrium, respectively.

3.4 Result and discussion

3.4.1 Zeolite L Synthesis

Figure 3.1 illustrates XRD patterns of zeolite L with different morphologies. To characterize K-LTL and H-LTL, the XRD patterns of synthesized zeolite were compared with simulated XRD patterns of zeolite (see Figure3.1) that all of the samples show characteristic main peaks at $2\theta = 5.5, 19.4, 22.7, 28.0, 29.1$ and

30.7. (Figure 3.2 and 3.3). The XRD patterns indicate that the crystallinity of the H-LTL samples is lower than that of K-LTL, and the percentage of the crystallinity of the H-LTL is reduced to 10 % of the K-LTL samples except that of ice hockey shape (35%). A possible explanation of this observation is that the calcination step led to destruction of the crystalline framework.

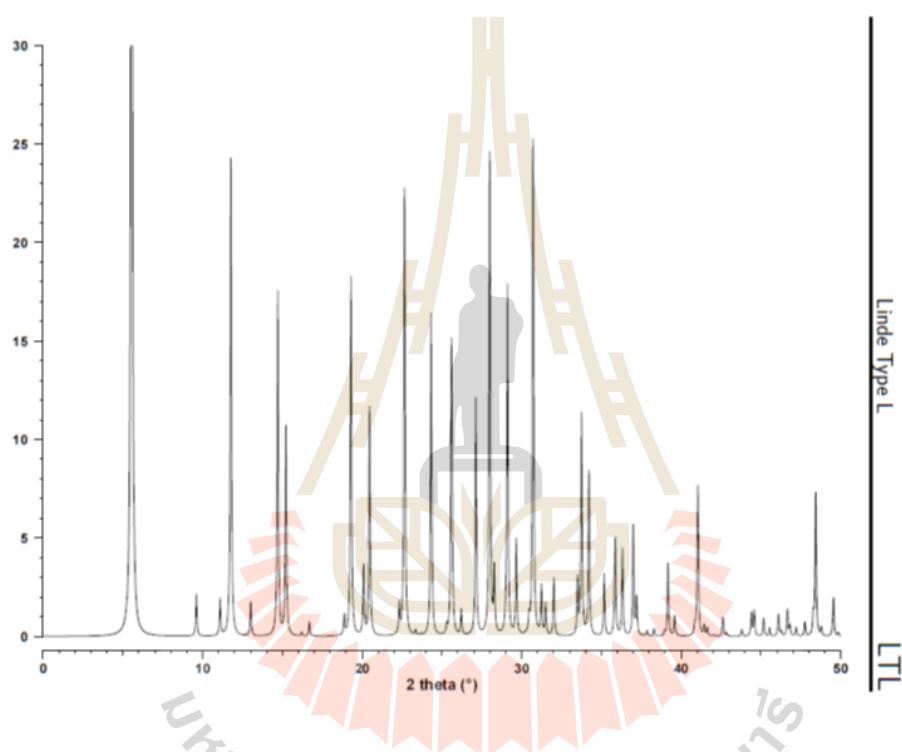


Figure 3.1 The simulated XRD powder pattern of LTL (Treacy et al., 2007).

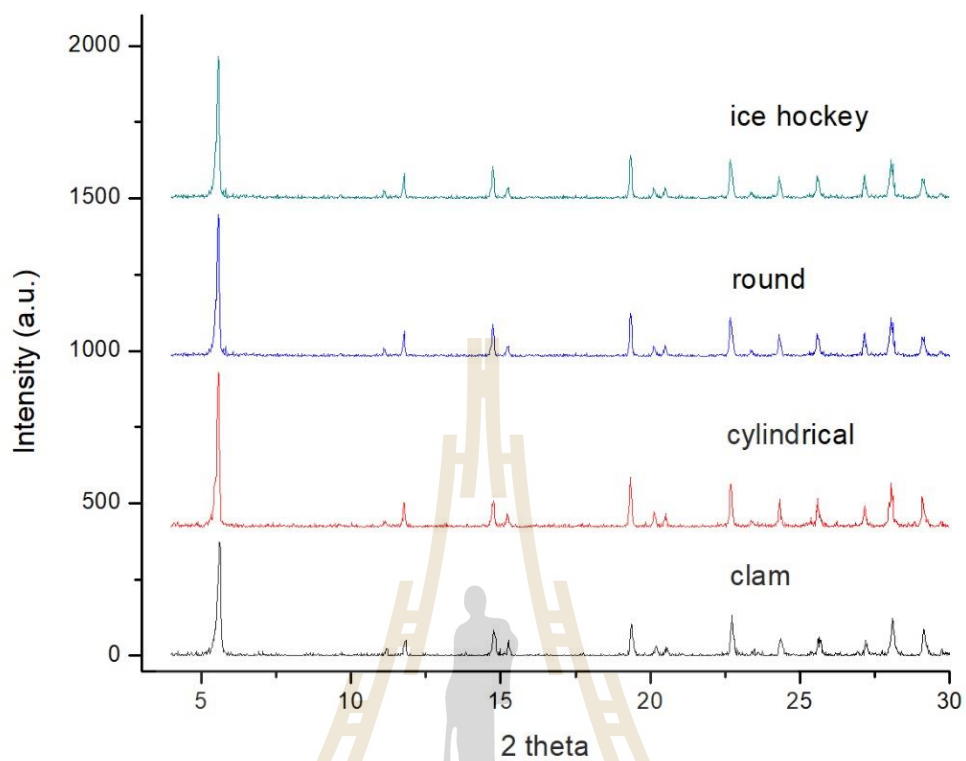


Figure 3.2 XRD patterns of K-LTL zeolite product in different morphologies.

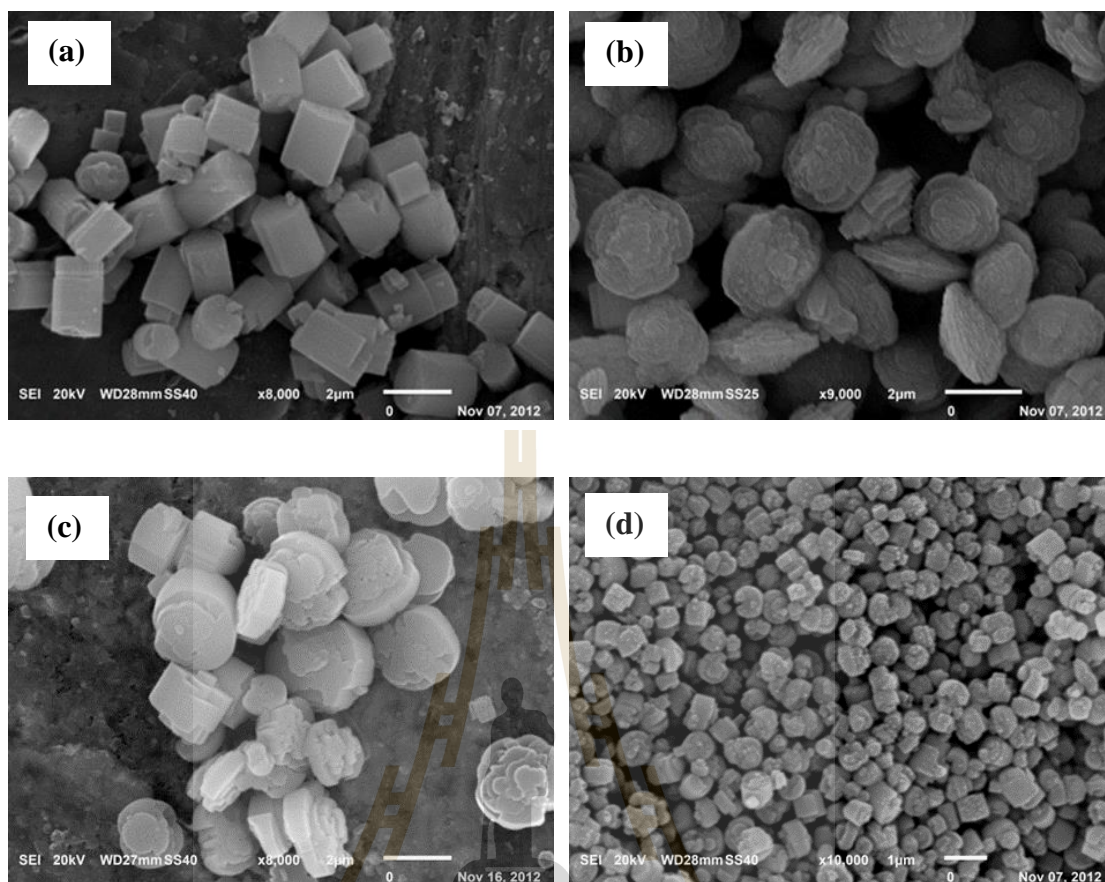


Figure 3.3 SEM images of zeolite L with different morphologies; cylindrical(a), clam(b), round(c) and ice hockey(d) shape.

Zeolite L can be synthesized in various sizes and shapes. Insuwan (Insuwan W. et al., 2012) studied the effects of chemical compositions of the starting gel on the synthesis, size and morphology of zeolite L crystals. In this study the K-LTL sample of an ice hockey shape ($2.62\text{K}_2\text{O}:\text{Al}_2\text{O}_3:8\text{SiO}_2:160\text{H}_2\text{O}$) with the size $0.5\ \mu\text{m}$, a round shape ($2.62\text{K}_2\text{O}:\text{Al}_2\text{O}_3:10\text{SiO}_2:100\text{H}_2\text{O}$) with the size $2.2\ \mu\text{m}$, a clam shape ($3.54\text{K}_2\text{O}:\text{Al}_2\text{O}_3:10\text{SiO}_2:160\text{H}_2\text{O}$) with the size $2.6\ \mu\text{m}$ and a cylindrical shape ($2.62\text{K}_2\text{O}:1.2\text{Al}_2\text{O}_3:10\text{SiO}_2:160\text{H}_2\text{O}$) with the size $2.2\ \mu\text{m}$ were obtained. The SEM images demonstrating a morphology of zeolite L K-LTL samples are shown in Figure 3.3. Due to a variety of morphology, a round shape and cylindrical shape were used for the study

of the adsorption isotherm and fluorescence resonance energy transfer (FRET), respectively.

The chemical composition (see Table 3.1) shows that the exchange of NH_4^+ with K^+ in K-LTL is not complete and the NH_4^+ exchange level attained is about 69–75%. This is in a line with the work of Insuwan (W. Insuwan et al., 2014; Meeprasert et al., 2013) on cation-exchange in K-LTL with NH_4^+ of about 77 % of K-LTL.

Table 3.1 Chemical composition of K-LTL and H-LTL with round shape (r) and cylindrical shape (cy).

Sample	Chemical composition (% mol)			
	Si	Al	K	Si/Al
K-LTL (r)	72.5	13.2	14.2	5.49
H-LTL (r)	78.3	13.9	7.8	5.63
K-LTL (cy)	68.9	12.5	18.6	5.59
H-LTL (cy)	78.2	14.4	7.4	5.43

The temperature-programmed desorption of NH_3 (NH_3 -TPD) was used to monitor the changes in the surface coverage of the probe molecules pre-adsorbed on the zeolite samples. The temperature from which the strength and the amount of total acid sites were determined. The NH_3 -TPD curves of the K-LTL and H-LTL samples are shown in Figure 3.4. The desorption peak of NH_3 on K-LTL showed a desorption peak at 176 °C. H-LTL obviously showed to desorption peaks at low and high temperature of 190 °C and 450 -500 °C, respectively. This result suggests the presence of weak acid sites and strong acid sites on the H-LTL. The first peak was assigned to

ammonia adsorbed on the extra-framework potassium, and the second one was assigned to the ammonia adsorbed on the Brønsted acid site.

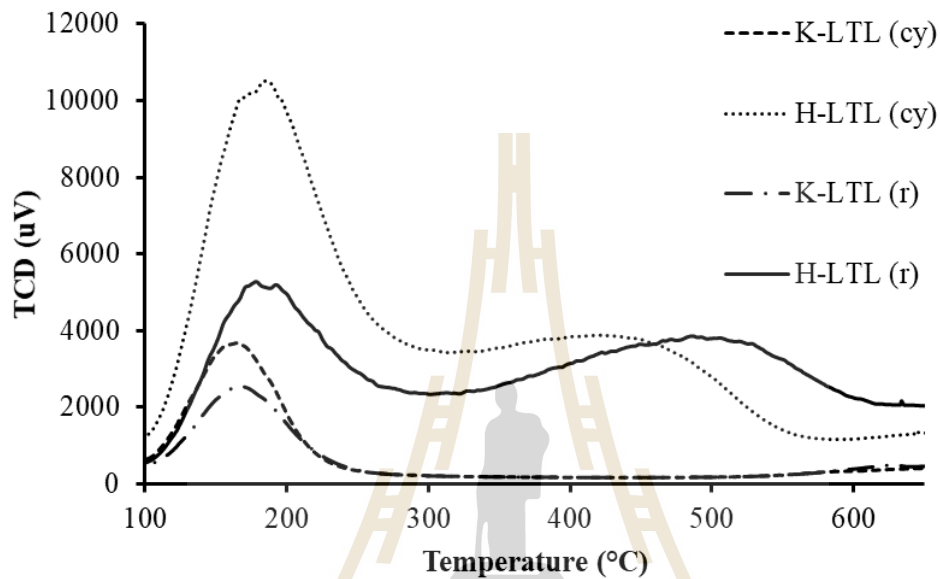


Figure 3.4 NH_3 -TPD adsorption pattern of K-LTL and H-LTL.

3.4.2 Adsorption isotherms of cationic dyes

The adsorption isotherm was studied with some cationic dyes such as AC, AF, Hemi and Th that was performed at 30, 40, and 50 °C, respectively. It was found that the experimental data were well-fitted with the Langmuir model. One of the assumptions of the Langmuir model is that the adsorption occurs at specific homogeneous sites within the adsorbent. The equation is as follows:

$$qe = \frac{q_m K_L C_e}{1 + K_L C_e} \quad (3.2)$$

where q_e (M/g) is the amount of dyes adsorbed on zeolite LTL at equilibrium and q_m (M/g) is the maximum adsorption monolayer capacity. K_L is the Langmuir

constant related to the affinity between adsorbate and adsorbent and is related to the free energy of adsorption. C_e (M) is the concentration of dyes at equilibrium. (Hameed et al., 2007)

The maximum loading (% Φ_{max}) of dyes

The maximum loading (% Φ_{max}) of dyes on the H-LTL and K-LTL can be calculated from equation (2).

$$\Phi = \frac{\text{number of molecule intercalated}}{\text{number of site available}} = \frac{n_{D^+}}{n_s} \quad (3.3)$$

where the number of sites n_s is available in zeolite L; n_{D^+} corresponds to the number of unit cells and the size of D^+ is calculated as follows:

$$n_s = \frac{g_z}{Mw_z \left(\frac{g}{mol}\right)} \quad (3.4)$$

Where g_z is amount of zeolite LTL in grams and Mw_z is a molecular weight/unit cell of sample. In addition, the number of molecules intercalated (n_{D^+}) can be obtained from adsorption study (q_m) that was fitted and described by the Langmuir model.

Thermodynamic parameters

The thermodynamic parameter such as the Gibbs free energy change (ΔG°), enthalpy change (ΔH°) and entropy change (ΔS°) were determined to understand better the effect of temperature on the adsorption. The change in Gibbs free energy (ΔG°) of the adsorption process is related to the equilibrium constant by the following equation (Sawasdee et al., 2015):

$$\Delta G^\circ = -RT \ln K_L \quad (3.5)$$

where R is the gas constant (8.314 J/mol·K); T is temperature (K) and K_L is adsorption constant in the Langmuir isotherm (Sawasdee et al., 2015). The values of ΔH° and ΔS° can be calculated from the slope and intercept of the linear variation of $\ln K_L$ with reciprocal of temperature (1/T) as in the following equation.

$$\ln K_L = -\frac{\Delta H^\circ}{RT} + \frac{\Delta S^\circ}{R} \quad (3.6)$$

3.4.2.1 Adsorption isotherm of Acridine (AC)

The adsorption isotherm determined at 303, 313, and 323 K are shown in Figure 3.5. It was found that the experimental data can be fitted well with the Langmuir model. One of the assumptions of Langmuir model is that the adsorption occurs at specific homogenous sites within the adsorbent.

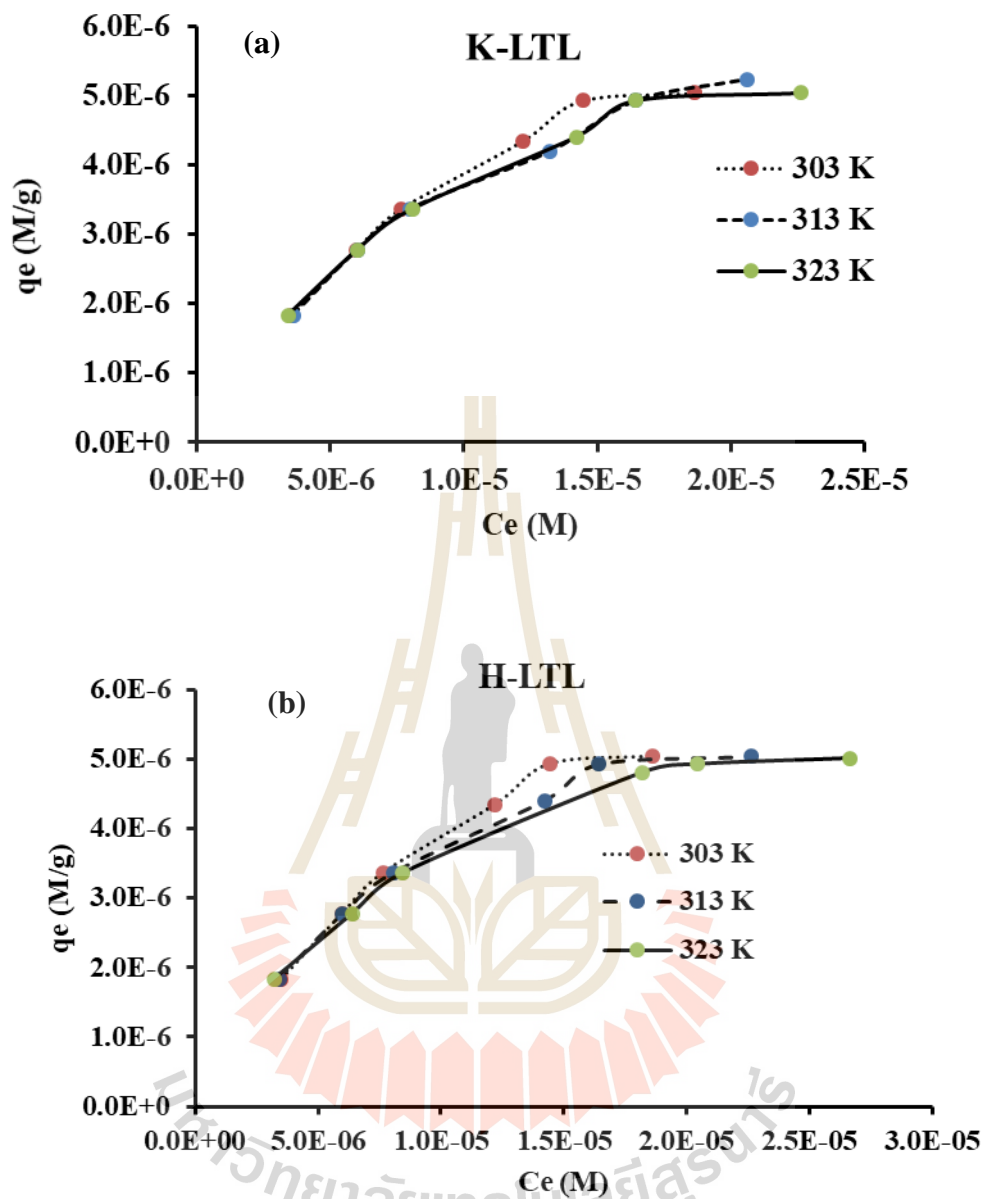


Figure 3.5 Adsorption isotherms of Ac on K-LTL(a) and H-LTL(b) at 303, 313 and 323 K.

Linear plots of Langmuir isotherms of the dyes adsorbed on the K-LTL and H-LTL samples are shown in Figure 3.6. The correlation coefficient values of the linearity were found to be satisfactory. The maximum adsorption monolayer capacity

(q_m), and the Langmuir constant (K_L) calculated from the slope and the intercept of the linear plot are shown in Table 3.2.

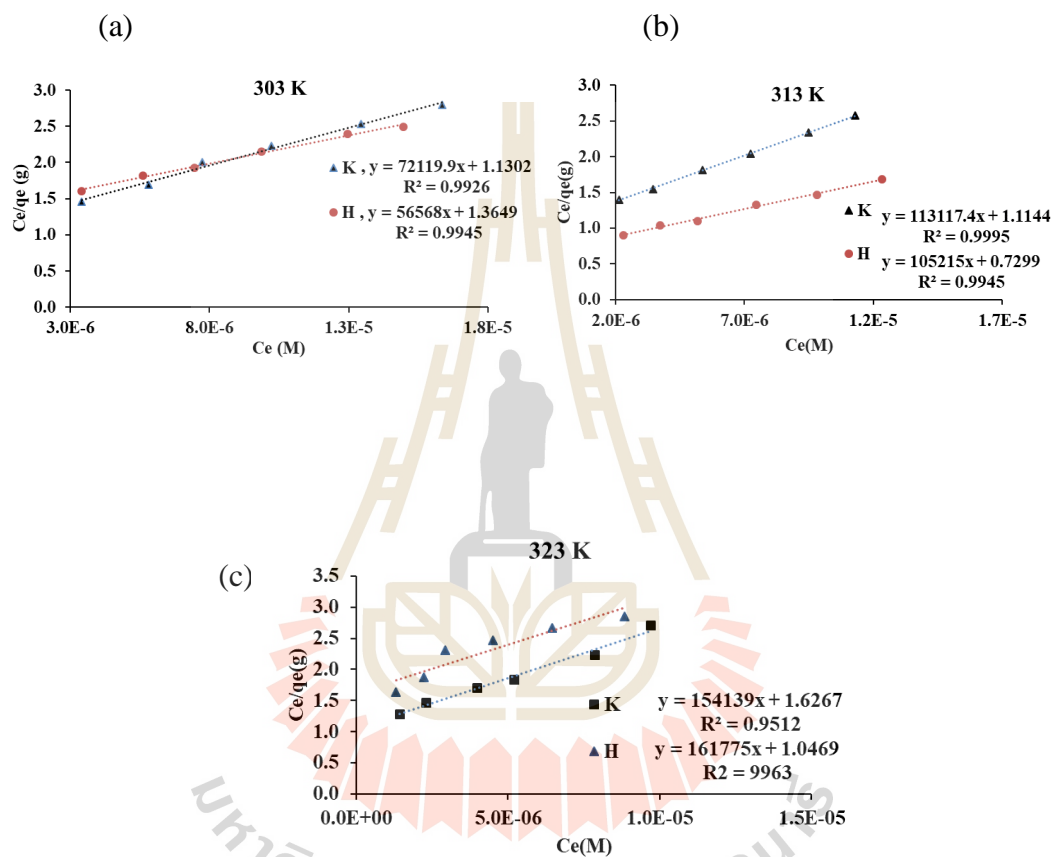


Figure 3.6 Linear plot of Langmuir isotherm of AC on K-LTL and H-LTL at 303 (a), 313 (b) and 323 K (c)

Table 3.2 Parameters for adsorption of AC on K-LTL and H-LTL.

Sample	temp (K)	Langmuir isotherm			
		q_m (M/g)	K_L (M ⁻¹)	R^2	$\% \Phi_{max}$
K-LTL	303	9.61×10^{-6}	72119.9	0.9926	1.72
	313	9.85×10^{-6}	113177.4	0.9995	2.29
	323	1.23×10^{-5}	154139.6	0.9512	2.57
H-LTL	303	1.29×10^{-6}	56568.3	0.9945	0.37
	313	1.30×10^{-6}	105215.8	0.9945	0.38
	323	6.18×10^{-6}	161775.0	0.9963	1.08

From Table 3.2, the maximum adsorption monolayer capacity (q_m) of AC inside the channel of zeolite L in K - LTL is higher than that in H - LTL. The Langmuir constant (K_L), which is related to the energy of the adsorption which quantitatively reflects the affinity between the adsorbent and the adsorbate, of the K-LTL is higher value than H-LTL indicating that the interaction of AC – K-LTL is stronger than that of AC - H-LTL. The strong interaction of AC – K-LTL can be described by cation - π interaction while the interaction of AC - H-LTL is an aromatic hydrogen bond occurring from HO-Brønsted acid site and π -electron of AC (OH/ π interaction) (Insuwan et al., 2014). In addition, the maximum loading ($\% \Phi_{max}$) of AC in H-LTL is smaller than that in K-LTL due to the interaction as mentioned above.

Table 3.3 Thermodynamic parameters for adsorption of AC on K-LTL and H-LTL.

Sample	temp (K)	ΔG (kJ/mol)	ΔH (kJ/mol)	ΔS (J/molK)
K-LTL	303	-28.82		291.33
	313	-30.31	21.15	268.39
	323	-32.11		268.02
H-LTL	303	-27.58		265.65
	313	-30.11	26.01	234.13
	323	-32.58		244.55

Thermodynamic parameters are shown in table 3.3. The negative values of ΔG° indicate that the dye adsorption is spontaneous in nature. The positive values of ΔH° indicate that the adsorption process is endothermic. This result agrees with the several reports on endothermic adsorption of reactive dyes on different types of adsorbents. Based on the magnitude of ΔH° (20.45 - 44.62 kJ/mol) (Hameed et al., 2007), the adsorption of AC dyes onto zeolite L (K-LTL and H-LTL) was classified as a physical adsorption process. Moreover, the positive value of ΔS° indicates the increasing randomness at the solid/liquid interface during the adsorption process.

3.4.2.2 Adsorption isotherm of Afriflavine (AF)

The adsorption isotherms of AF dye at 303, 313, and 323 K were determined, and linear plots of Langmuir isotherms are shown in Appendix (Figure A1

and A2). The experimental data can be fitted well with the Langmuir model and the parameters for adsorption of AF on K-LTL and H-LTL are shown in table 3.4

Table 3.4 Parameters for adsorption of AF on K-LTL and H-LTL.

Sample	temp (K)	Langmuir isotherm			
		q_m (M/g)	K_L (M ⁻¹)	R^2	% Φ_{max}
K-LTL	303	4.67×10^{-6}	73705.4	0.9959	1.35
	313	5.62×10^{-6}	126924.3	0.9950	1.62
	323	9.20×10^{-6}	283947.9	0.9980	2.65
H-LTL	303	4.79×10^{-6}	99818.1	0.9942	1.37
	313	5.87×10^{-6}	128083.1	0.9917	1.68
	323	1.12×10^{-5}	293726.8	0.9971	2.84

According to the data, the maximum adsorption monolayer capacity (q_m) and K_L of AF in H-LTL are higher than that in K-LTL. This result can be described from the interaction of lone pair electron of amino group (-NH₂) of AF with HO-Brønsted acid sites of H-LTL via a strong hydrogen bond interaction, while the interaction of AF in K-LTL is described by cation- π interaction (Ruan et al., 2004), which K⁺ ion in zeolite points toward the face of the electron-rich π system of the dyes.

In table 3.5, the thermodynamic parameters show the negative value of ΔG° and the positive values of ΔH° indicating that dye adsorption is spontaneous in nature and the adsorption process is endothermic, respectively. The ΔH° of K-LTL and H-LTL are 36.7 and 42.2 kJ/mol, respectively, which are classified as a physical

adsorption process. Moreover, the positive value of ΔS° indicates the increasing randomness at the solid/liquid interface during the adsorption process.

Table 3.5 Thermodynamic parameters for adsorption of AF on K-LTL and H-LTL.

Sample	temp (K)	ΔG°	ΔH°	ΔS°
		(kJ/mol)	(kJ/mol)	(J/molK)
K-LTL	303	-28.26	32.79	306.41
	313	-30.61		278.39
	323	-33.75		334.54
H-LTL	303	-29.01	26.01	323.21
	313	-30.62		321.44
	323	-32.09		298.55

3.4.2.3 Adsorption isotherm of Hemicyanine (Hemi)

The adsorption isotherms of Hemi dyes at 303, 313, and 323 K were determined and linear plots of Langmuir isotherms are shown in Appendix (Figure A3 and A4). The experimental data can be fitted well with the Langmuir model and the parameters for the adsorption of Hemi on K-LTL and H-LTL are shown in table 3.6

Table 3.6 Parameters for adsorption of Hemi on K-LTL and H-LTL.

Sample	temp (K)	Langmuir isotherm			
		q_m (M/g)	K_L (M ⁻¹)	R^2	% Φ_{max}
K-LTL	303	5.46×10^{-6}	93749.2	0.9914	0.54
	313	9.24×10^{-6}	116934.6	0.9933	0.72
	323	1.13×10^{-5}	147239.8	0.9900	1.01
H-LTL	303	4.09×10^{-6}	57994.5	0.9931	0.44
	313	8.06×10^{-6}	80626.9	0.9807	0.65
	323	9.63×10^{-6}	119687.6	0.9821	0.95

The results in Table 3.6 suggest that the Langmuir affinity constant of K-LTL is much higher than that of H-LTL which is attributed to the strong interaction of cation- π interaction and the maximum loading (% Φ_{max}) of Hemi dye is quite low in both K-LTL and H-LTL. This result can be described from a large molecule of Hemi that is hard to insert into channel of zeolite L.

Table 3.7 Thermodynamic parameters for adsorption of Hemi on K-LTL and H-LTL.

Sample	temp (K)	ΔG° (kJ/mol)	ΔH° (kJ/mol)	ΔS° (J/molK)
K-LTL	303	-27.65	29.37	234.45
	313	-29.42		243.22
	323	-31.43		231.32
H-LTL	303	-28.23	30.25	234.21
	313	-29.72		253.13
	323	-31.28		245.34

The thermodynamic parameters from table 3.7, shows the negative value of ΔG° and the positive values of ΔH° indicating that the dye adsorption is spontaneous in nature and adsorption process is endothermic, respectively. The ΔH° of K-LTL and H-LTL are 29.37 and 30.25 kJ/mol, respectively, classifying as a physical adsorption process of Hemi dyes onto zeolite L (K-LTL and H-LTL).

3.4.2.4 Adsorption isotherm of Thionine (Th)

The adsorption isotherm of Th dyes at 303, 313, and 323 K were determined and linear plots of Langmuir isotherms are shown in Appendix (Figure A5 and A6). The experimental data can be fitted well with the Langmuir model and the parameters for adsorption of Th on K-LTL and H-LTL are shown in table 3.8. The values of q_m and K_L of Th in K-LTL are higher than that in H-LTL. It can be described from the strong interactions between lone pair electrons of S and N atoms of Th with

K^+ of K-LTL and $-NH_2$ groups act as hydrogen-bond donor to the zeolite framework (Gigli et al., 2015).

Table 3.8 Parameters for adsorption of Th on K-LTL and H-LTL.

Sample	temp (K)	Langmuir isotherm			
		q_m (M/g)	K_L (M ⁻¹)	R^2	% Φ_{max}
K-LTL	303	1.03×10^{-6}	65996.33	0.9989	1.54
	313	5.04×10^{-6}	92784.72	0.9937	2.44
	323	1.28×10^{-5}	141692.9	0.9913	2.95
H-LTL	303	1.03×10^{-6}	59206.75	0.9919	1.42
	313	5.04×10^{-6}	119399.03	0.9845	2.56
	323	9.28×10^{-6}	196056.14	0.9598	2.68

The thermodynamic parameters from table 3.9, shows the negative value of ΔG° and the positive values of ΔH° indicating that the dye adsorption is spontaneous in nature and adsorption process is endothermic, respectively. The ΔH° of K-LTL and H-LTL are 31.06 and 28.25 kJ/mol, respectively, classifying as a physical adsorption process of Th dyes onto zeolite L.

Table 3.9 Thermodynamic parameters for adsorption of Th on K-LTL and H-LTL.

Sample	temp (K)	ΔG° (kJ/mol)	ΔH° (kJ/mol)	ΔS° (J/molK)
K-LTL	303	-27.98		241.23
	313	-29.79	31.06	261.43
	323	-31.88		244.66
H-LTL	303	-27.10		268.74
	313	-29.78	28.25	265.89
	323	-32.03		298.66

3.5 Conclusions

The zeolite L with different morphologies are successfully prepared by hydrothermal synthesis with different ratios of K_2O and H_2O gel composition. The round shape was used for adsorption isotherm study with cationic dyes such as AC, AF, Hemi and Th. The Langmuir constant for the interaction of the dyes and zeolite L is in the order of Th>AF> Hemi> AC. The maximum loading ($\%Q_{max}$) of Hemi is very low (1.01%) compared to the other dyes such as 2.57%(AC), 2.65%(AF) and 2.95%(Th) in K-LTL at 323 K resulting from the steric hindrances of the Hemi dyes molecule. All of cationic dyes show the thermodynamic parameter with negative value of ΔG° (28-32 kJ/mol) and the positive values of ΔH° (21 - 32 kJ/mol) that refer to the higher adsorption capacity observed and the adsorption process is endothermic, respectively. Based on the magnitude of ΔH° (20.45 - 44.62 kJ/mol), the adsorption of these dyes onto zeolite L (H-LTL and K-LTL) is classified as a physical adsorption process.

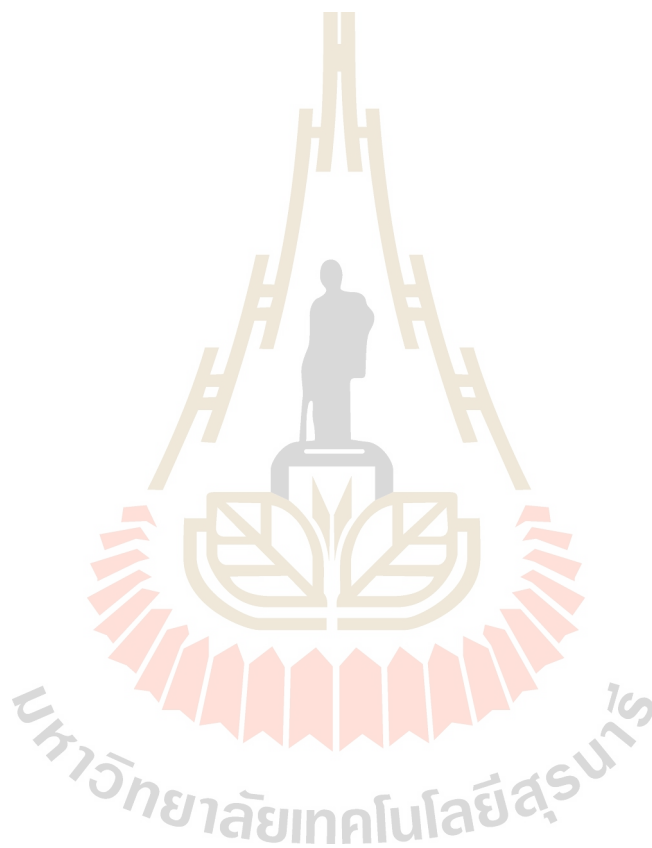
Moreover, all of dyes have the positive value of ΔS° indicating an increase in randomness at the solid/liquid interface during the adsorption process.

3.6 References

- Ban, T., Saito, H., Naito, M., Ohya, Y., and Takahashi, Y. (2007). Synthesis of zeolite L crystals with different shapes. **Journal of Porous Materials**. 14: 119-126.
- Calzaferri, G. (2012). Nanochannels: hosts for the supramolecular organization of molecules and complexes. **Langmuir**. 28: 6216-6231.
- Calzaferri, G., Huber, S., Maas, H., and Minkowski, C. (2003). Host-guest antenna materials. **Angewandte Chemie International edition in English**. 42: 3732-3758.
- Devaux, A., and Calzaferri, G. (2009). Manipulation of Energy Transfer Processes in Nanochannels International Journal of Photoenergy (Vol. 2009).
- Easwaramoorthi, S., and Natarajan, P. (2008). Spectral and electrochemical studies of methylene blue and thionine encapsulated in zeolite-Y. **Journal of Porous Materials**. 15: 343-349.
- Fois, E., Tabacchi, G., Devaux, A., Belser, P., Bruhwiler, D., and Calzaferri, G. (2013). Host-guest interactions and orientation of dyes in the one-dimensional channels of zeolite L. **Langmuir**. 29: 9188-9198.
- Gigli, L., Arletti, R., Vitillo, J.G., Alberto, G., Martra, G., Devaux, A., and Vezzalini, G. (2015). Thionine Dye Confined in Zeolite L: Synthesis Location and Optical Properties. **The Journal of Physical Chemistry C**. 119: 16156-16165.

- Hameed, B.H., Ahmad, A.A., and Aziz, N. (2007). Isotherms, kinetics and thermodynamics of acid dye adsorption on activated palm ash. **Chemical Engineering Journal**. 133: 195-203.
- Hennessy, B., Megelski, S., Marcolli, C., Shklover, V., Bärlocher, C., and Calzaferri, G. (1999). Characterization of Methyl Viologen in the Channels of Zeolite L. **The Journal of Physical Chemistry B**. 103: 3340-3351.
- Ihle, G., Schüth, F., Krauß, O., Vietze, U., and Laeri, F. (1998). Alignment of a Laser Dye in the Channels of the AlPO₄-5 Molecular Sieve (Vol. 10).
- Insuwan, W., and Rangriwatananon, K. (2012). Morphology-Controlled Synthesis of Zeolite and Physicochemical Properties. **Engineering Journal**. 16: 1-12.
- Insuwan, W., and Rangriwatananon, K. (2014). Evaluation of adsorption of cationic dyes on H-LTL and K-LTL zeolite (Vol. 21).
- Insuwan W., and Kunwadee, R. (2012). Morphology-Controlled Synthesis of Zeolite and Physicochemical Properties. **Engineering Journal**. 16: 1-12.
- Meeprasert, J., Jungsuttiwong, S., and Namuangruk, S. (2013). Location and acidity of Brønsted acid sites in isomorphously substituted LTL zeolite: A periodic density functional study. **Microporous and Mesoporous Materials**. 175: 99-106.
- Ruan, C., and Rodgers, M.T. (2004). Cation- π Interactions: Structures and Energetics of Complexation of Na⁺ and K⁺ with the Aromatic Amino Acids, Phenylalanine, Tyrosine, and Tryptophan. **Journal of the American Chemical Society**. 126: 14600-14610.
- Sawasdee, S., and Watcharabundit, P. (2015). Equilibrium, Kinetics and Thermodynamic of Dye Adsorption by Low — Cost Adsorbents (Vol. 6).

- Treacy, M.M.J., and Higgins, J.B. (2007). LTL - Linde Type L. In M. M. J. Treacy & J. B. Higgins (Eds.), Collection of Simulated XRD Powder Patterns for Zeolites (Fifth Edition) (pp. 256-257). Amsterdam: Elsevier Science B.V.
- Wang, Y., Li, H., Feng, Y., Zhang, H., Calzaferri, G., and Ren, T. (2010). Orienting Zeolite L Microcrystals with a Functional Linker. **Angewandte Chemie International Edition**. 49: 1434-1438.



CHAPTER IV

INSERTION OF SINGLE CATIONIC AND NEUTRAL DYE ON H-LTL AND K-LTL ZEOLITE

4.1 Abstract

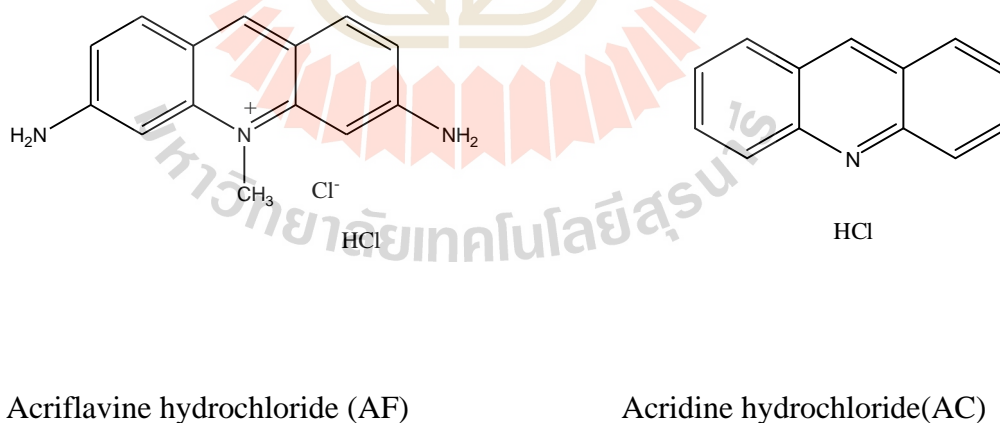
The inclusion of organic dye onto zeolite L was prepared using cation exchange and gas phase method (thermal diffusion). According to the limitation for inclusion of dye via cation exchange, gas phase methods are used for improvement. Cationic dyes such as acridine hydrochloride (AC), acriflavine hydrochloride (AF), hemicyanine iodide (Hemi) and thionine acetate (Th) and a neutral dye of thioindigo (Thio) are encapsulated onto K-LTL and H-LTL zeolite by gas phase method in which the amount of dye with different occupation probabilities (ρ) of 0.1, 0.25, 0.5 and 1.0 were used. It was found that the occupation probability at 0.25 is suitable for the preparation of the dye_zeolite as its prevent the dye aggregation in the zeolite and the quenching emission of the dye. The gas method produces the dye_K-LTL zeolite with high fluorescence properties while a partial dye in H-LTL zeolite (dye_H-LTL) was degraded in reducing the luminescence. Additionally, this study shows that the way to prepare dyes confined in zeolite L plays a very important role on the enhancement of fluorescence and development of optical materials.

4.2 Introduction

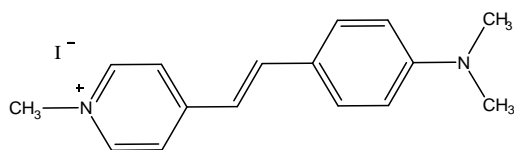
The host-guest materials such as dye-LTL gain increasing attention during the years. The pore structure of LTL consists of one-dimensional channels running across the whole crystal axis. The performance of zeolite LTL in the applications relies upon their physical properties such as crystal size and morphology. For example, disc-like LTL crystals can be used in photonic devices to produce higher trapping efficiency. Disk-like shapes can also facilitate c-oriented layering for the preparation of thin-film technologies (Veiga-Gutierrez et al., 2012). In contrast, cylinder shapes is easy for studying the dye incorporate on the channel of LTL with a confocal microscope. Excited state processes of dyes in host materials adjust novel applications in various systems. It can be used as an artificial antenna and potential use of these compounds as microlaser are well reported (Calzaferri et al., 2003). The cationic dyes such as hemicyanine have been widely used to obtain live cell images in fluorescence and second harmonic generation (SHG) microscopies due to two distinctive properties (Yamaguchi et al., 2006) Recently, it has been reported with hemicyanine dyes in MOF and zeolite L for enhancing fluorescence properties (Kim et al., 2017; Yu et al., 2013). Moreover, thionine dyes attracted considerable attention over the years due to their appropriate biological, chemical, photochemical, and photophysical properties such used as photosensitisers and redox mediators in electrocatalytic systems (Easwaramoorthi et al., 2007; Gigli et al., 2015). The small enough acridine hydrochloride (Ac) and acriflavine hydrochloride (AF) molecule have been widely applied for organic light-emitting diode (OLED) materials, photovoltaic cell (PVC), pH sensor and fluorescent probe and recently, there are reported for FRET application (Insuwan et al., 2015; Kaewsuya et al., 2008; Kazim et al., 2007; Li et al., 2008).

Neutral dyes like thioindigo are known as vat dyestuffs and have been used for coloring textiles since ancient times. (Alvarado et al., 2012; Uno et al., 2004)

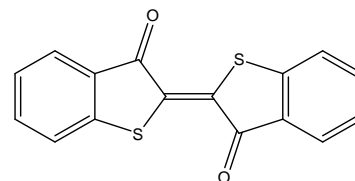
This chapter concentrates on the synthesis of dye-loaded zeolite L that can be used for antenna system that emits cover 400 - 700 nm (blue – red region) in which the emission is from acridine (AC), acriflavine (AF), hemicyanine (Hemi), thionine (Th) and thioindigo (Thio) and the structure formula of these dyes are shown in scheme 4.1. The methods for incorporating dye molecule such the cation exchange and gas phase method were used for cationic and neutral dye, respectively. In addition, the gas phase method was also used for cationic dyes besides neutral dye in order to increase the amount of cationic dye in the zeolite L. The samples were investigated the photophysical properties and the behavior of electronic excitation energy of these cationic and neutral guest species intercalated in the zeolite L.



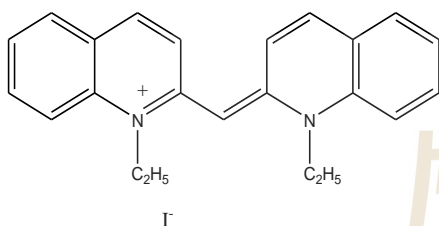
Scheme 4.1 Structure formula of cationic and neutral dye.



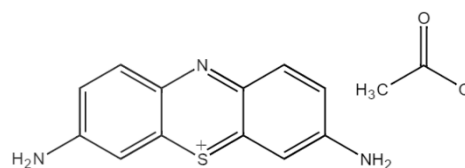
trans-4-[4-(Dimethylamino)styryl]
-1-methylpyridinium (Hemi)



Thioindigo (Thio)



1,1'-Diethyl-2,2'-cyanine iodide (Cy)



3,7-Diamino-5-phenothiazinium
acetate (Th)

Scheme 4.1 Structure formula of cationic and neutral dye (Continued).

4.3 Materials and method

4.3.1 Synthesis of zeolite LTL

Materials and Chemicals

The silica sources is colloidal silica sol (Ludox HS-40 from Dupont, 40% SiO₂), while alumina source is aluminium hydroxide (CARLO ERBA, 98%). Potassium hydroxide (CARLO ERBA, 85%) was used for alkali metal cations.

Synthesis

Zeolite L crystals were synthesized by a method from the literature (Ban et al., 2007; Insuwan et al., 2012), 0.59 g of aluminium hydroxide was dissolved in boiling potassium hydroxide solution (1.28 g of potassium hydroxide was added to 2.51 g of double distilled water until a clear solution). This solution was added to 5.52 g of Ludox HS-40 with 4.82 g of double distilled water in a mixer. The clear solution mixture was stirred for 3 minutes to obtain a gel with viscosity and turbidity. The starting gel was then transferred into a Teflon-lined autoclave for crystallization at 180 °C for 2 days without stirring. After crystallization, the Teflon-lined autoclave was cooled in cold water before opening. The product was washed with distilled water until the pH of liquid was close to 7. Finally, the crystalline solid was dried for overnight at 80 °C in hot air oven. All materials used in this study were of reagent grade.

NH₄LTL was prepared by ion-exchanging the K-LTL with 0.5M NH₄Cl solution. Ion exchange was carried out at 50 °C for 12 hours. After that the zeolite samples were washed with distilled water and dried at 100 °C for 12 hours. NH₄LTL was calcined at 450 °C for 4 hours to decompose NH₄⁺ ions to NH₃, then NH₄LTL was transformed to H-LTL.

Characterization

The products were analyzed by XRD using a Bruker D2 PHASER radiations scanning from 3-45° at a rate of 0.05 °/s with current 30 kV and 10 mA. The chemical compositions were analyzed by energy dispersive X-ray fluorescence (EDXRF, Horiba XGT-5200 X-ray Analytical Microscope) with Rh X-ray tube with a 50 kV and 1 mA. For the examination of LTL morphology, scanning electron microscope (SEM, JEOL JSM-6010LV) at an acceleration voltage of 10-20 kV were

used. Acidity strength was determined by ammonium temperature programmed desorption (NH₃-TPD) with a Bel Japan Model BelcatB. The NH₃-TPD spectra were measured using a conventional flow-through reactor connected to a thermal conductivity detector (TCD). The TCD responses were calibrated by a dose containing known amounts of ammonia.

4.3.2 Dyes-loaded on zeolite LTL

Cation exchange method

Incorporation of cationic dyes such as AC, AF and hemi onto K-LTL, and H-LTL zeolite were performed at 30 °C using 0.5 g of accurately weighed dehydrated zeolite LTL in a 125 mL conical flask. Then 50 mL of the dye solution with concentration of 0.1 mM was added to a flask. The flask was sealed and transferred to a shaker bath for 24 hours to equilibrate the system. The dyes loaded zeolite LTL were collected by separation of solid from solution by centrifugation and dried at 100 °C overnight. To remove the dyes molecules on the zeolite surface, the following washing procedure was used. The suspension was transferred into a 125 mL conical flask with 50 mL n-butanol, sonicated for 10 minutes then stirred at room temperature for 24 hours. The n-butanol washing was repeated until the supernatant did not show dyes luminescence.

Gas phase procedure

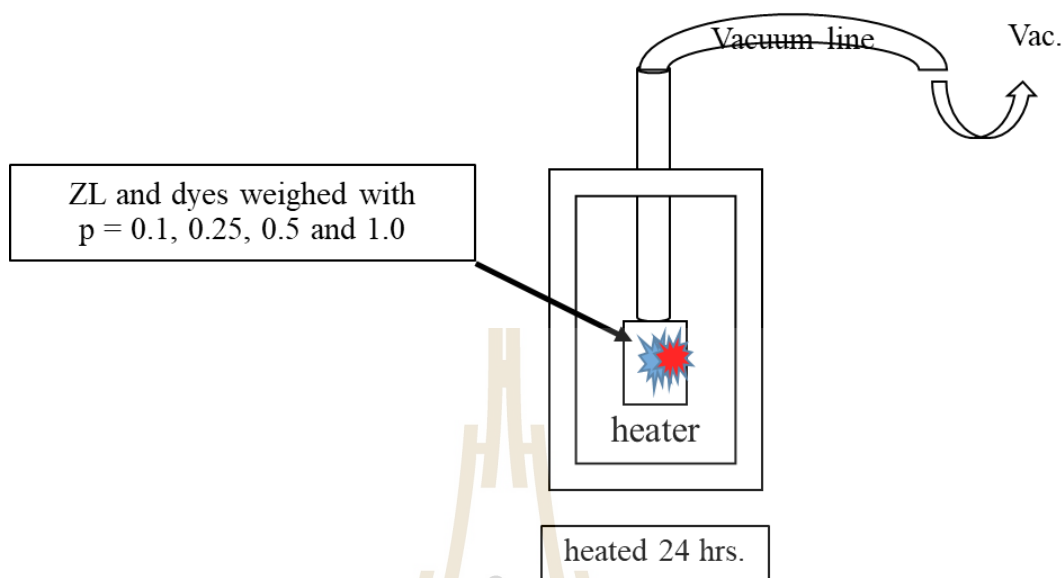
In the experiment, 100 mg of zeolite L was mixed with neutral dye or cationic dye with various occupation probability ($\rho = 0.1, 0.25, 0.5$ and 1.0). Then 1.0 ml. of solvent (chloroform, toluene and water for Thio, hemi, AC and AF, respectively) was added to the mixture. The mixture was sonicated for 10 min to dissolve the dye and ensure a good dispersion of the zeolite. The solvent was removed by vacuum oven at $50\text{ }^{\circ}\text{C}$ for 2 hrs, thus leading to a homogeneous coating of the zeolite surface with dyes. Then the coated zeolite was transferred into an agate mortar, ground into a fine powder. The powder was filled into a holder and dried in a vacuum line for 2.0 hours at a pressure of 1×10^{-2} mbar. The gas phase insertion process took place over 24 hours at an appropriate melting point temperature of each dye (Scheme 2). The colored powder was washed with appropriate solvent until the supernatant washing was colorless. The loading, or occupation probability (ρ) of the loaded dye on zeolite LTL is defined as follows (Hennessy et al., 1999);

$$\rho = \frac{\text{number of occupied sites}}{\text{total amount of sites}} \quad (4.1)$$

From (Eq. 4.1), one gets the following expression to calculate the loading or occupation probability (Calzaferri and Devaux, 2010);

$$\rho = \frac{m_D}{M_D} \left(\frac{M_Z n_s}{m_Z} \right) \quad (4.2)$$

where M_D is the molar mass of dye molecule; M_Z is the molar mass of zeolite LTL per one unit cell (2883 g/mol); m_D and m_Z are weight of dye and zeolite LTL in grams, respectively; n_s represents the number of unit cells occupied by one dye that determined by the length of the dye molecule.



Scheme 4.2 The apparatus of the gas phase method.

Determination of Loading Level by HF Analysis

The effective loading levels were determined by first suspending 10 mg of the loaded material in 3 mL ethanol in a polystyrene cuvette. Then 300 μL of a 4% aqueous HF solution was added to dissolve the zeolite. The process was completed after 20 min, leaving a transparent solution. The loading degree was then calculated from the dye concentration obtained from the UV-vis absorption spectrum

Physical Measurements

UV/vis spectra were recorded on a UV-2550 UV/vis Spectrophotometer. Dye molecules were dissolved in various solvents and quartz cuvette was used in the measurement. Diffuse reflectance spectra of dyes loaded on zeolite LTL was recorded using a Carry UV-2550 UV-Visible spectrometer with the condition of slit width (5

nm), sampling interval (0.1 nm) and wavelength range of 200-800 nm. Fluorescence spectra were recorded on a luminescence spectrometer LS 50B (Perkin-Elmer). Dye molecules were measured either in various solvents in quartz cuvette, or incorporated in zeolite LTL by suspending dyes/zeolite LTL in chloroform (~1 mg in 100 mL).

4.4 Results and discussion

4.4.1 Synthesis of LTL zeolite

The product in the zeolite L synthesis through SEM is shown in Figure 4.1. The SEM image shows the morphology of K-LTL (1a) and H-LTL (1b) with round shape and with the crystal size around $1 \times 2 \mu\text{m}$. The round shape of zeolite L are used further in the study in this chapter.

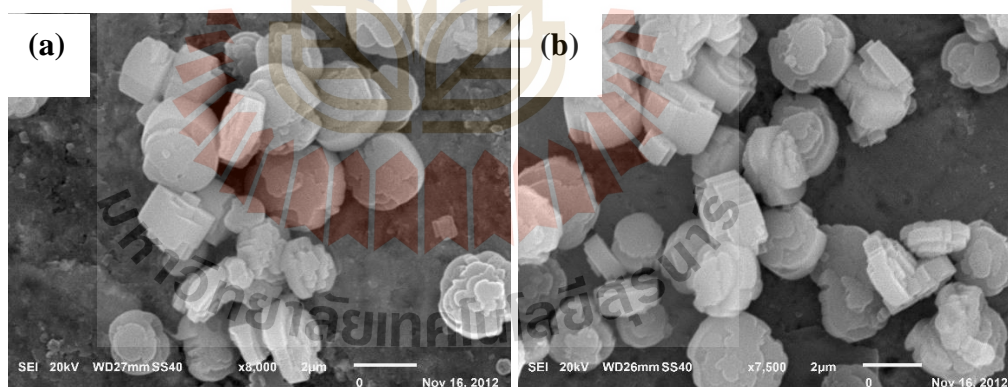


Figure 4.1 The morphology of zeolite a) K-LTL zeolite and b). H-LTL zeolite.

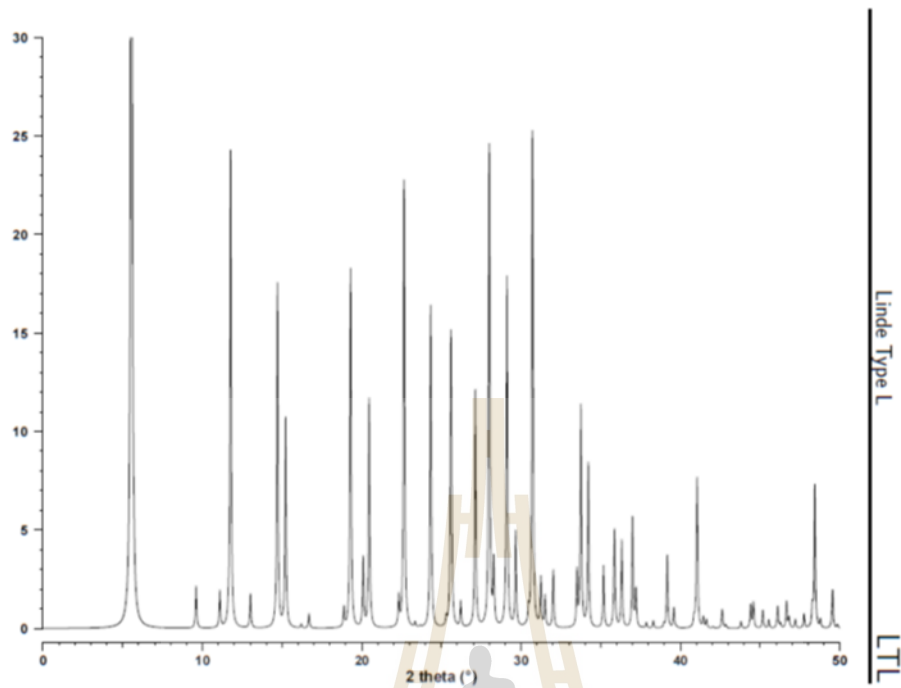


Figure 4.2 The simulated XRD powder pattern of LTL (Treacy et al., 2007).

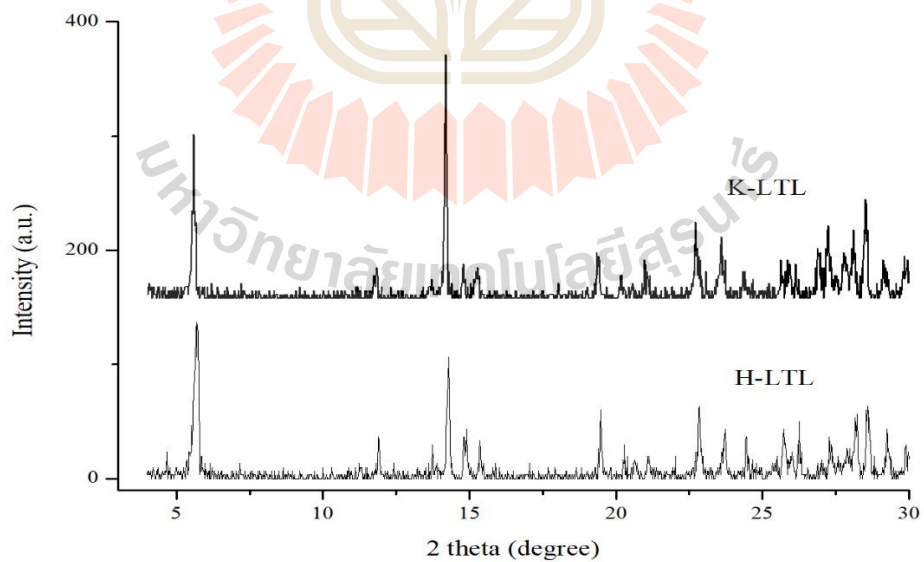


Figure 4.3 XRD patterns of K-LTL and H-LTL zeolite with round shape.

Figure 4.3 shows XRD patterns of the synthesized zeolite L with round shape in K form and H form (protonated form), all of the samples show the same 2 theta (2θ) that the main peaks located at $2\theta = 5.5, 19.4, 22.7, 28.0,$ and 29.1 degree indicating the XRD patterns corresponding to zeolite L (Figure 4.2). The crystallinity of H-LTL is decreased compared to K-LTL due to the process in changing K-LTL form to H-LTL form with high temperature causing to the structure collapse. However, from the SEM image, the crystal shapes are still the same with K-LTL.

4.4.2 Dye insertion onto zeolite L

4.4.2.1 Acridine hydrochloride (AC) on to zeolite (AC_LTL)

1) Acridine in solution

The absorption spectra of acridine hydrochloride (AC) in water and acidic solution is revealed in Figure 4.4. Acridine molecule exist as protonated form when it was dissolved in water and acidic solution (0.1 M HCl) that shows the absorption peak at 355 nm suggesting that the band was a π - π^* character (V.K. Sharma et al., 2003) and shows a broad band around 400-450 nm. Furthermore, the absorption maxima of Ac in neutral, hydrogen-bonded and protonated species appeared at 355 nm (Ryder et al., 2003), only the spectrum of protonated species (AcH^+) has a broad shoulder within 370-430 nm range. The protonated form of AC (AcH^+) appeared in both water and 0.01M HCl solution but AcH^+ in 0.01M HCl shows a broad shoulder with higher intensity than that in water referring to AC favorite to represent in protonate form. (Wilaiporn Insuwan et al., 2014; Ryder et al., 2003)

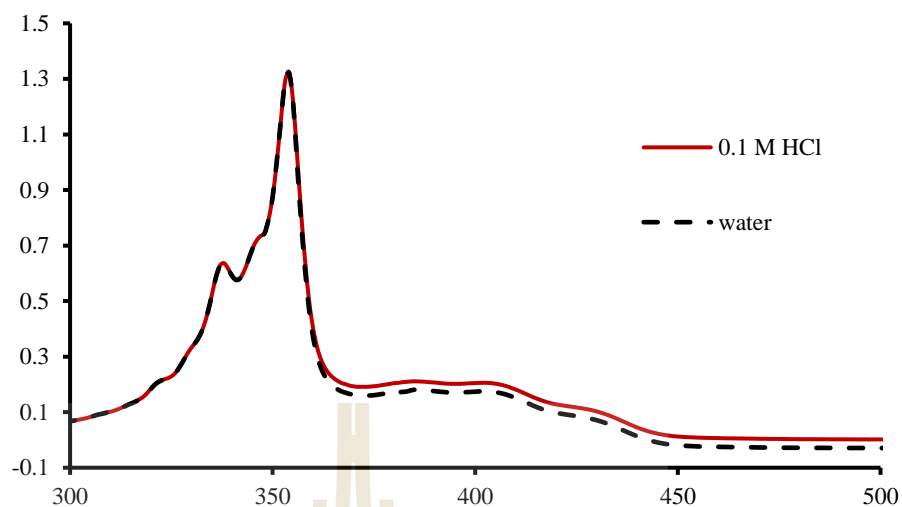


Figure 4.4 The absorption spectra of AC in water and 0.1 HCl solution.

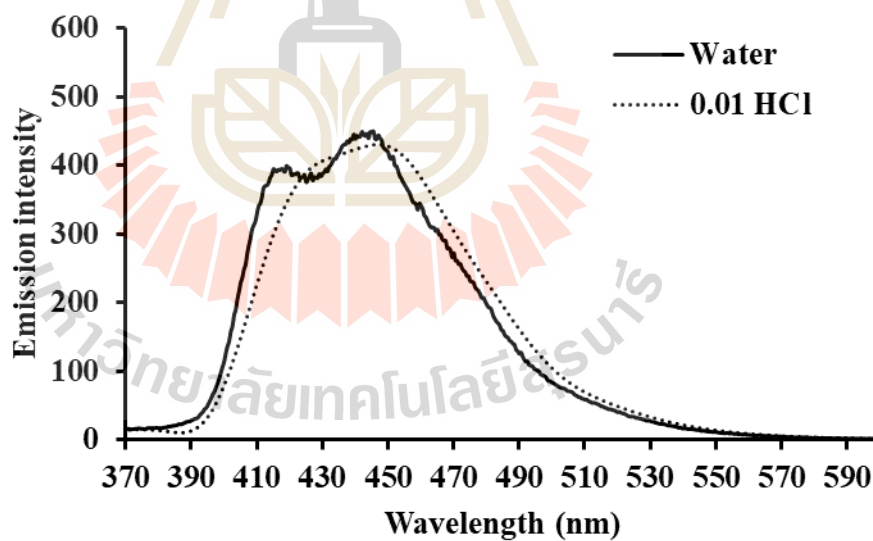


Figure 4.5 The emission spectrum of AC in water and 0.01 HCl solution, excited at 355 nm.

The steady state fluorescence emission spectra taken using 355 nm excitation shows that the AC in water has a fluorescence maximum at 447 nm and

hypsochromic shoulder at 410 nm which is characteristic of AC in neutral form. While a protonated form (ACH^+) in 0.01 M HCl solution are slightly red shift at 455 nm (Figure 4.5).

2) Insertion by cation exchange method.

The diffuse reflectance spectra of Ac adsorbed on K-LTL and H-LTL zeolite were shown in Figure 4.6. Due to the limit of our instrument, we cannot observe the main absorption spectra thus it was considered only the broad band at 400-450 nm. The spectra show a characteristic of protonated form of acridine in both forms of zeolite, but the intensity of this band belonging to protonated acridine in H-LTL is higher than K-LTL.

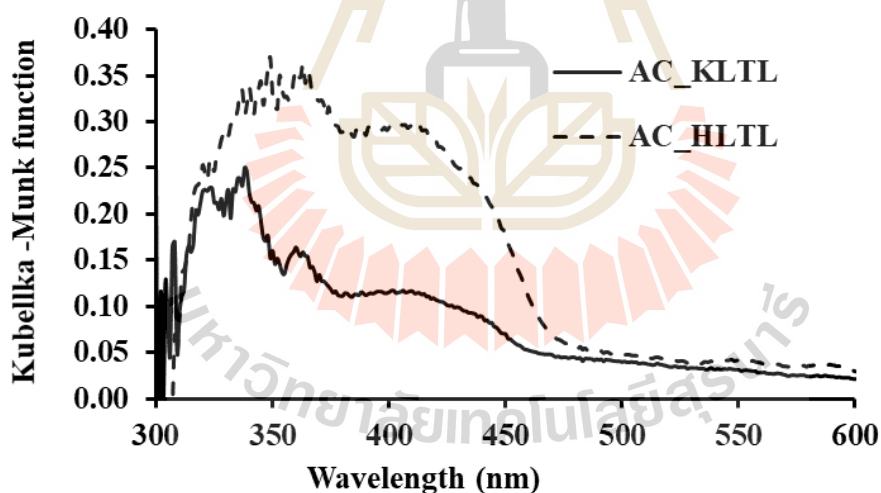


Figure 4.6 Diffuse reflectance spectra of Ac in K-LTL and H-LTL.

Figure 4.7 illustrates emission spectra of Ac incorporated in K-LTL and H-LTL zeolite; the emission maximum of K-LTL appeared at 465 nm with a shoulder at 446 nm. While AC undergoes an excited state of proton transfer reaction on H-LTL, appeared with broad band and the emission maximum spectra appeared at 486

nm. This can be described from the nitrogen atom being more negative in the excited state that facilitates for adding proton due to the pKa of the excited state of Ac being 9.2 which is much larger than its ground state (pKa 5.4) (Bowen, Holder, and Woodger, 1962). Therefore, the protonated form is produced through a proton abstraction reaction by excited Ac that is possible on H-LTL. The difference between the maximum emission of protonated species in H-LTL and neutral species in K-LTL is about 21 nm. As a result, H-LTL form can be considered as an acidic surface. From the above mention Ac can be used as a fluorescent probe for an estimation the pH of surface as well.

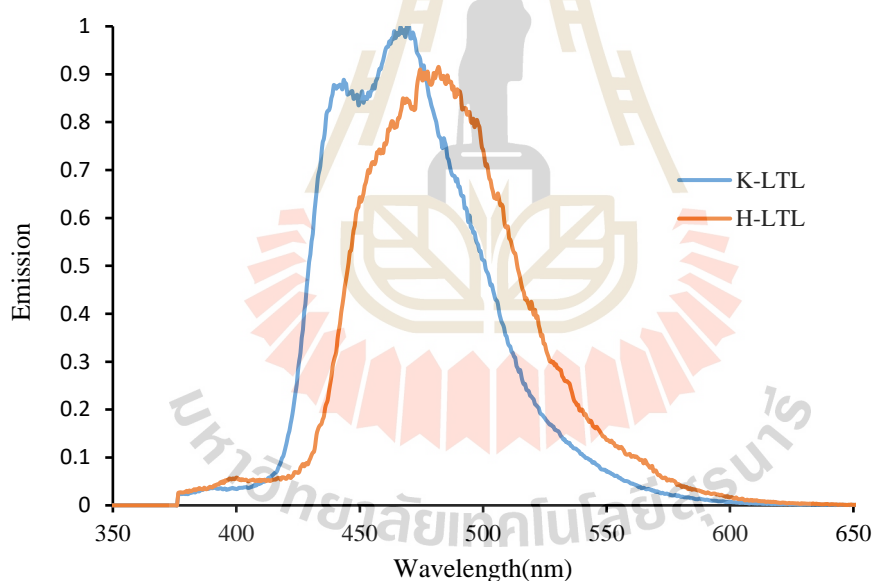


Figure 4.7 Emission spectra of Ac on K-LTL and H-LTL zeolite with an excitation at 355 nm.

3) Insertion AC by the gas phase method

Because only a slight amount of cationic dye of Ac inserted in the channel of K-LTL and H-LTL by the cation exchange process, so a gas phase method was used for insertion of cationic dye besides neutral dye. Similarly, a neutral dye AC, was prepared with the occupation probability of 0.10, 0.25, 0.50 and 1.00, and heated at 120 °C (melting point of AC) under vacuum condition. The sample was prepared successfully and characterized the luminescence properties.

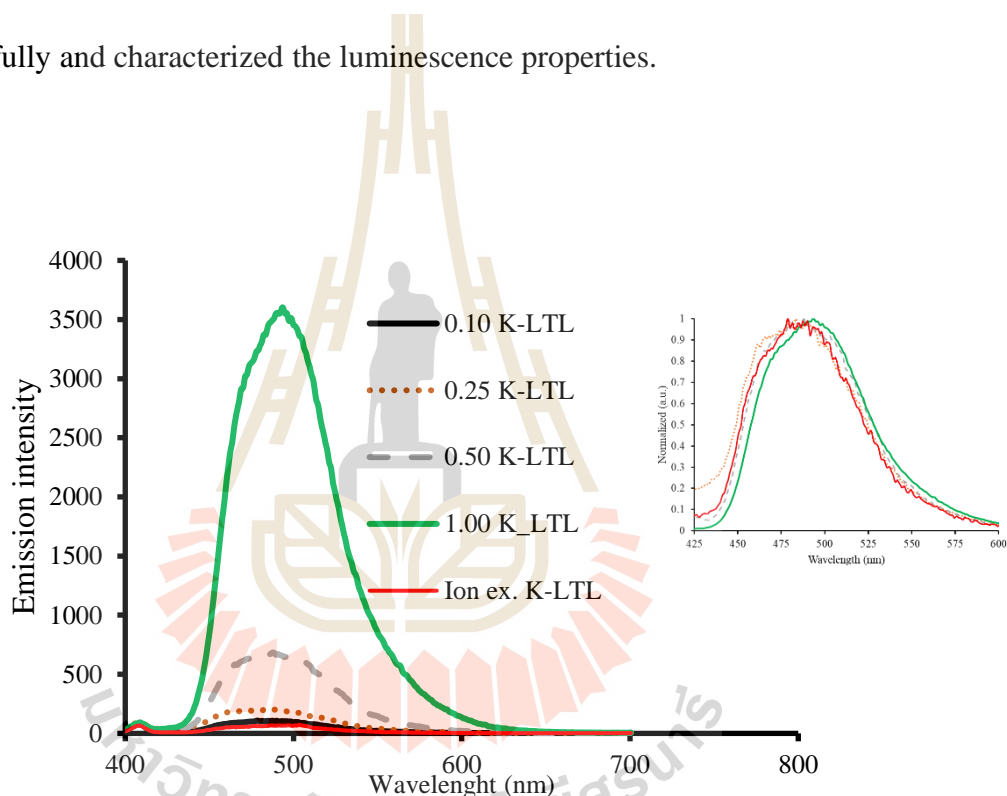


Figure 4.8 Emission spectra of AC with different loadings onto K-LTL zeolite by gas phase method, excited at 355 nm.

The samples of AC_K-LTL zeolite with the different occupation probability ($p = 0.10, 0.25, 0.50$ and 1.0) are prepared by the gas phase method. The emission spectra show the $\lambda_{\text{max}} = 470 - 500$ nm when excited at 355 nm. A superimpose picture of Figure 4.8 shows the normalized emission position of all samples and the

emission positions shift slightly to longer wavelength (red shift) from 475 to 500 nm with an increase in the occupation probability. That refers the dye aggregation in the channel of zeolite L. Whereas the emission intensity of AC_K-LTL, prepared by ion exchange and the gas phase method increases with increasing occupation probability. It suggests that an increase in the amount of dye onto zeolite L affects the fluorescence intensity of dye_zeolite system.

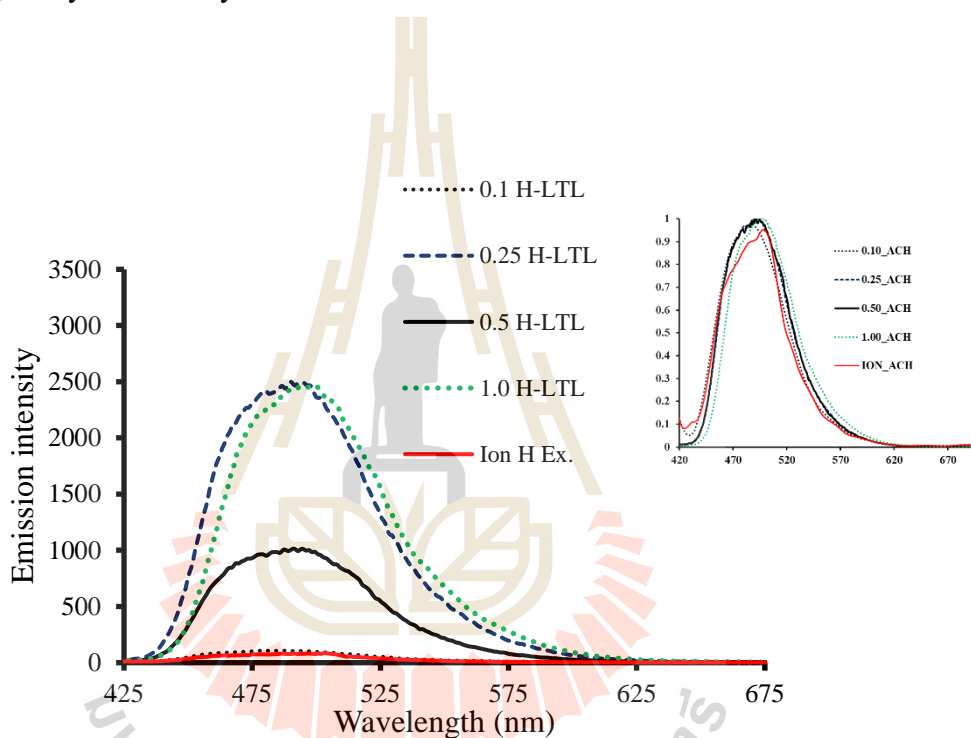


Figure 4.9 Emission spectra of AC with different loadings onto H-LTL zeolite by gas phase method, excited at 355 nm.

The systems of AC_H-LTL is similarly to AC_K-LTL that the emission intensity increases with an increase in the occupation probability. The emission position of the AC_H-LTL occurs around 475 – 520 nm with longer wavelength than that of AC_K-LTL (450 – 500 nm) due to the protonated properties of LTL and AC structure. Likewise, the emission position shifts slightly to red shift with

an increase in the occupation probability (a superimpose picture of Figure 4.9). The Figure 4.9 shows a comparison of the emission intensity of AC_H-LTL that was prepared by cation exchange and gas phase method with different occupation probabilities ($p=0.10, 0.25, 0.50$ and 1.00). The result shows the increase in the emission intensity corresponding to an increase in an amount of AC. Table 4.1 shows the amount of dye with the cation exchange and the gas phase method. The amounts of dye prepared by the gas phase method for AC_K and H-LTL are rising with increasing occupation probability. While, the limitation for loading of AC_K and H-LTL arises with the cation exchange method.

Table 4.1 The amount of dyes in the K and H-LTL after loading with gas phase and cation exchange method.

p	K-LTL		H-LTL	
	Dye offer (mol g ⁻¹)	Dye uptake (mol g ⁻¹)	Dye offer (mol g ⁻¹)	Dye uptake (mol g ⁻¹)
0.10	1.73×10^{-5}	8.15×10^{-6}	1.73×10^{-5}	9.97×10^{-6}
0.25	8.76×10^{-5}	1.87×10^{-5}	4.33×10^{-5}	2.05×10^{-5}
0.50	4.33×10^{-5}	2.85×10^{-5}	8.76×10^{-5}	3.88×10^{-5}
1.00	1.73×10^{-4}	1.51×10^{-4}	1.73×10^{-4}	1.59×10^{-5}
Ion Ex.	1.00×10^{-4}	1.8×10^{-7}	1.00×10^{-4}	1.60×10^{-7}

4.4.2.2 Acriflavine hydrochloride (AF) on to zeolite (AF_LTL)

1) AF in solution

The absorption spectra of AF in water and ethanol with different solvent polarities (1.00 and 0.66, respectively) are shown in Figure 4.10. The characteristic absorption band stabilizes the ground state of π - π^* transition and amino group in the mero-phenyl ring is protonated to give high fluorescent. This behavior is similar to that reported earlier (Kumar et al., 2012).

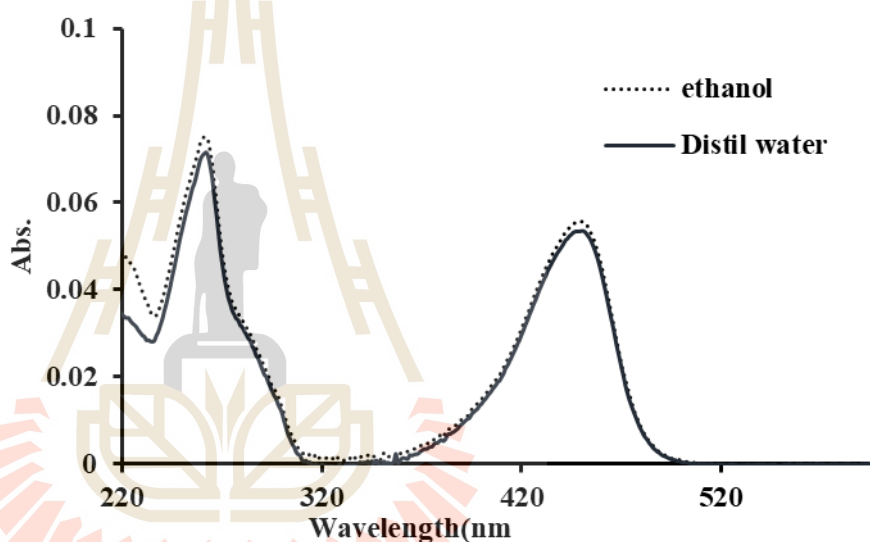


Figure 4.10 The absorption spectra of AF in solution.

Figure 4.10 shows the effect of the solvent polarity on the fluorescence spectra. The fluorescence intensity decreases with an increase in polarity because the molecule absorbed the light and transitioned to the excited electronic state causing change in molecular electronic configuration and hence solute-solvent molecule interacts (dipole-dipole) (Kitai, 2008). It suggests that it is a locally excited intra molecular charge transfer (ICT) state. Amino group in the mero-phenyl ring is protonated to give high fluorescent and as a result, twisted ICT (TICT) states are not

formed in the case of AF dye or interacting between solute with molecule solvent as dipole-dipole interacts. (Petit et al., 1993; V.K. Sharma et al., 2003)

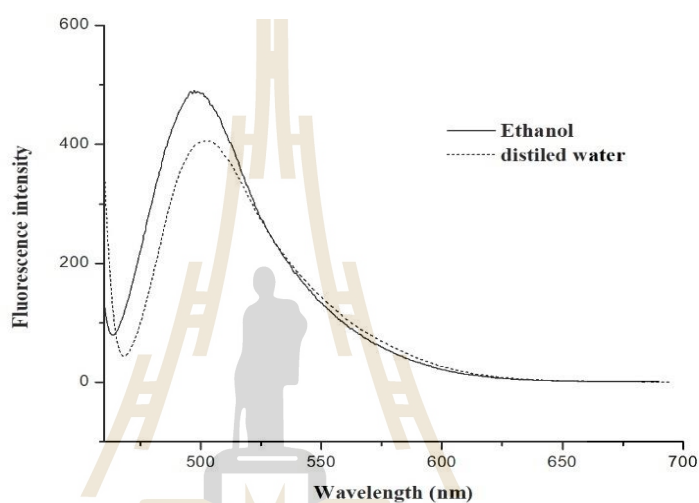


Figure 4.11 The emission spectrum of AF in water and 0.01 M HCl solution, excited at 460 nm.

One can observe that, a little shift of fluorescence spectrum from λ_{\max} at 500 nm (in ethanol) to 515 nm (in water) (Figure 4.11). It indicates that the fluorescence spectrum shifts to a long wavelength (red shift) and decreases in the intensity with an increase in polarity of the solvent. This shift value is dependent on the dielectric constant (ϵ) value of solvent and the difference between dipole moment values of solvent. (N. Sharma et al., 2007).

2) Insertion AF by cation exchange method.

The absorption bands of AF_K-LTL and H-LTL zeolite are shown in Figures 4.12. AF exchange K-LTL samples exhibit the characteristic absorption band at 465 nm and emission band at 500 nm, that shifted to longer wavelength compared to AF in water (448 to 465 nm) and shorter wavelength (515 to 500 nm), respectively (Figures 4.12 and 4.13). This behavior is due to the channels of K-LTL less polar than that in the aqueous environment (W. Insuwan et al., 2014)

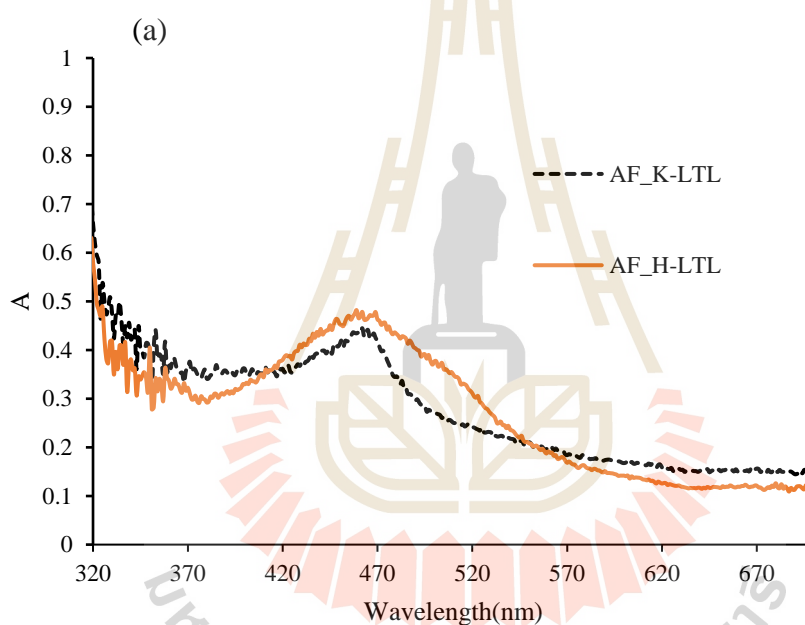


Figure 4.12 (a) The diffuse reflectance and (b) emission spectra of AF on K-and H-LTL zeolite.

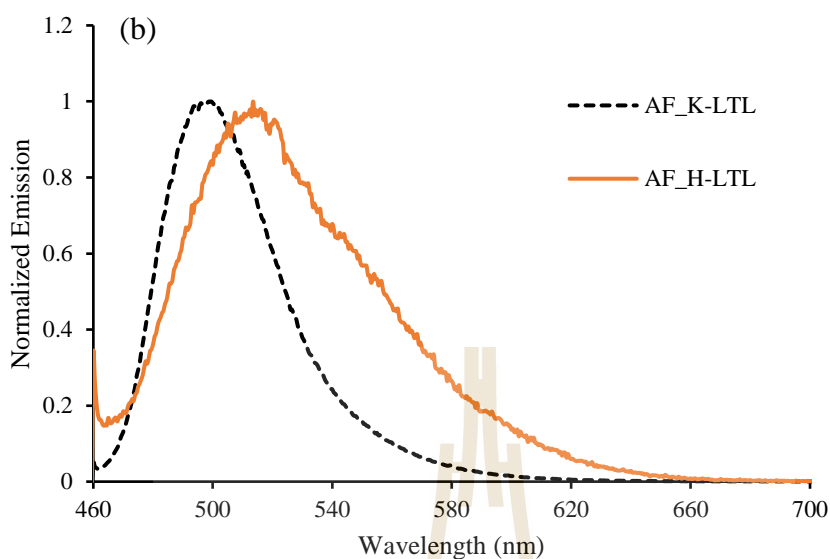


Figure 4.12 (a) The diffuse reflectance and (b) emission spectra of AF on K- and H-LTL zeolite (Continued).

Considering AF confined on H-LTL, the absorption bands appeared at 473 nm (see 4.12(a)) and the emission band at around 520 nm with slightly red shift on shoulder (see Figure 4.12(b)) indicating that AF in H-LTL exhibits as protonated forms ($\text{AFH}^+/\text{AFH}_2^{2+}$). That refers to AF existing as cationic and protonated species depending upon the pH of the aqueous medium.

3) AF insertion by the gas method.

For acriflavine hydrochloride (AF) inserted on both K-LTL and H-LTL by the gas phase method at 130 °C, their diffuse reflectance spectra shown in Fig 4.13 are similar to those by cation exchange method with absorption band at 470 and 473 nm in K and H-LTL, respectively (see Figure 4.13). While, AF on H-LTL (Figure 12(b)) shows a shoulder broad band around 510 nm that refers to protonated form of AF produced in channel of zeolite L.

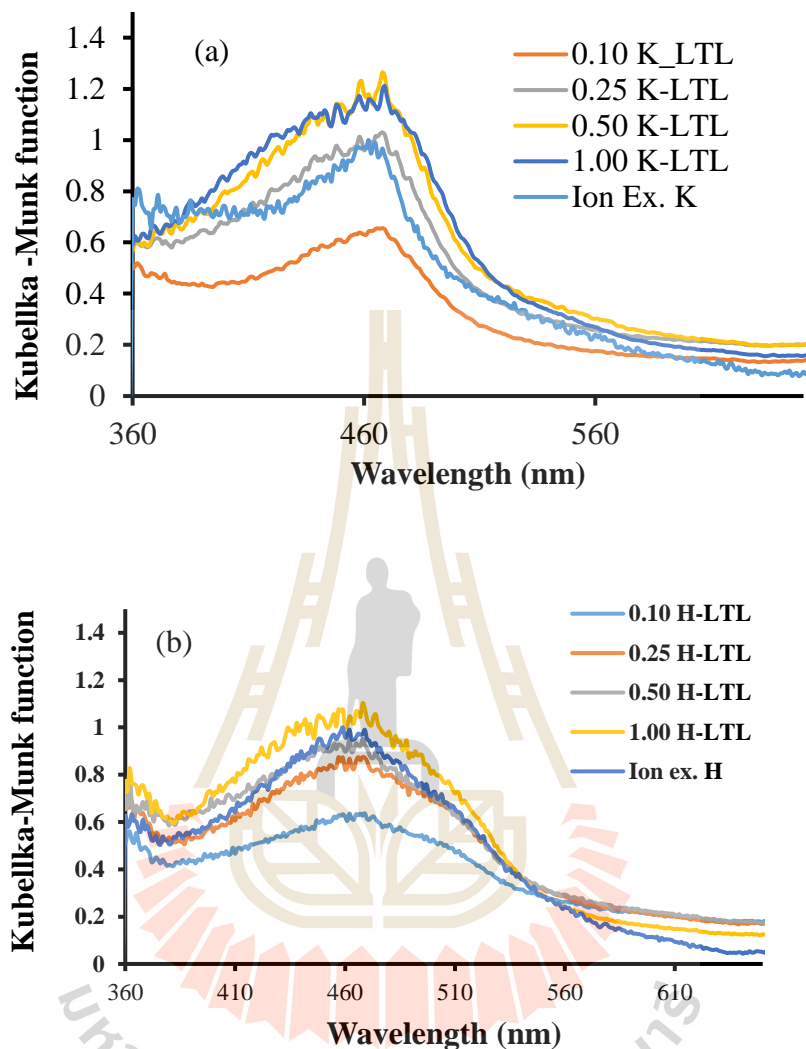


Figure 4.13 Diffuse reflectance spectra of AF in (a) K-LTL and (b) H-LTL zeolite with different occupation probabilities.

The emission spectra of AF on K-LTL (Figure 4.14) show the emission band at λ_{\max} around 520 -530 nm and excited at 470 nm (corresponding with the absorption energy). A slight skewing and red shift of the peak with an increase in the occupation probability cause from self-adsorption effect and aggregation of the AF dye.

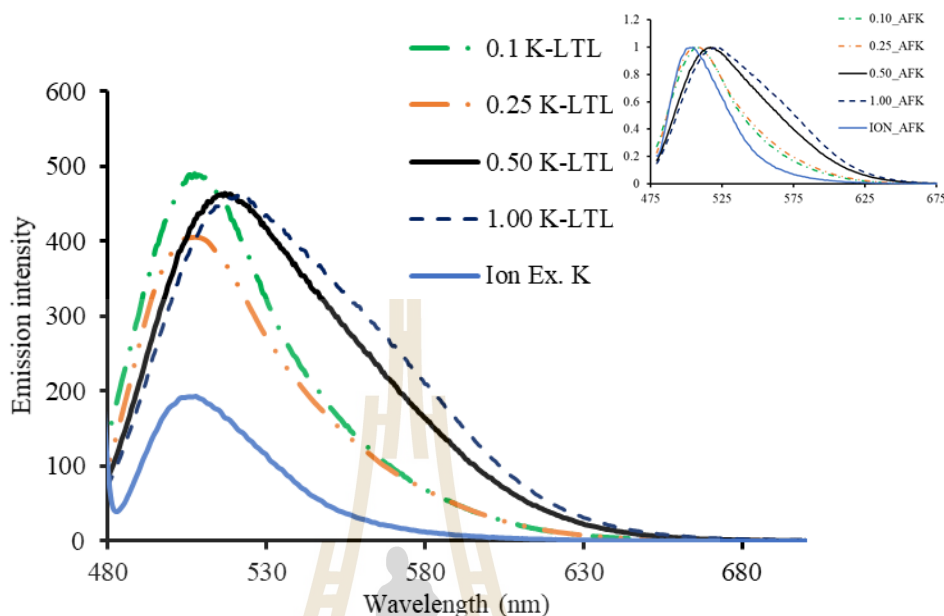


Figure 4.14 The emission spectra of AF in K-LTL with different occupation probabilities with excited at 475 nm.

A superimpose picture in Figure 4.14. shows the normalized emission position of all samples in AF_K-LTL and the emission shifts slightly to longer wavelength (red shift) from 475 to 525 nm with an increase in the occupation probability. As a result, AF_K-LTL prepared by the cation exchange exhibits the λ_{\max} at 480 nm while the emission prepared by the gas phase method with $p = 0.10 - 0.25_AFK$ and $p = 0.50 - 1.00_AFK$ shows the λ_{\max} at 485 and 525 nm, respectively, demonstrating that self-adsorption arrives with higher concentration causing an aggregate in the channel of zeolite L. Whereas, the increase in the emission intensity of AF_K-LTL are belonging to the occupation probability. It suggests that the increase in the amount of dye onto zeolite L affects the fluorescence intensity of dye_zeolite system.

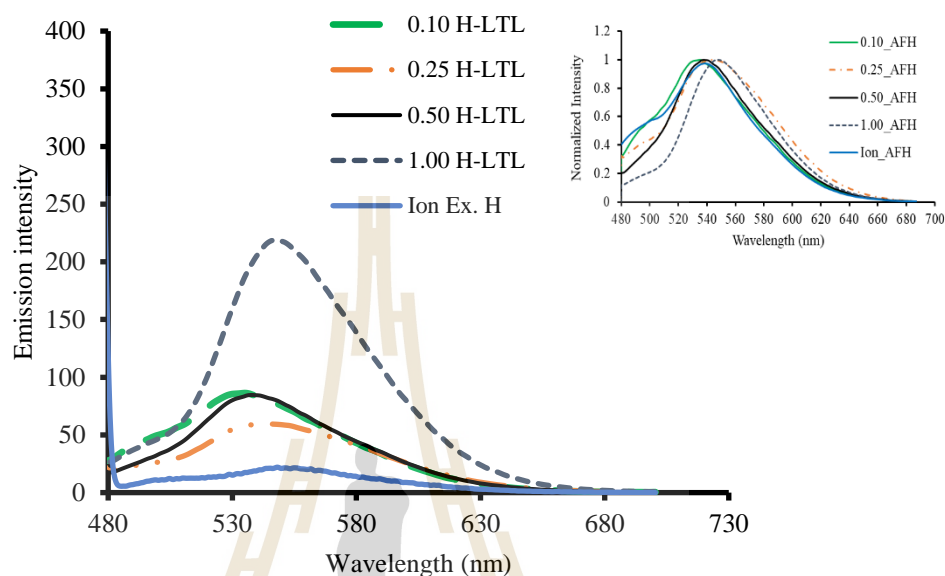


Figure 4.15 The emission spectra of AF_H-LTL zeolite with different occupation probabilities with excited at 475 nm.

Moreover, the emission spectra of AF on H-LTL show the band around 530 – 550 nm which is similar to K-LTL. The red shift occurs with the increase in occupation probability (see Figure 4.15). However, the emission intensity of AF_K-LTL are higher than that of AF_H-LTL that is affected from H-LTL zeolite structure offering protonate to AF molecule that decreases the emission intensity. The amount of dye contents of K-LTL and H-K-LTL trends to increase with increasing the occupation probability. Fortunately, the gas phase method provides a more insertion of AF dye than the cation exchange method (table 4.2)

Table 4.2 The amount of AF dyes content in the K and H-LTL after loading.

p	K-LTL		H-LTL	
	Dye offer (mol g ⁻¹)	Dye uptake (mol g ⁻¹)	Dye offer (mol g ⁻¹)	Dye uptake (mol g ⁻¹)
0.10	1.73×10^{-5}	9.52×10^{-6}	1.73×10^{-5}	1.20×10^{-6}
0.25	8.76×10^{-5}	2.55×10^{-5}	8.76×10^{-5}	1.27×10^{-6}
0.50	4.33×10^{-4}	3.95×10^{-5}	4.33×10^{-5}	2.45×10^{-6}
1.00	1.73×10^{-4}	6.00×10^{-5}	1.73×10^{-4}	4.54×10^{-6}
Ion Ex.	1.00×10^{-4}	4.6×10^{-7}	1.00×10^{-4}	5.50×10^{-7}

4.4.2.3 Hemicyanine Iodide (Hemi) on to zeolite (Hemi_LTL)

1) Hemi in solution.

Normally, hemicyanine dye has low emission quantum yield in polar solvent ($\Theta = 0.07$) (Cerdán et al., 2012). It is well-known that Hemi has a strong absorption band around 500 nm, which comes from the charge-transfer transition and its derivatives in the past two decades show that Hemi chromophore has negative solvatochromic behavior (absorption peak position blue-shifts through the increase of the solvent polarity), indicating that the ground state has larger dipole moments than excited state. Figure 4.16 and 4.17 show the absorption and fluorescence spectra of Hemi in four different common solvents: Acetone, chloroform, ethanol and water. Generally, speaking, the polarities of these solvents are in the following order: Water > ethanol > acetone > chloroform. The absorption spectra evidently show the negative solvatochromic behavior of Hemi (Figure 4.16). The red-shifted absorption spectra of the molecule were observed in solvents with higher polarity, indicating progressively

greater stabilization of the excited state in a polar environment. But there is relatively greater stabilization of ground than excited state of hydrophobic Hemi molecule in water, due to the quinonoid to benzenoid transformation (Abdel-Halim, 2011; Huang et al., 2002; Sahoo et al., 2011), and the absorption band gets blue-shifted compared to other polar solvents. Figure 4.17 shows the fluorescence spectra of the probe molecule in different solvents. A significant shift in the peak position from 430 nm in a nonpolar solvent (like acetone) to 588 nm in a more polar solvent (like water) was observed. The fluorescence excitation spectra of Hemi in other solvent match well with the absorption spectra in the same solvent which indicates that each of the emission bands arises from excitation of the same ground-state species.

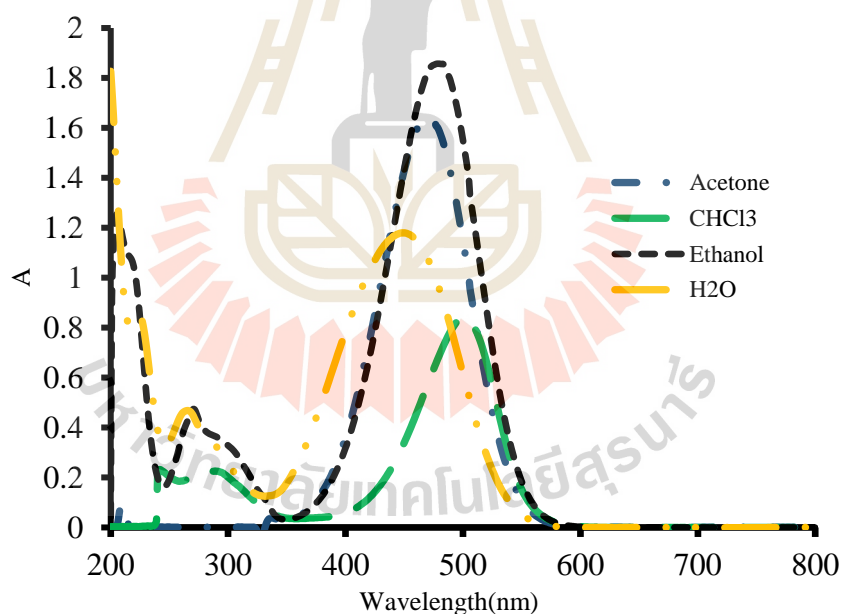


Figure 4.16 The absorption spectra of hemicyanine in various solvents.

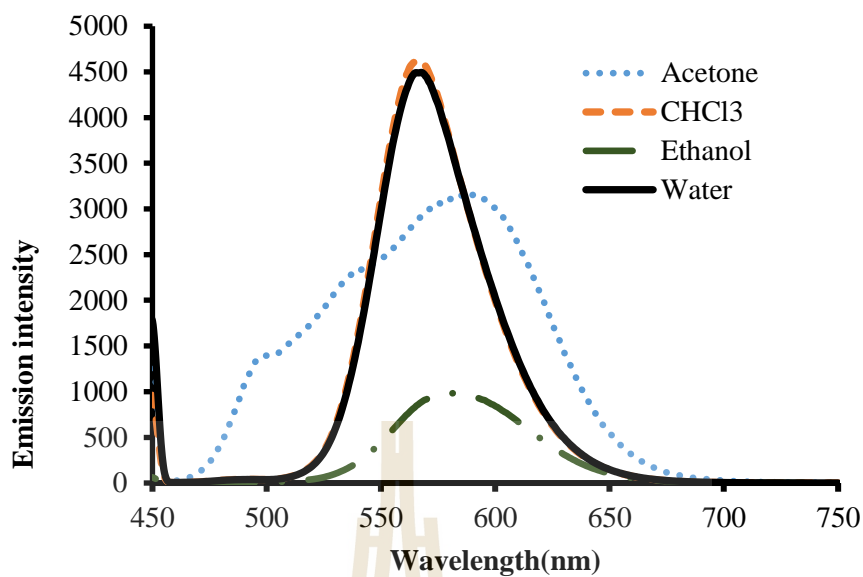


Figure 4.17 Emission spectra of Hemi in different solvents, excited at 450 nm

2) Insertion of Hemi onto K_LTL and H_LTL zeolite by cation exchange method

Figure 4.18 shows the diffuse reflectance of adsorbed Hemi on K-LTL and H-LTL zeolite. The result shows that the absorption broad band with maxima at 460 nm appeared on K-LTL. In contrast, hemi on H-LTL zeolite shows a sharp peak with the absorption maxima at 470 nm that is similar to the absorption spectra of hemi in water solvent. Furthermore, an acid surface of H-LTL zeolite can protonate the Hemi molecule resulting in a red shift of the absorption. The emission spectra of Hemi confined in K-LTL and H-LTL zeolite is revealed in Figure 4.18 that both of the samples appeared the similar emission maxima around 580 nm. Thus, the Hemi in K-LTL and H-LTL have the same excited state species.

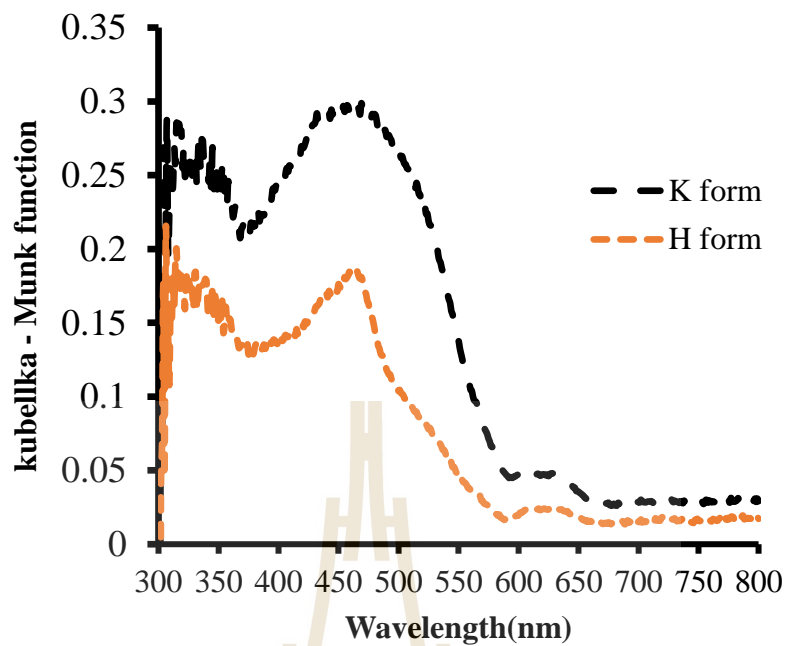


Figure 4.18 Diffuse reflectance spectra of AF in (a) K-LTL and (b) H-LTL

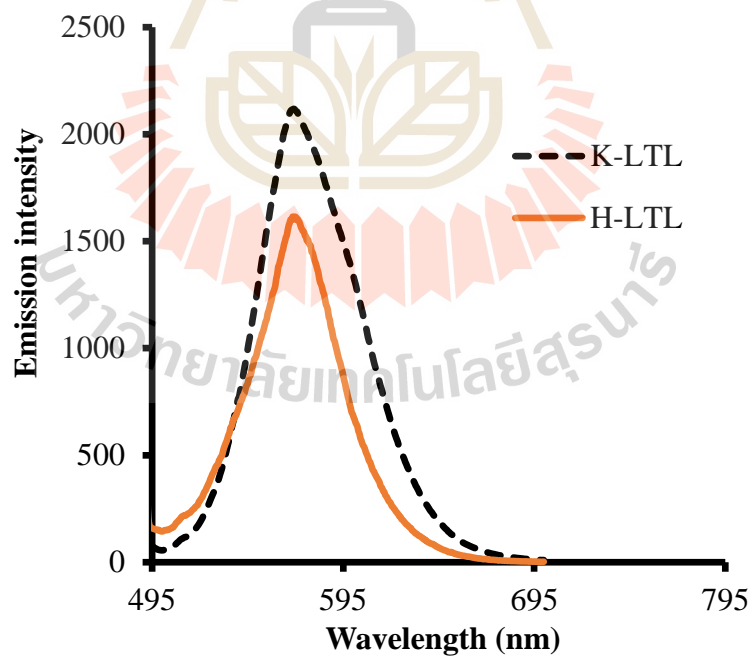
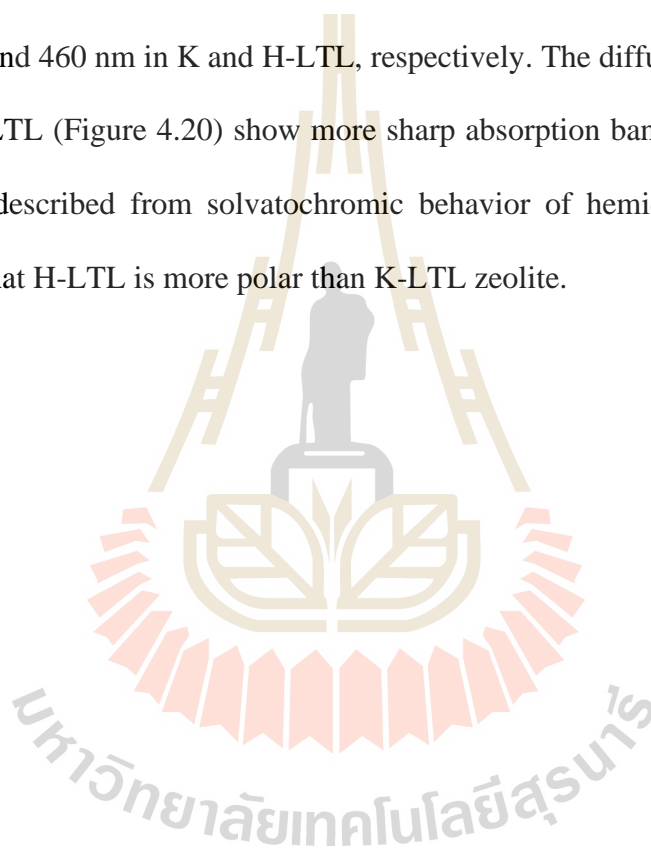


Figure 4.19 The emission spectra of Hemi in K-LTL and H-LTL zeolite, excited at 470 nm.

3) Insertion of hemicyanine iodide onto K_LTL and H-LTL zeolite by the gas phase method

A large molecule of hemicyanine is hard to insert onto zeolite L by the cation exchange due to the pore diameter and steric hindrances of the dye molecule. Thus, the gas phase approaches for insert with 180 °C. The gas phase insertion shows diffuse reflectance spectra with similar to the cation exchange method in the absorption band at 465 and 460 nm in K and H-LTL, respectively. The diffuse reflectance spectra of Hemi_H-LTL (Figure 4.20) show more sharp absorption band than Hemi_K-LTL, that can be described from solvatochromic behavior of hemicyanine chromophore confirming that H-LTL is more polar than K-LTL zeolite.



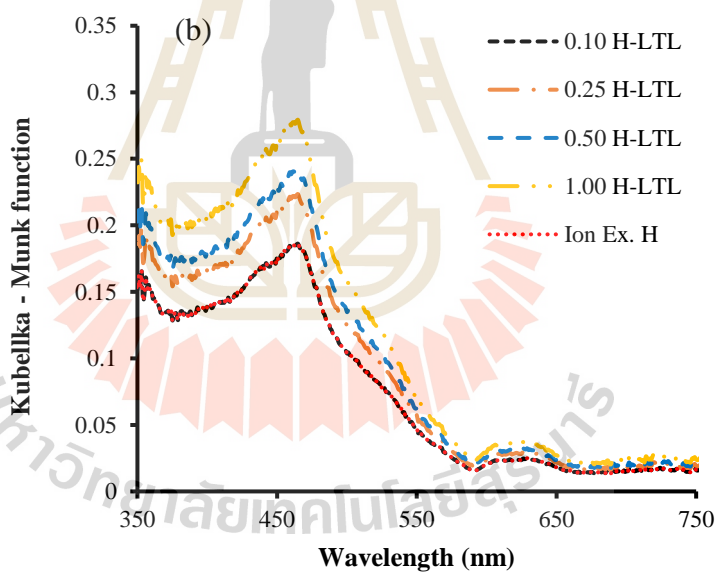
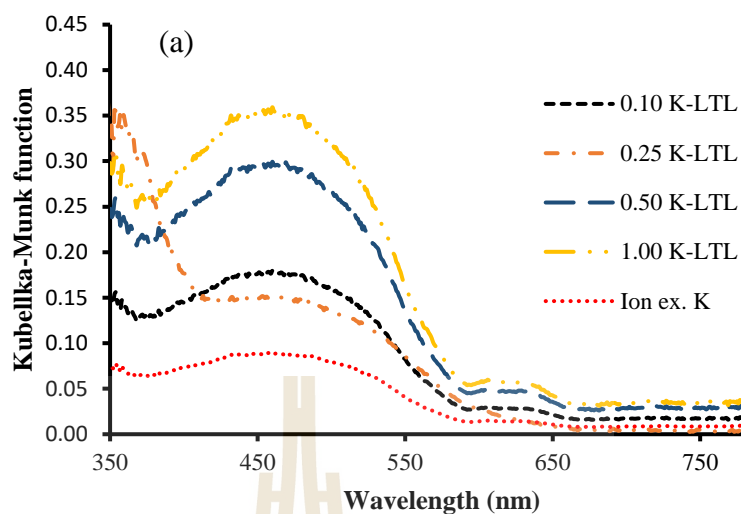


Figure 4.20 Diffuse reflectance spectra of hemi in (a) K-LTL and (b) H-LTL zeolite with various occupation probabilities.

Figure 4.21 reveals the emission of Hemi_K-LTL. It shows the λ_{max} around 560 nm. The emission intensity increases until $p = 0.25$ and then decreases with increasing occupation probability ($p = 0.5$ and 1.0). This can be described that the

aggregation of hemi dye is easy to occur with a large molecule and branch of amine group effect the quenching emission intensity.

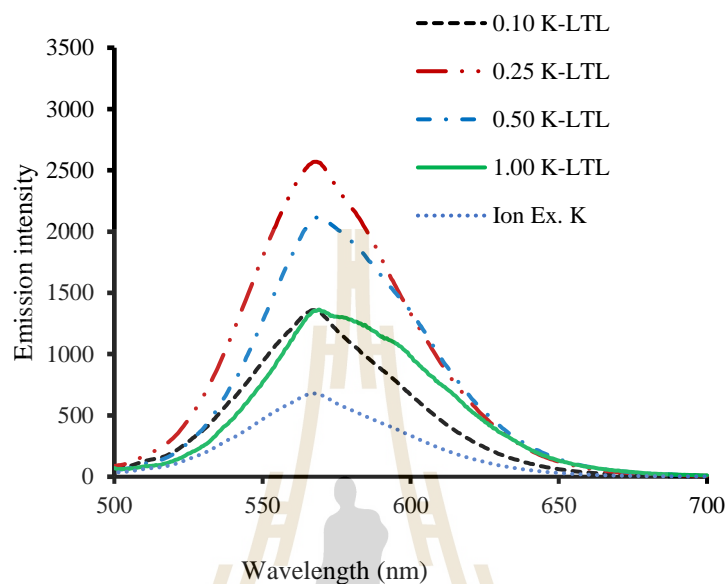


Figure 4.21 The emission spectra of Hemi_K-LTL zeolite with various occupation probabilities, excited at 470 nm.

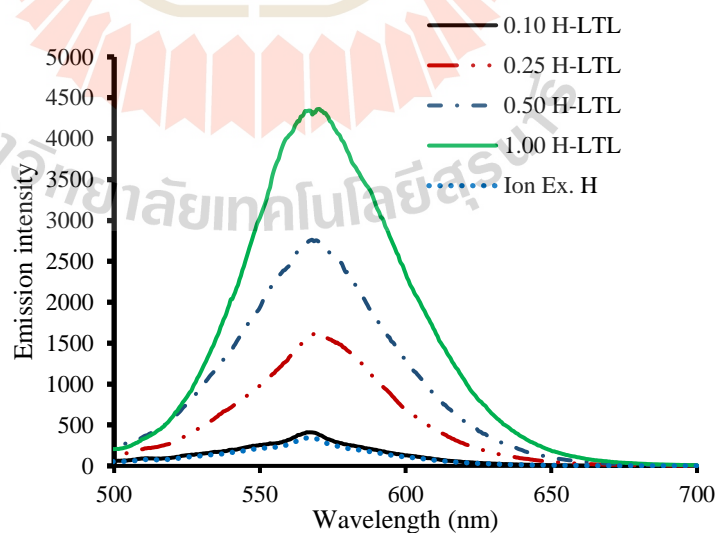
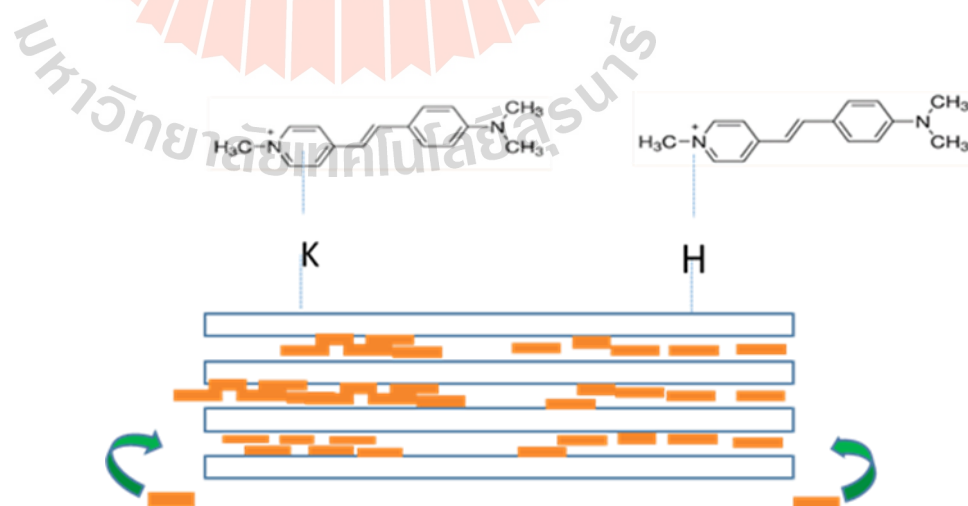


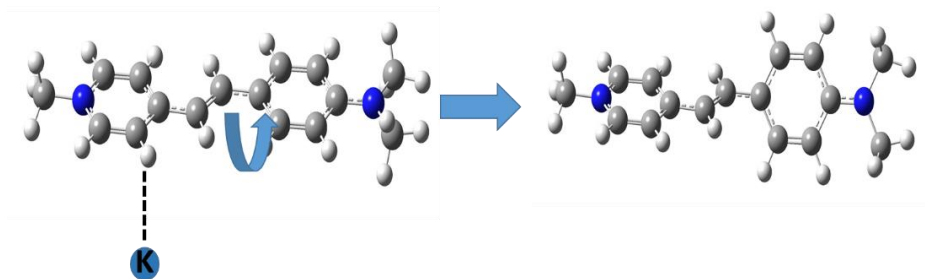
Figure 4.22 The emission spectra of Hemi_H-LTL zeolite with various occupation probabilities, excited at 470 nm.

The emission of Hemi_H-LTL appears at $\lambda_{\max} = 575$ nm (Figure 4.22) and the emission intensity tends to increase with increasing the occupation probability contrasting with Hemi_K-LTL, as a result, we have two ways for explanation:

1. The surface of K-LTL zeolite is K $\cdots\pi$ interaction between K-LTL and benzene ring of hemi dye which is strong interaction and 1 molecule of hemi dye has 2 positions to occur thus it is possible that the dye stacks with each other and close the pore of the zeolite. In addition, the surface of H-LTL can interact with hemi dye through H \cdots N interaction which is weaker than K $\cdots\pi$ interaction resulting in the dye aggregation in K-LTL (Scheme 4.3) (Escudero et al., 2008; Ruan et al., 2004).
2. An internal twisting of aniline ring of hemi dye is favor to occur in K-LTL zeolite due to the strong K $\cdots\pi$ interaction more than H-LTL zeolite as can be seen in the Scheme 4.4



Scheme 4.3 Illustrate the interaction of hemicyanine dye with the surface of K-LTL and H-LTL zeolite.



Scheme 4.4 Twisting motion of hemicyanine chromophore through the torsion of C-C bond (the aniline ring)

Moreover, the amount of the dye after insertion tends to increase with increasing the occupation probability in the Hemi_K and H-LTL zeolite as revealed in table 4.3.

Table 4.3 The amount of Hemi dyes in the K-LTL and H-LTL after loading.

P	K-LTL		H-LTL	
	Dye offer (mol g ⁻¹)	Dye uptake (mol g ⁻¹)	Dye offer (mol g ⁻¹)	Dye uptake (mol g ⁻¹)
0.10	1.15×10^{-5}	2.91×10^{-7}	1.15×10^{-5}	6.46×10^{-7}
0.25	2.86×10^{-5}	8.78×10^{-7}	2.86×10^{-5}	1.31×10^{-6}
0.50	5.76×10^{-5}	1.83×10^{-6}	5.76×10^{-5}	2.36×10^{-6}
1.00	1.15×10^{-4}	4.46×10^{-6}	1.15×10^{-4}	1.79×10^{-6}
Ion Ex.	1.00×10^{-4}	2.0×10^{-7}	1.00×10^{-4}	1.5×10^{-7}

4.4.2.4 Thioindigo (Thio) on to zeolite (Thio_LTL)

1) Thio in solution

Thio is a neutral dye with a beautiful red color and widely used in fabric red color. The absorptions of Thio are shown in Figure 4.23. The absorption maxima appear at 545 nm in acetone, ethanol, and toluene and the hypsochromic shoulders on 504 nm that is a character of $n \rightarrow \pi^*$ transition. In contrast, the absorption maxima of Thio in CHCl_3 appear at 505 nm and the bathochromic shoulders at 545 nm. According to cis – trans isomer of Thio dye, the cis isomer appears the emission spectra at shorter wavelength (Grellmann et al., 1978). (Figure 4.22). The emission spectra of Thio in each solvent shows around 573 nm. however, the emission in ethanol shows the very low intensity (Figure 4.23) because ethanol has more polar which affect on the molecule of Thio dye.

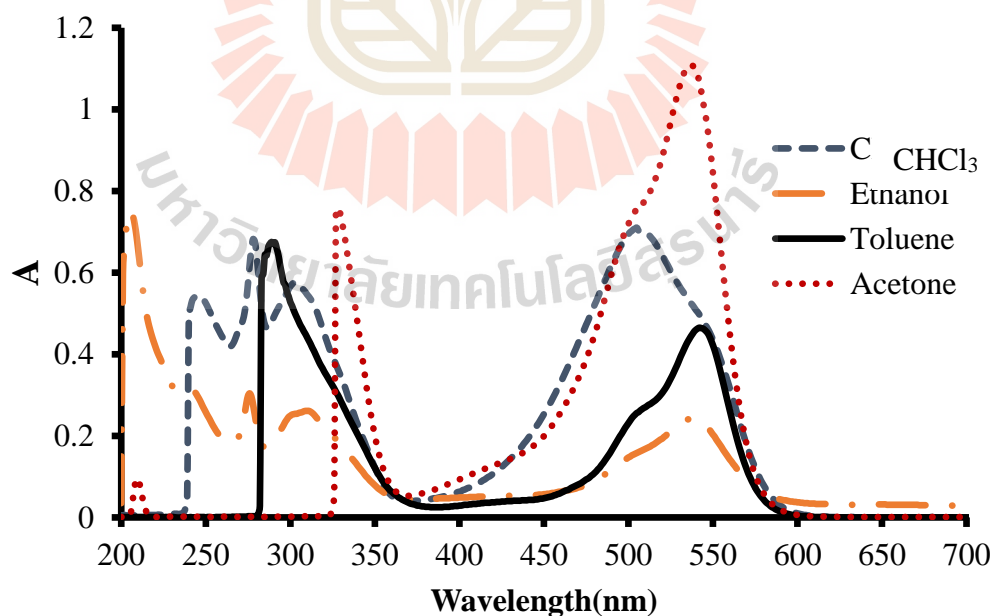


Figure 4.23 The absorption spectra of Thio in various solvents.

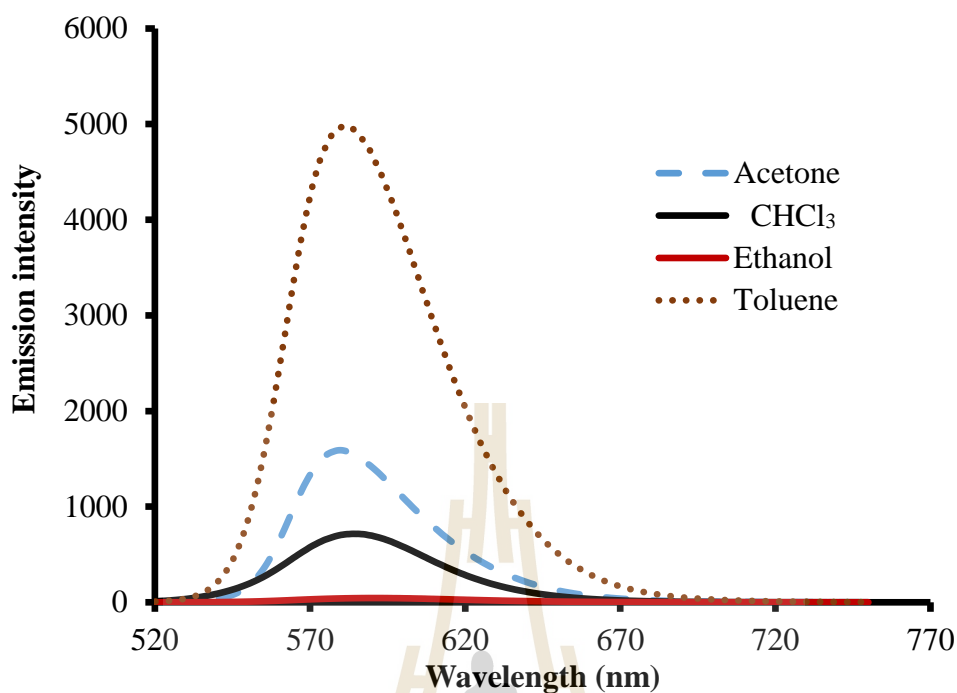


Figure 4.24 Emission spectra of Thio in different solvents, the samples were excited at 500 nm

2) Thioindigo inclusion to K-LTL and H-LTL zeolite by the gas phase method

Thio_zeolite composite is successfully prepared by the gas phase method at the temperature 150 °C. The diffuse reflectance shows the absorption spectra of Thio_K-LTL and H-LTL zeolite composite appear the maxima absorption peak at 550 nm with a bathochromic shoulder in both samples (Figure 4.25). As a result, the Thio species are possible to form of trans- species molecule in the channel of zeolite L (Fukunishi et al., 1990).

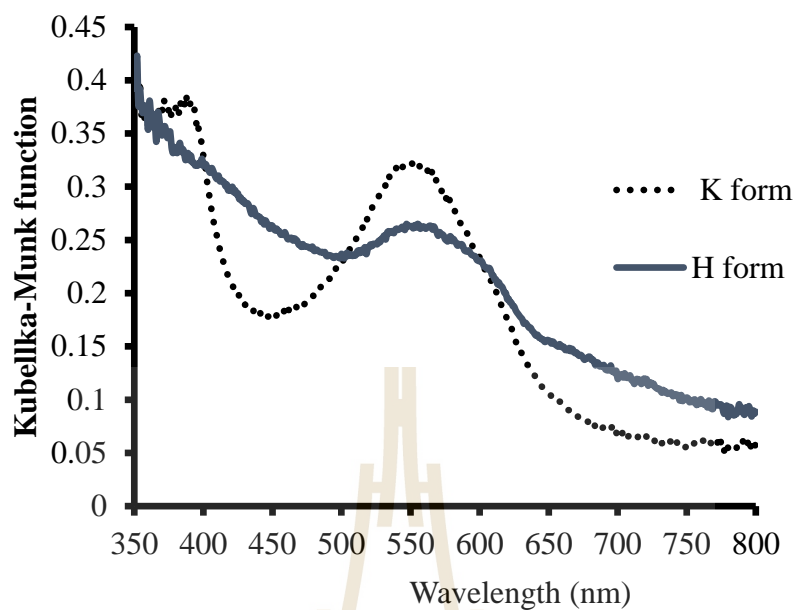


Figure 4.25 Diffuse reflectance spectra of Thio confined in K-LTL and H-LTL zeolite.

Figure 4.26 illustrates the emission spectra of Thio absorbed on K-LTL zeolite with different probabilities with excited at 500 nm. The result shows that all samples appear the emission peak around 575 nm that is similar to Thio in the solution.

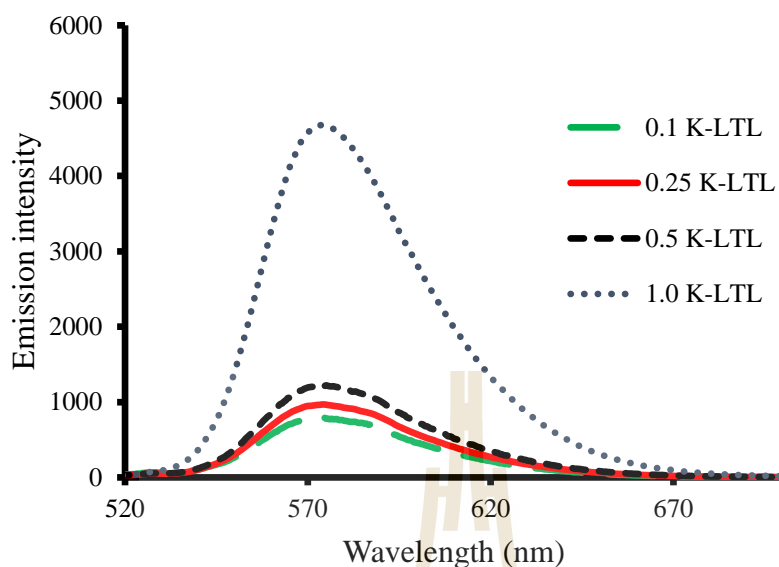


Figure 4.26. The emission spectra of Thio in K-LTL zeolite with various occupation probabilities, excited at 500 nm.

In addition, the emission intensity of Thio_K-LTL zeolite composite is significantly increased with increasing the occupation probability due to an increase in the amount of dye with the probability increased (table 4.4).

Table 4.4 The amount of Thio dye on the K-LTL and H-LTL zeolite.

ρ	K-LTL		H-LTL	
	Dye offer (mol g ⁻¹)	Dye uptake (mol g ⁻¹)	Dye offer (mol g ⁻¹)	Dye uptake (mol g ⁻¹)
0.10	1.15×10^{-5}	7.76×10^{-8}	1.15×10^{-5}	-
0.25	2.86×10^{-5}	2.03×10^{-7}	2.86×10^{-5}	-
0.50	5.76×10^{-5}	8.26×10^{-7}	5.76×10^{-5}	-
1.00	1.15×10^{-4}	2.82×10^{-6}	-	-

The gas phase method cannot prepare because of the protonated zeolite L and temperatures degrade the Thio dyes, that achieved a black powder and disappear the luminescence properties.

4.4.2.5 Cyaninine (Cy) on to zeolite (Cy_LTL)

The absorption spectra belong to the media such as the acidic and polar of solvent. A clear aggregation of the dye in Figure 4.27, shows the absorption spectra of Cy in 0.01 M HCl and water solvent.

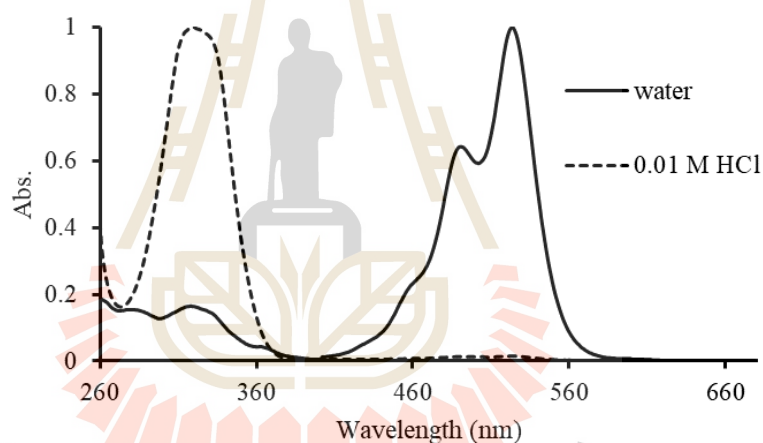
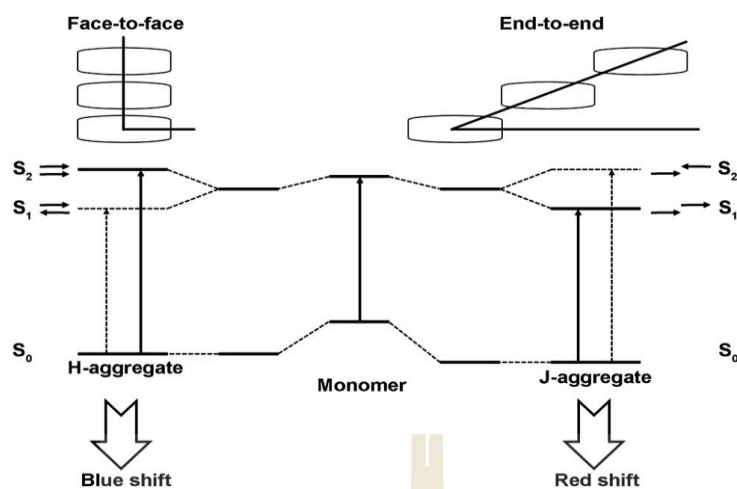


Figure 4.27 The absorption spectra of Cy in 0.01 HCl and water solvents.



Scheme 4.5 Representation of the relationship between chromophore arrangement and spectral shift based on the molecular exciton theory (Zhai et al., 2014).

The acidic solvent turns the Cy to H-aggregation causing the absorption band to appear at 320 nm while Cy in water solution shows the absorption band at 520 nm with a secondary peak at 490 nm, which is caused by the vibrational actions of the dye molecule. The H and J aggregate are described in Scheme 5. The dye molecule, according to excitation theory, is regarded as a point dipole and the excitonic state of the dye aggregate splits into two levels through the interaction of transition dipoles. The dye molecules may aggregate in a parallel way (plane to plane stacking) to form a sandwich type arrangement (H-dimer) or in a head-to-tail arrangement (end to end stacking) to form a J-dimer. A transition to the upper state in parallel aggregates having parallel transition moments and to a lower state in a head-to-tail arrangement with perpendicular transition moments leads to hypsochromic (red) and bathochromic (blue) shifts, respectively.

2) Insertion by cation exchange method

The inclusion of Cy on zeolite L by cation exchange method, the adsorption and emission energy of K-LTL and H-LTL zeolite appear in the same position at 320 nm and 415 nm, respectively (Figure 4.28 and 4.29). The emission intensity of Cy in H-LTL is lower than that of K-LTL resulting from the protonated properties of the Cy molecule (Zhai et al., 2014)

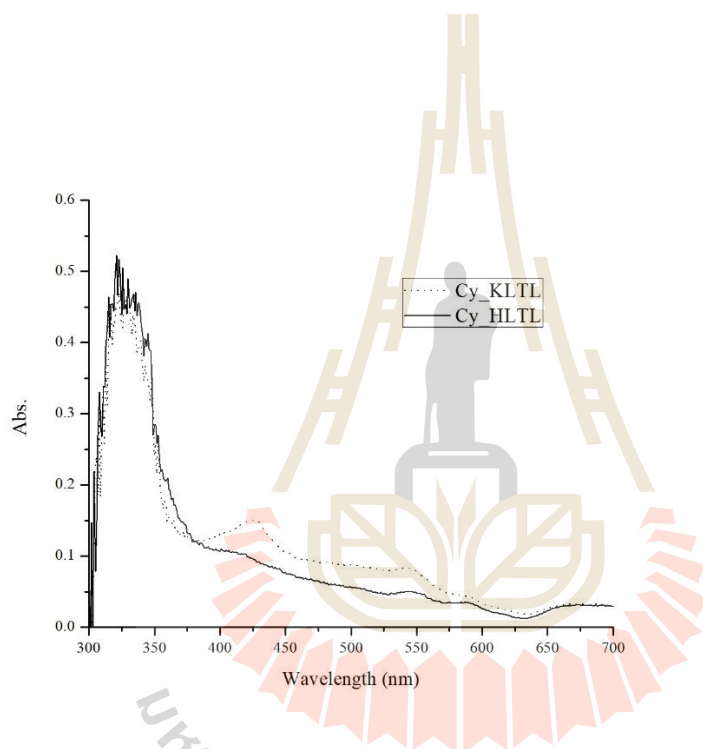


Figure 4.28 Diffuse reflectance spectra of Cy confined in K-LTL and H-LTL zeolite prepared by the cation exchange method.

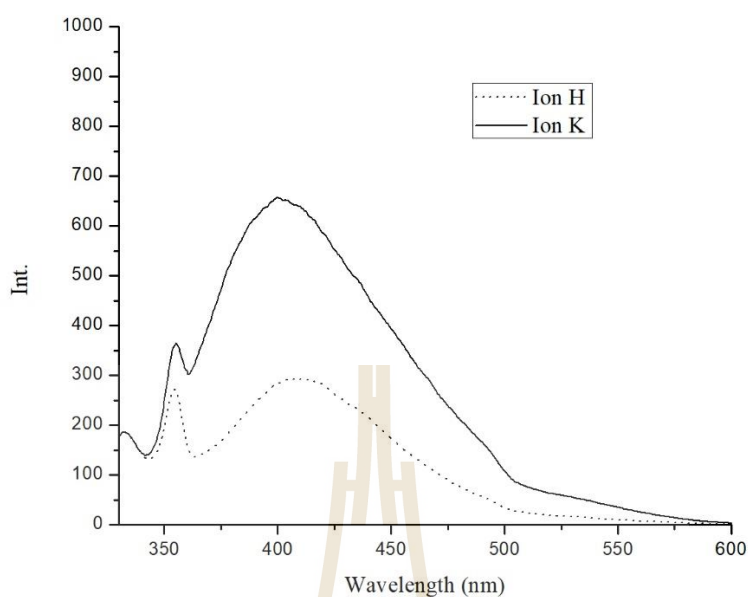


Figure 4.29 The emission spectra of Cy on K-LTL and H-LTL zeolite prepared by ion exchange, excited at 320 nm.

3) Insertion of Cy by the gas phase method

Cy is a cationic with a branch of ethyl group and the molecular size of cyanine dyes is very tight to enter into the pore diameter of zeolite L, consequently, it is hard to included into zeolite L. Thus, the gas phase method was employed to this dye with difference in occupation probability. Figure 4.30 displays the absorption band of Cy_K and H-LTL prepared with $p = 0.25$ and 1.0 . The result shows that the main excitation energy of those samples appears at 320 nm and the J-aggregate produced in the Cy_H-LTL appears two small absorption bands at 420 and 550 nm seen more clearly in Cy_ H-LTL than Cy_K-LTL.

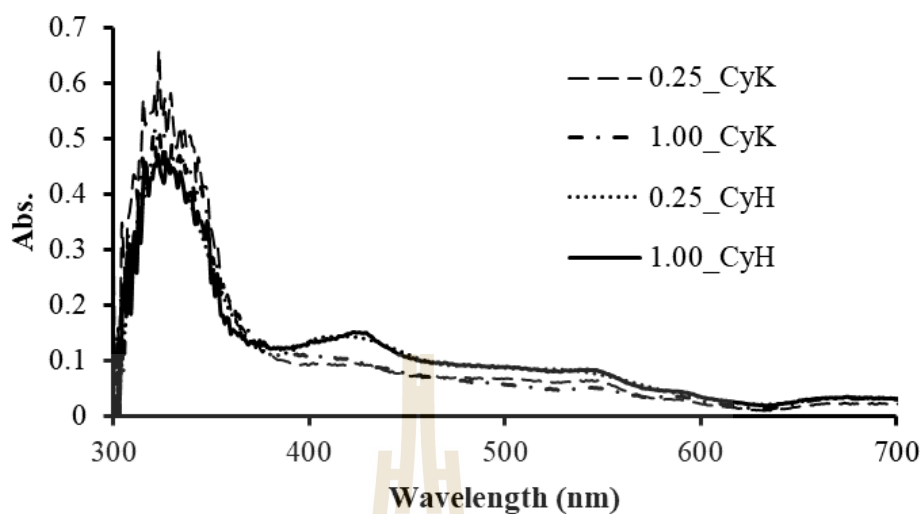


Figure 4.30 Diffuse reflectance spectra of Cy confined in K-LTL and H-LTL zeolite prepared by gas phase method.

Figure 4.31(a) demonstrates the emission spectra of all Cy_K-LTL samples with excitation at 320 nm and the emission spectra of the prepared samples by gas phase method with different probabilities appear at 400 nm and at 415 nm for those prepared by the cation exchange method. While Cy_H-LTL sample prepared by gas phase method shows the emission spectra at 425 nm and 415 nm for the samples prepared by the cation exchange method (see Figure 31b). The explanation of this result is that the j-aggregate of Cy dye produced in H-LTL with a high concentration in the channel of zeolite L resulting in the emission at longer wavelength (red shift) (415 to 425 nm). Moreover, the emission intensity of Cy_K-LTL increases with increasing probability until p is 0.25 and decreases with p higher than 0.25. This effect is from high packing with H-aggregate produced in K-LTL channel. Whereas the emission intensity of Cy_H-LTL increases with increasing p until 0.50 and decreases with p higher than 0.5. However, the j-

aggregate affects on the high emission intensity of Cy_H-LTL is greater than that of Cy_K-LTL. The amount of the dye in Cy_K-LTL and Cy_H-LTL are reported in table 4.5.

Table 4.5 The amount of Cy dye on the K and H-LTL zeolite.

p	K-LTL		H-LTL	
	Dye offer (mol g ⁻¹)	Dye uptake (mol g ⁻¹)	Dye offer (mol g ⁻¹)	Dye uptake (mol g ⁻¹)
0.1	1.15×10^{-5}	7.78×10^{-8}	1.15×10^{-6}	7.07×10^{-8}
0.25	2.86×10^{-5}	7.47×10^{-8}	2.86×10^{-5}	1.87×10^{-6}
0.5	5.76×10^{-5}	7.14×10^{-7}	5.76×10^{-5}	3.48×10^{-6}
1	1.15×10^{-4}	1.32×10^{-6}	1.15×10^{-4}	2.21×10^{-5}
Ion Ex.	1.00×10^{-4}	1.65×10^{-7}	1.00×10^{-4}	1.72×10^{-7}

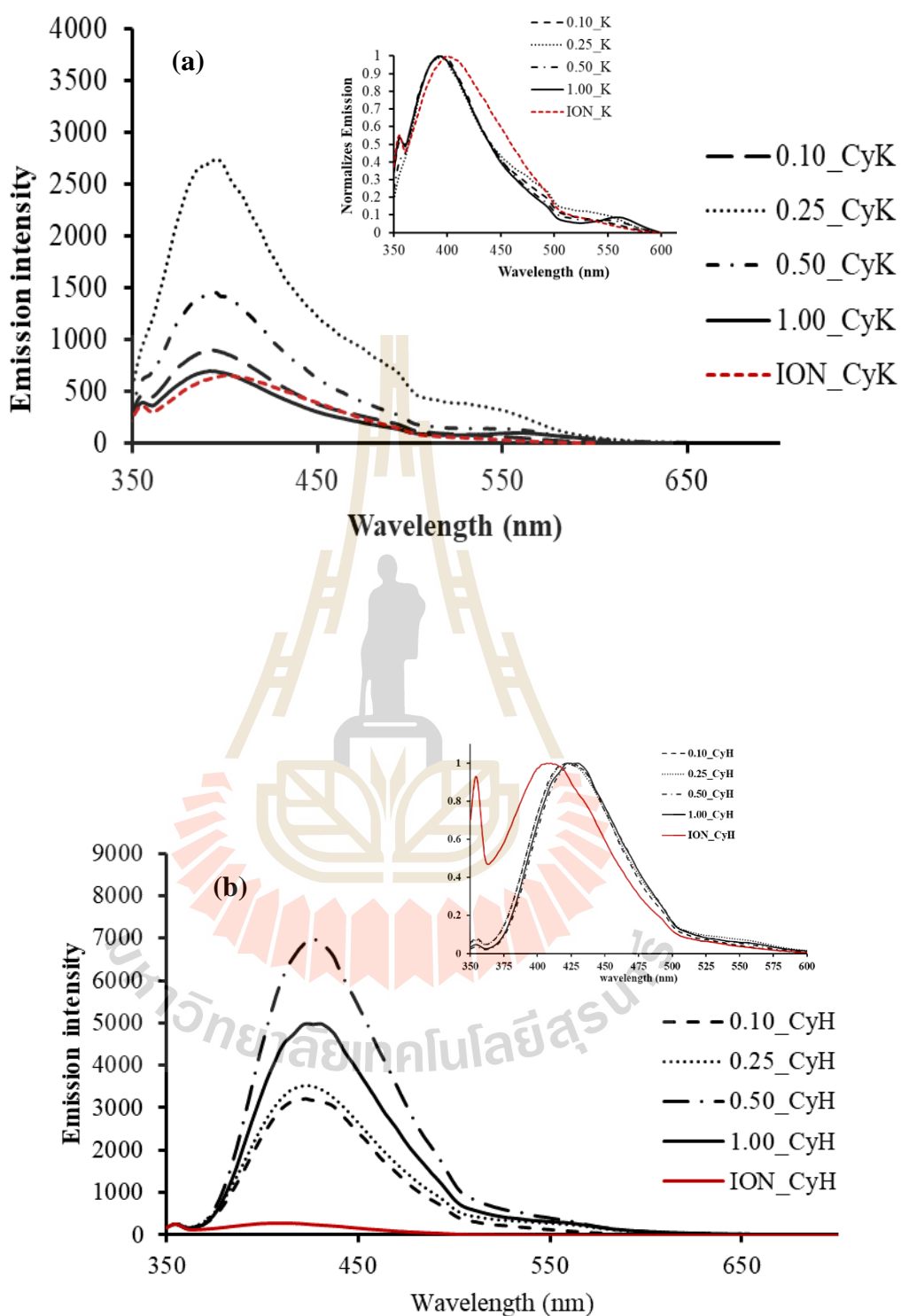


Figure 4.31 The emission spectra of Cy on K-LTL (a) and H-LTL (b) zeolite, excited at 320 nm.

4.4.2.6 Thionine Acetate (Th) on to zeolite (Th_LTL)

1) Thionine in solution

Thionine is a cationic species dye with S atom in the structure. The spectrum of thionine acetate in water and methanol solution exhibits the typical profile expected for the monomeric form, with a main peak at 600 nm and hypsochromic shoulders at 550 nm (see Figure 4.32), due to $0 \leftarrow 0$, $1 \leftarrow 0$, and $2 \leftarrow 0$, $\pi^* \leftarrow \pi$ transitions (Gigli et al., 2015)

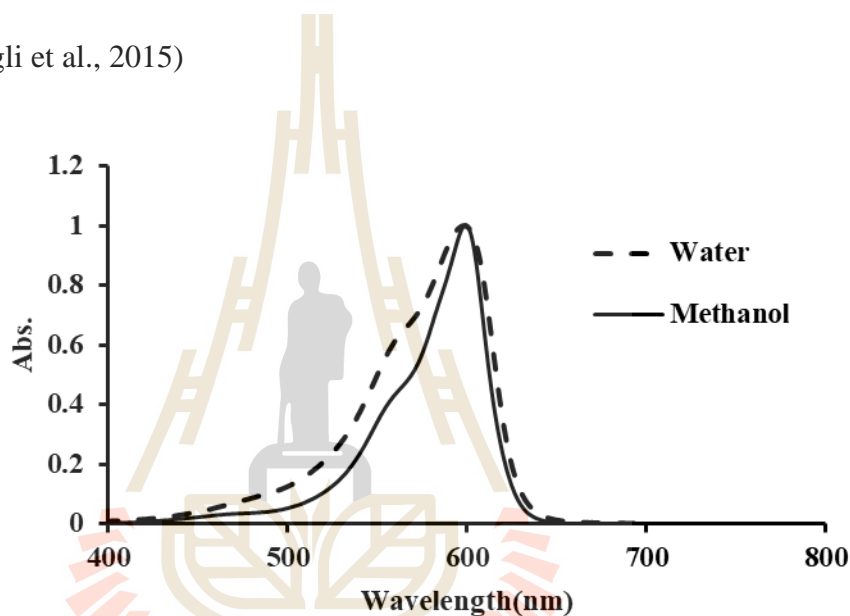


Figure 4.32 The absorption spectra of Th in water and methanol solvents.

2) Insertion by cation exchange method

The absorption band of Th_K-LTL and Th_H-LTL zeolite are independent of emission band changes with the peak position remaining at 610 and 615 nm, respectively (Figure 4.33), and a slight skewing of the peak results from the effect of self-absorption of dye in environment of zeolite. (Haugen et al., 1965).

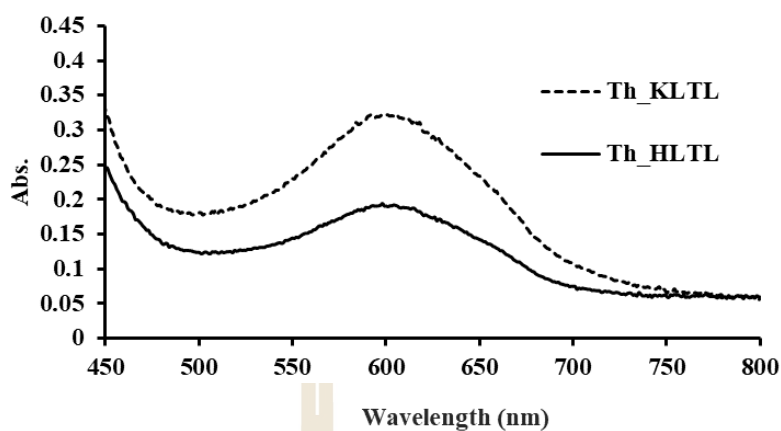


Figure 4.33 Diffuse reflectance spectra of Cy confined in K-LTL and H-LTL zeolite.

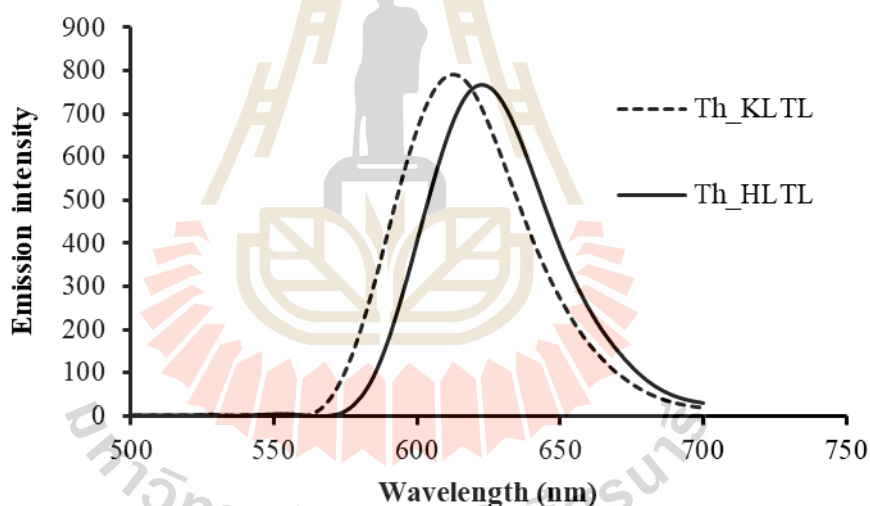


Figure 4.34 The emission spectra of Th_K-LTL and Th_H-LTL zeolite, excited at 610 nm.

When comparing the emission spectra of Th in solution to the Th_K-LTL and Th_H-LTL zeolite (Figure 4.34), a red-shift of emission maxima was observed, in agreeing with the analogous shift of the absorption spectra. Moreover, the photoemission of Th_H-LTL appears at higher position than that of Th_K-LTL,

agreement with the intramolecular charge transfer (ICT) favored in this system (Gigli et al., 2015).

3) Insertion by the gas phase method

Unfortunately, the gas phase method cannot apply to thionine acetate dye due to the acetate anion combusted at high temperature and it changed to black powder of Th_K-LTL and H-LTL with non-fluorescence properties. Thus, for application of this dye into zeolite LTL, a low temperature and a long time for insertion are required. Even though, the experiment under this condition was done and the product was achieved, but the product is non-fluorescence. Therefore, other species of thionine such as thione chloride is worth to try with this method.

4.5 Conclusions

A variety of fluorescent dyes such as acridine (AC), acriflavine (AF), hemicyanine (Hemi), cyanine (cy), thionine (Th) and thioindigo (Thio) are used in the dye-zeolite L composite. The appropriate cationic and neutral dye can be inserted onto K-LTL and H-LTL zeolite. Not only the cation exchange but also the gas phase method are used for preparation of cationic dyes onto zeolite LTL at different occupation probabilities ($p = 0.10, 0.25, 0.50$ and 1.00). The samples of dye_K-LTL and dye_H-LTL zeolite prepared by the gas phase method show the high amount of the dye intercalated in the channel of zeolite. The high loading ($p = 0.50$ and 0.10) produces the aggregation of the dye molecule in the channel of zeolite L causing a self-absorption and a reduction of luminescence properties. In the case of zeolite H-LTL the gas phase method is not suitable for some dye such as Thio due to the protonated form able to

degrade with high temperature. In the gas phase method, the occupation probability at 0.25 was chosen for applying in FRET study due to an achievement of high luminescence property and avoidance of the aggregation of dye molecule.

4.6 References

- Abdel-Halim, S.T. (2011). Steady-state fluorescence and photo-isomerization study of 1-methyl-4'-(p-N,N dimethyl-amino styryl) pyridinium iodide. **Journal of Luminescence**. 131: 30-35.
- Alvarado, M., Jr., Chianelli, R.C., and Arrowood, R.M. (2012). Computational study of the structure of a sepiolite/thioindigo mayan pigment. **Bioinorganic Chemistry and Applications**. 2012: 672562.
- Ban, T., Saito, H., Naito, M., Ohya, Y., and Takahashi, Y. (2007). Synthesis of zeolite L crystals with different shapes. **Journal of Porous Materials**. 14: 119-126.
- Calzaferri, G., Huber, S., Maas, H., and Minkowski, C. (2003). Host-guest antenna materials. **Angewandte Chemie International edition in English**. 42: 3732-3758.
- Cerdán, L., Costela, A., García-Moreno, I., Bañuelos, J., and López-Arbeloa, I. (2012). Singular laser behavior of hemicyanine dyes: unsurpassed efficiency and finely structured spectrum in the near-IR region. **Laser Physics Letters**. 9: 426-433.
- Easwaramoorthi, S., and Natarajan, P. (2007). Spectral and electrochemical studies of methylene blue and thionine encapsulated in zeolite-Y. **Journal of Porous Materials**. 15: 343-349.

- Escudero, D., Frontera, A., Quiñonero, D., and Deyà, P.M. (2008). Interplay between cation- π and hydrogen bonding interactions. **Chemical Physics Letters**. 456: 257-261.
- Fukunishi, K., Tatsuma, M., M. Fatah Ur Rahman, S., Kuwabara, M., Yamanaka, H., and Nomura, M. (1990). Cis/trans isomerization of thioindigo derivatives adsorbed on silica gel modified with octadecyl groups (Vol. 63).
- Gigli, L., Arletti, R., Vitillo, J.G., Alberto, G., Martra, G., Devaux, A., and Vezzalini, G. (2015). Thionine Dye Confined in Zeolite L: Synthesis Location and Optical Properties. **The Journal of Physical Chemistry C**. 119: 16156-16165.
- Grellmann, K.H., and Hentzschel, P. (1978). Mechanism of the photochemical cis \rightleftharpoons trans isomerization of thioindigo and 6,6'-diethoxy-thioindigo in solution. **Chemical Physics Letters**. 53: 545-551.
- Haugen, G., and Hardwick, R. (1965). Ionic Association in Solutions of Thionine. II. Fluorescence and Solvent Effects. **The Journal of Physical Chemistry**. 69: 2988-2996.
- Huang, Y., Cheng, T., Li, F., Luo, C., Huang, C.-H., Cai, Z., and Zhou, J. (2002). Photophysical Studies on the Mono- and Dichromophoric Hemicyanine Dyes II. Solvent Effects and Dynamic Fluorescence Spectra Study in Chloroform and in LB Films. **The Journal of Physical Chemistry B**. 106: 10031-10040.
- Insuwan, W., Jungstittiwong, S., and Rangsrivatananon, K. (2015). Host-guest composite materials of dyes loaded zeolite LTL for antenna applications. **Journal of Luminescence**. 161: 31-36.
- Insuwan, W., and Kunwadee, R. (2012). Morphology-Controlled Synthesis of Zeolite and Physicochemical Properties. **Engineering Journal**. 16: 1-12.

- Insuwan, W., and Rangriwatananon, K. (2014). Evaluation of adsorption of cationic dyes on H-LTL and K-LTL zeolite (Vol. 21).
- Insuwan, W., and Rangriwatananon, K. (2014). Evaluation of adsorption of cationic dyes on H-LTL and K-LTL zeolite. **Journal of Porous Materials**. 21: 345-354.
- Kaewsuya, P., Miller, J.D., Danielson, N.D., Sanjeevi, J., and James, P.F. (2008). Comparison of N-alkyl acridine orange dyes as fluorescence probes for the determination of cardiolipin. **Analytica Chimica Acta**. 626: 111-118.
- Kazim, S., Zulfequar, M., Mazharul Haq, M., Bhatnagar, P.K., and Husain, M. (2007). Electrical and optical properties of thin films based on poly [2-methoxy-5 (2'-ethyl hexyloxy)-1,4-phenylene vinylene] doped with acridine orange dye with possible photovoltaic applications. **Solar Energy Materials and Solar Cells**. 91: 1462-1466.
- Kim, D., and Kim, H.S. (2017). Enhancement of fluorescence from one- and two-photon absorption of hemicyanine dyes by confinement in silicalite-1 nanochannels. **Microporous and Mesoporous Materials**. 243: 69-75.
- Kitai, A. (2008). Luminescent Materials and Applications.
- Kumar, K.S., Selvaraju, C., Malar, E.J.P., and Natarajan, P. (2012). Existence of a New Emitting Singlet State of Proflavine: Femtosecond Dynamics of the Excited State Processes and Quantum Chemical Studies in Different Solvents. **The Journal of Physical Chemistry A**. 116: 37-45.
- Li, C., Sun, P., Yan, L., Pan, Y., and Cheng, C.-H. (2008). Synthesis and electroluminescent properties of Ir complexes with benzo[c]acridine or 5,6-dihydro-benzo[c]acridine ligands. **Thin Solid Films**. 516: 6186-6190.

- Petit, J.-M., Denis-Gay, M., and Ratinaud, M.-H. (1993). Assessment of fluorochromes for cellular structure and function studies by flow cytometry. **Biology of the Cell**. 78: 1-13.
- Ruan, C., and Rodgers, M.T. (2004). Cation- π Interactions: Structures and Energetics of Complexation of Na⁺ and K⁺ with the Aromatic Amino Acids, Phenylalanine, Tyrosine, and Tryptophan. **Journal of the American Chemical Society**. 126: 14600-14610.
- Ryder, A., Power, S., and Glynn, T. (2003). Evaluation of Acridine in Nafion as a Fluorescence-Lifetime-Based pH Sensor (Vol. 57).
- Sahoo, D., Bhattacharya, P., and Chakravorti, S. (2011). Spectral signature of 2-[4-(dimethylamino)styryl]-1-methylquinolinium iodide: a case of negative solvatochromism in water. **The Journal of Physical Chemistry B**. 115: 10983-10989.
- Sharma, N., Jain, S.K., and Rastogi, R.C. (2007). Solvatochromic study of excited state dipole moments of some biologically active indoles and tryptamines. **Spectrochimica Acta Part A: Molecular and Biomolecular Spectroscopy**. 66: 171-176.
- Sharma, V.K., Sahare, P.D., Rastogi, R.C., Ghoshal, S.K., and Mohan, D. (2003). Excited state characteristics of acridine dyes: acriflavine and acridine orange. **Spectrochimica Acta Part A: Molecular and Biomolecular Spectroscopy**. 59: 1799-1804.
- Treacy, M.M.J., and Higgins, J.B. (2007). LTL - Linde Type L. In M. M. J. Treacy and J. B. Higgins (Eds.), Collection of Simulated XRD Powder Patterns for Zeolites (Fifth Edition) (pp. 256-257). Amsterdam: Elsevier Science B.V.

- Uno, H., Moriyama, K., Ishikawa, T., Ono, N., and Yahiro, H. (2004). Thioindigo precursor: control of polymorph of thioindigo. **Tetrahedron Letters**. 45: 9083-9086.
- Veiga-Gutierrez, M., Woerdemann, M., Prasetyanto, E., Denz, C., and De Cola, L. (2012). Optical-tweezers assembly-line for the construction of complex functional zeolite L structures. **Advanced Materials**. 24: 5199-5204, 5198.
- Yamaguchi, A., Nakano, M., Nochi, K., Yamashita, T., Morita, K., and Teramae, N. (2006). Longitudinal diffusion behavior of hemicyanine dyes across phospholipid vesicle membranes as studied by second-harmonic generation and fluorescence spectroscopies. **Analytical and Bioanalytical Chemistry**. 386: 627-632.
- Yu, J., Cui, Y., Xu, H., Yang, Y., Wang, Z., Chen, B., and Qian, G. (2013). Confinement of pyridinium hemicyanine dye within an anionic metal-organic framework for two-photon-pumped lasing. **Nature Communications**. 4: 2719.
- Zhai, D., Xu, W., Zhang, L., and Chang, Y.-T. (2014). The role of “disaggregation” in optical probe development. **Chemical Society Reviews**. 43: 2402-2411.

CHAPTER V

FLUORESCENCE RESONANCE ENERGY TRANSFER

FROM THE DONOR -ACCEPTER OF ORGANIC DYE

ONTO ZEOLITE LTL

5.1 Abstract

To synthesis the two dyes into channel of zeolite L which are used for antenna system, a donor-acceptor such as Acridine - Hemicyanine (AC_Hemi), Acridine - Acriflavine (AC_AF) and Acriflavine - Thioindigo (AF_Thio) were prepared. The sequence of method to insert the dyes is cation exchange – gas phase (i -g), gas phase - cation exchange (g – i), gas phase - gas phase (g – g) or/and cation exchange_ gas phase (i – g). The results show that all the systems have a high quenching in the K-LTL and each system has a high quenching efficiency which is AC(g)_AF(i) K-LTL (72.2%), AC(i)_Hemi(g) (65.9%) and AF(i)_Thio(g) (52.6%). This result shows a high efficiency that can be applied for antenna material.

5.2 Introduction

Fluorescence Resonance Energy Transfer (FRET) is a distance dependent interaction between two molecules where the energy is transferred non radiatively from an excited donor molecule to an acceptor in ground state via an induced dipole–dipole interaction. Typically, the distance between donor–acceptor within 1–10 nm is ideal for energy transfer to occur (Lakowicz, 2006; Saha et al., 2016). Also, the energy transfer depends on the inverse sixth power of the distance between the two chromophores, the donor and acceptor. Fluorescence Resonance Energy Transfer (FRET) between an organic or laser dye in zeolite LTL channels are efficient processes for antenna applications such as solar cells sensitized by dye loaded zeolite LTL antenna and Luminescent solar concentrators (LSC) (Calzaferri, 2012; Insuwan et al., 2015). The zeolite LTL pore structure consists of one-dimensional channels that cross the crystal axis that acts as an organic dye support for host-guest composite materials by exploiting their one-dimensional structure. The different forms of zeolite K-LTL and H-LTL are significant as a host material with organic dye as a guest (Calzaferri, 2012; Insuwan et al., 2015; Szulbinski et al., 2001). These work concentrates on synthesis of dye-loaded zeolite L acting as artificial antenna system. In this material two different kinds of dyes with appropriate donor – acceptor properties are organized as monomers in spatially separated domains. The structure of the system allows the excitation of donor dye in the central part and fast transport of the energy to acceptor along the channel axis to the end of faces of crystals. The systems of donor-acceptor in the channel of zeolite L used in the study are Acridine (AC) – hemicyanine (hemi), acridine (AC) – acriflavine (AF), acriflavine (AF) – thioindigo (thio) and hemicyanine (hemi) - thionine (Th) (see Figure 5.1). The selective light absorbed by the donor dye located in the middle part of crystal

with cylindrical morphology then the energy migrates to the end of crystal which captured by the acceptor and then emitted as luminescence of acceptor molecule (Pauchard et al., 2000). In the previous chapter we organized the single dye molecule by cation exchange method for cationic dye and gas phase method (or thermal diffusion) for cationic and neutral dye with successful in preparation. The zeolite L sandwich material with dye1 in the middle part and the indicated dye2 at the both of the ends of the crystal (Figure 5.2) was prepared. However, the method for insertion of dye1 and dye2 plays an important role to an efficiency of the FRET. The efficiency of FRET was investigated on the systems prepared with different insertions of the dyes by ion exchange and gas phase method for donor (D) – acceptor (A) molecule such as ion exchange (i) – ion exchange (i), gas phase (g) – ion exchange (i) and gas phase (g) – gas phase (g).

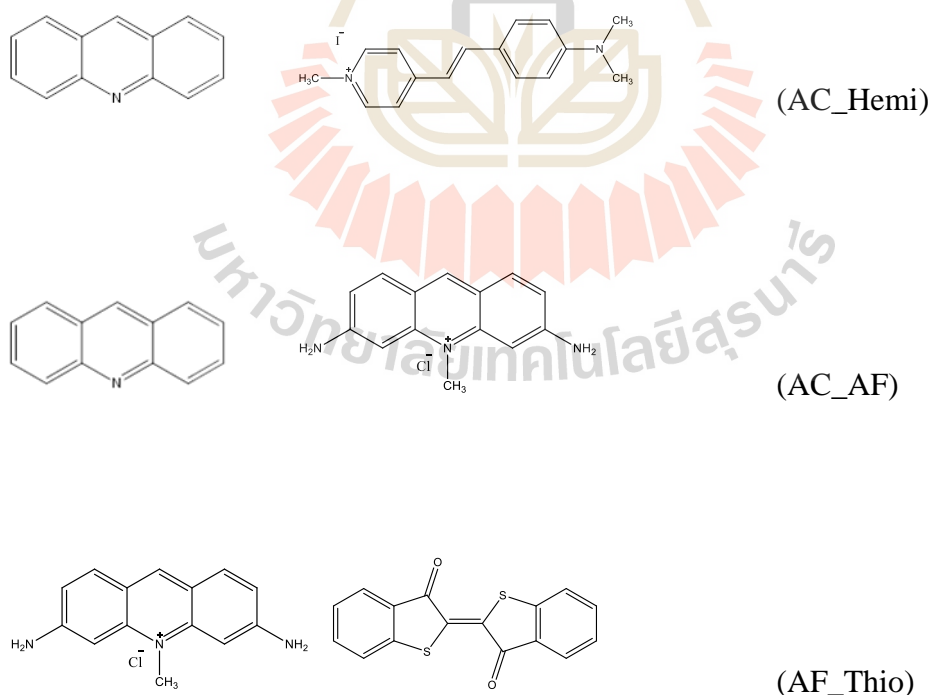


Figure 5.1 The donor - acceptor molecule for FRET study.

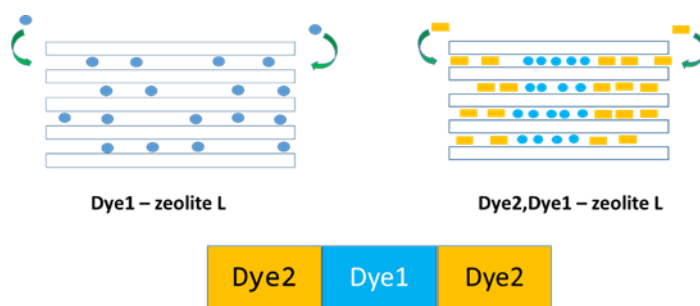


Figure 5.2 Insertion of two different dyes into the zeolite framework.

5.3 Material and Method

5.3.1 Synthesis of zeolite LTL

All materials used in this study are of reagent grade. The typical procedure for the preparation of synthesis gel of K-LTL zeolite was modified according to a Chapter III (page 32)

5.3.2 Dyes-loaded on zeolite LTL

Cation exchanged method

Incorporation of cationic dyes such as AC, AF, hemi and Th onto K-LTL, and H-LTL zeolite were performed at 30 °C using accurately weighed dehydrated zeolite LTL 0.5 g in a 125 mL conical flask. Then 50 mL of the dye solution with concentration of 0.1 mM added to a flask. The flask was sealed and transferred to a shaker bath for 24 hours to equilibrate the system. The dyes loaded zeolite LTL were collected by separation of solid from solution by centrifugation and dried at 100 °C overnight. To remove the dyes molecules on the zeolite surface, the following washing procedure was used. The suspension was transferred into a 125 mL conical flask with 50 mL n-butanol, sonicated for 10 minutes then stirred at room temperature for 24 hours. The n-butanol washing was repeated until the supernatant did not show dyes luminescence.

Gas phase procedure

For the gas phase method, the experiment corresponds with Chapter IV (page 62), 100 mg of zeolite L was mixed with neutral dye or cationic dye by using occupation probability = 0.25 ($p = 0.25$) which is appropriate for insertion that shows the high packing and low aggregation of dye in the channel of zeolite L.

Energy transfer measurement

The insertion of two different dyes was prepared by combination of ion exchange and gas phase method. We named dye1-zeolite L in the first step of the insertion and eventually, dye1 adsorbed on the outer surface of zeolite was removed. After that the second dye, dye2, was inserted. The conditions must be chosen such that dye1 has no chance to exit the channels when start of the second step. Once a dye2 molecule entered in each channel from both the ended sides of cylinder, the dye1 molecules have no chance to escape. In fact, they are pushed deeply into the channels by the incoming dye2 species, and formed the dye2, dye1-zeolite L material. The system of donor - acceptor in zeolite L that is (AC_Hemi), (AC_AF), (AF_Thio) and (AF_Th) was done by combined different insertions of dye1 and dye2 such as ion exchange - ion exchange (i-i), ion exchange – gas phase (i-g) and gas phase -gas phase (g-g) method.

Physical Measurements

UV/vis spectra were recorded on a T80+ UV-Vis spectrophotometer PG instruments. Dye molecules were dissolved in various solvents and quartz cuvette was used in the measurement. Diffuse reflectance spectra of dyes loaded on zeolite LTL was recorded using a Shimadzu UV-2550 UV-Visible spectrometer with the condition of slit width (5 nm), sampling interval (0.1 nm) and wavelength range of 200-800 nm. Fluorescence spectra were recorded on a luminescence spectrometer LS 50B (Perkin-Elmer). Dye molecules were measured either in various solvents in quartz cuvette or incorporated in zeolite LTL by suspending dyes/zeolite LTL in chloroform (~1 mg in 100 mL).

5.4 Result and discussion

5.4.1 Fluorescence resonance energy transfer (FRET) experiments.

FRET performance between donor and acceptor in zeolite

Efficiency of FRET

The Quenching efficiency (%Q) value and Förster distance (R_{DA}) indicates a proficiency of the artificial antenna which can be calculated as follows. The efficiency of the energy transfer (quenching efficiency, %E) was estimated by comparing the donor fluorescence with and without acceptor

$$\%Q = \left(1 - \frac{F_{DA}}{F_D}\right) \times 100\% \quad (5.1)$$

where F_{DA} is the fluorescence intensity of the donor in the presence of acceptor and F_D is the fluorescence intensity in the absence of the acceptor (Gfeller et al., 1997; Lakowicz, 2006; Minkowski et al., 2006)

The critical transfer distance (R_{DA})

The value of critical transfer distance (R_{DA}) between donor and acceptor molecules was calculated with Eq. (5.2) by using Förster's energy transfer relation (Cucinotta et al., 2014). Conceptually, the Förster critical distance is the maximal separation length between donor and acceptor molecules in which resonance energy transfer will still occur.

$$R_{DA}^6 = \frac{9000(\ln 10)\kappa_p^2\Omega_{DA}\Theta_D}{128\pi^5N_A n^4} \quad (5.2)$$

when κ_p^2 is the orientation factor set to equal 2/3, this assumes a random orientation of the emission and absorption dipole moments of the donor and acceptor respectively. While Ω_{DA} is an overlap integral for overlapping emission spectra of donor with absorption spectra of acceptor; Θ_D is quantum yield of donor; N_A is the Avogadro constant and n is the refractive index of the solvent (1.33 for H₂O and 1.4 for zeolite). The overlap integral, Ω_{DA} , between donor emission spectrum and an excitations spectrum of acceptor, are measured upon excitation energy of donor (Insuwan et al., 2015; Saha et al., 2016; Viani et al., 2016).

The rate constant for energy transfer (k_{ET})

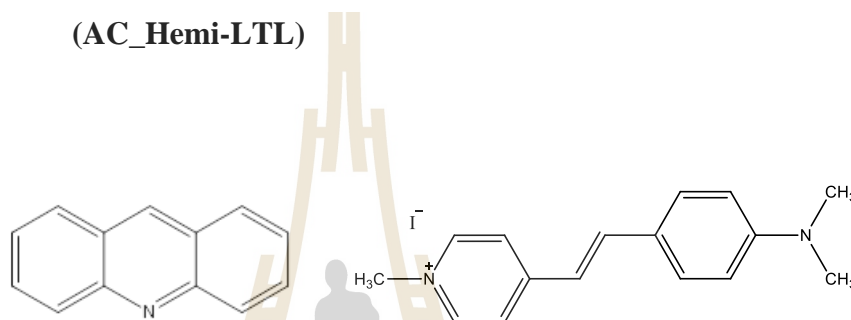
The rate constant for energy transfer from a donor into an acceptor as follows:

$$k_{ET} = \left(\frac{9000 \ln 10 \Phi_D}{128\pi^5 N_A n^4 \tau_D}\right) \Omega_{DA} G_{DA} \rho_D \rho_A \quad (5.3)$$

Where Φ_D and τ_D [s⁻¹] are the fluorescence quantum yield and the intrinsic fluorescence lifetime of the donor; N_A [mol⁻¹] is Avogadro's number; n is the refractive index of the medium; Ω_{DA} [cm³m⁻¹] is the spectral overlap integral between

the normalized donor emission and the acceptor absorption spectra; G_{DA} is the geometrical factor; p_D and p_A are the occupation probabilities of the sites with donors and acceptors, respectively (Lakowicz, 2006).

5.4.1.1 Acridine (AC)- Hemicyanine (hemi) Zeolite L system (AC_Hemi-LTL)



Scheme 5.1 AC and Hemi molecules.

The objective of the present work is to investigate the possibilities of energy transfer within antenna material. This material was prepared by inserted Ac (donor) and hemi (acceptor) molecules onto zeolite L. Energy transfer and migration in this system is governed by long-rang dipole-dipole interactions known as Förster mechanism due to the absence of any orbital overlap between the dye molecules. Energy transfer processes occur when the separation distance between donor and acceptor species is at least 10 Å. (Saha et al., 2016). Figure 5.3 illustrates the absorption and emission spectra of both dyes (AC and hemi) in the aqueous solution.

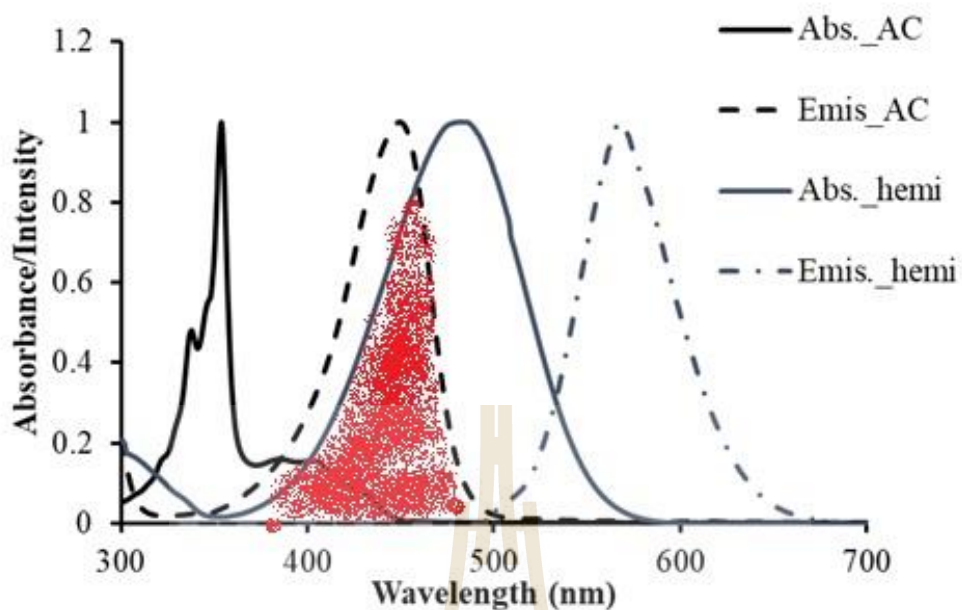


Figure 5.3 Energy transfer experiment, absorption and emission spectra of Ac and Hemi dissolved in aqueous solution.

The samples of AC_Hemi zeolite L prepared by different sequences of the used method under the concentration of loaded dye by ion exchange are 0.01 mM and by gas phase with an occupation probability of loaded dye is 0.25 ($p=0.25$). The emission spectra of these samples are shown in Figure 5.4. The excitation wavelength of the dyes loaded on zeolite LTL was fixed at 355 nm that only Ac (donor) can absorb.

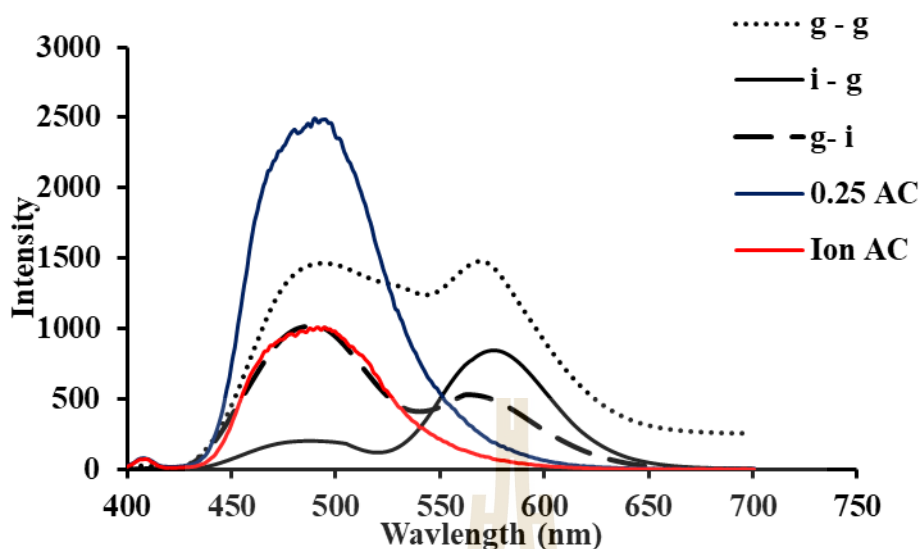


Figure 5.4 The emission spectra of AC – K-LTL prepared by the ion exchange and gas phase method (red line and blue line) and the emission spectra of AC and Hemi in the system of AC_Hemi K-LTL with different sequences of the method for inclusion and that excited at 355 nm for the energy transfer experiment.

Figure 5.4a shows the emission spectra of Ac loaded on zeolite K-LTL with the ion exchange and gas phase method. The emission spectra observed at $\lambda_{em} = 485$ nm that is overlap with the excitation spectra of Hemi on K-LTL ($\lambda_{ex} = 485$ nm) implying that the energy transfer might happen in an appropriate distance. The sequence for using the method to insert AC and Hemi onto zeolite L is important to energy transfer efficiency. The parameters of FRET shown in Table 5.1 were calculated from Figure 5.4

Table 5.1 Calculated overlap integral, quantum yield, Förster distance and quenching efficiency for the donor–acceptor pairs of AC_Hemi K-LTL.

Sequence of the loading method AC_Hemi - K-LTL	Overlap integral (Ω_{DA}) $10^{12} \text{ cm}^{-1} \text{ M}^{-1} (\text{nm})^4$	Quantum yield (Θ_D)	Forster distance, R_{DA} (Å)	Quenching efficiency (%Q)
i - g	15.58	0.66	26.5	65.9
g - i	10.75	0.66	24.3	46.5
g - g	12.56	0.66	24.7	58.7

Table 5.1 shows the results of the calculated overlap integrals (Ω_{DA}) and critical transfer distance (R_{DA}) for AC_Hemi K-LTL pair using Eqs. (5.1) and (5.2), in which Θ_D was 0.66 (Insuwan et al., 2015; Kubota et al., 1977) and κ_p^2 was 2/3. The theoretical efficiency of energy transfer between donor and acceptor can be estimated by calculating the Förster distance for the pair. Typically, the Förster distance is 20–90 Å. In this case, AC- Hemi-K-LTL prepare by i - g, in which AC was loaded by ion exchange method and Hemi by gas phase method, has higher quenching efficiency (65.9%) than that g – i (46.5%) and g -g (58.7%) due to Hemi (acceptor) able to insert into zeolite more by gas phase method. In contrast, high loading by gas phase method can reduce the R_{DA} distance and quenching efficiency. The longer the Förster distance of the donor – acceptor pair is, the more efficient the energy transfer between them becomes (Insuwan et al., 2015; Ryder et al., 2003).

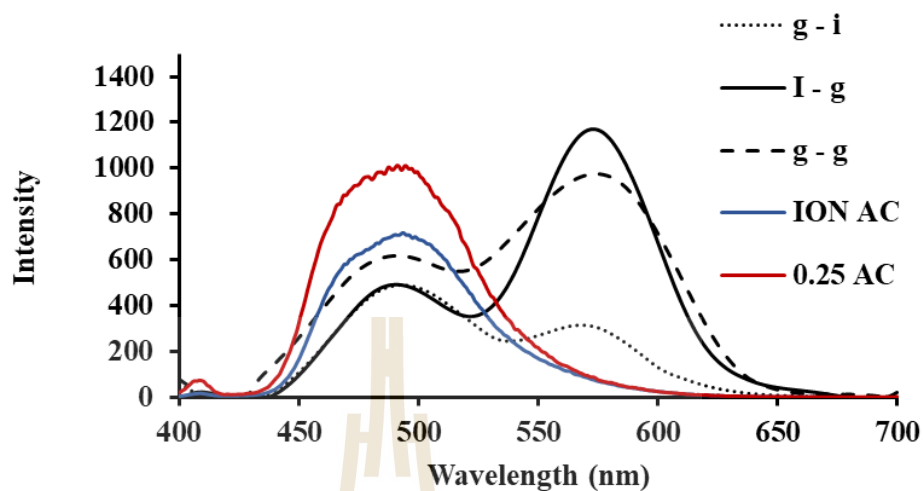


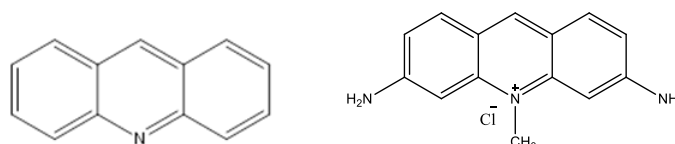
Figure 5.5 The emission spectra of AC – H-LTL prepare by the ion exchanged and gas phase method (blue and red line) and the emission spectra of AC and Hemi in the system of AC_Hemi-H-LTL with different sequences of the method for inclusion and that excited at 355 nm for the energy transfer experiment.

Table 5.2 Calculated overlap integral, quantum yield, Förster distance and quenching efficiency for the donor–acceptor pairs of AC_Hemi H-LTL.

Sequence of the loading method AC_Hemi - H-LTL	Overlap integral (Ω_{DA}) $10^{12} \text{ cm}^{-1} \text{ M}^{-1} (\text{nm})^4$	Quantum yield (Θ_D)	Forster distance, R_{DA} (Å)	Quenching efficiency (%Q)
i - g	20.53	0.66	26.5	50.1
g - i	14.85	0.66	24.3	42.1
g - g	15.15	0.66	24.7	41.3

Figure 5.5 shows the emission spectra of AC – Hemi loaded on H-LTL zeolite (red and blue line that is a protonated form of LTL zeolite). The preparation of this system is the same as AC – Hemi loaded on LTL zeolite (K form of LTL) as mentioned above. But in this case the gas phase method seems to be unsuitable to load AC on H-LTL. It shows the emission spectrum with quite low intensity compared to AC loaded on K-LTL. AC might be partially degraded in protonated form of zeolite at the same temperature used to load AC in K form. The FRET performance and parameter can be calculated and shown in Table 5.2. AC_Hemi H-LTL prepared by i - g , is still higher quenching efficiency (50.1%) than that by g – i (42.1%) and g -g (41.3%) but AC_Hemi H-LTL systems still remain lower quenching efficiency than AC_Hemi K-LTL system due to the degradation of the dye. As the results, the fluorescence intensity of Hemi is increased with an increase in loading of Hemi by the gas phase method. These results demonstrated clearly that Hemi would be proximity to the AC molecules when loaded on zeolite LTL, resulting in an efficient resonance energy transfer from Ac to Hemi in the AC_hemi K-LTL and H-LTL system.

5.4.1.2 Acridine (AC)- Acriflavine (AF) Zeolite L system (AC_AF - LTL)



Scheme 5.2 AC and AF molecules.

From the previous work, the system of (AC_AF - LTL) prepared by ion exchange method, the low loading of donor (AC) and acceptor according from the limiting case of the kinetic diameter of the channel opening and the diffusion species (Insuwan et al., 2015). In this work the sequence and the different methods for insertion of two dyes into zeolite LTL was investigated for improvement and prepared samples as artificial antenna system

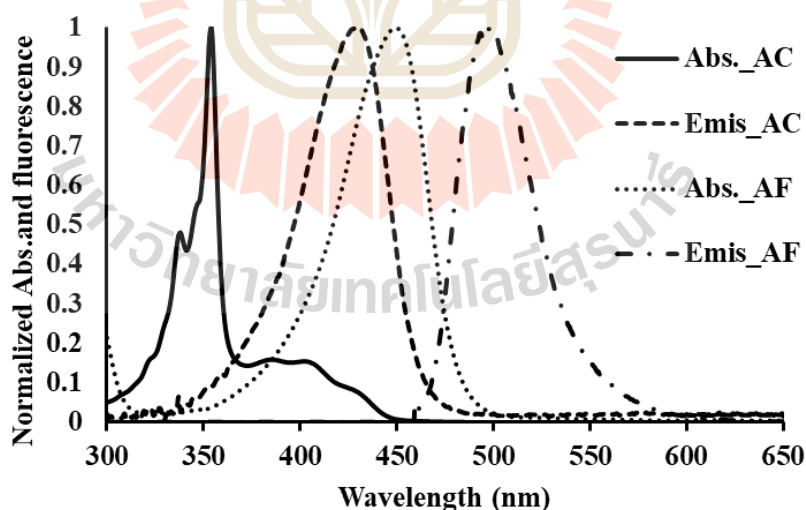


Figure 5.6 Absorption and emission spectra of Ac and hemi dissolved in aqueous solution for the energy transfer experiment.

For AC_AF zeolite L system, the preparation of these samples is the same as the systems of AC_Hemi zeolite L as mentioned above. The emission spectra of AC_AF zeolite K-LTL are shown in Figure 5.7, respectively. The excitation wavelength of the dyes loaded on zeolite LTL was fixed at 355 nm that only Ac (donor) can absorb.

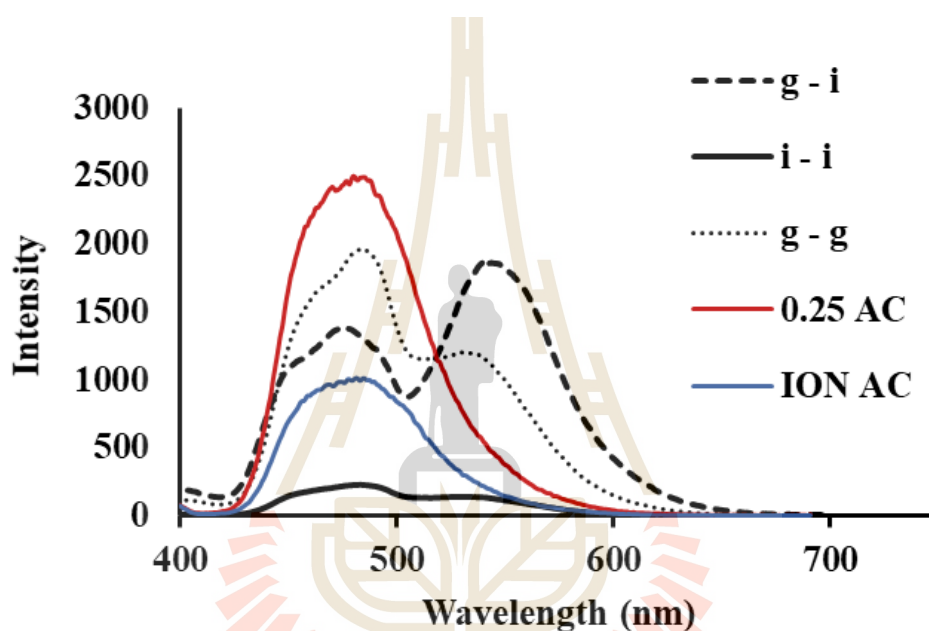


Figure 5.7 The emission spectra of AC – K-LTL prepared by the ion exchanged and gas phase method (blue and red line). The emission spectra of AC and AF in the system of AC_AF-K-LTL with different sequences of the method for inclusion and that excited at 355 nm for the energy transfer experiment.

Figure 5.7 shows the emission spectra of Ac loaded on zeolite K-LTL with the ion exchange and gas phase method (red and blue line). The observed emission is at $\lambda_{em} = 485$ nm which overlaps with the excitation spectra of AF on K-LTL ($\lambda_{ex} = 475$ nm). The FRET occurs from AC to AF molecule when AC molecule is excited ($\lambda_{ex} = 355$ nm). The quenching efficiency and performance of FRET used for antenna material

were calculated from the system of AC_AF zeolite LTL (Figure 5.7) prepared with the difference in the sequence and the method. The results are shown in Table 5.3.

Table 5.3 Calculated overlap integral, quantum yield, Förster distance and quenching efficiency for the donor–acceptor pairs of AC_AF_K-LTL.

Sequence of the loading method AC_AF -K- LTL	Overlap integral (Ω_{DA}) $10^{12} \text{ cm}^{-1} \text{ M}^{-1} (\text{nm})^4$	Quantum yield (Θ_D)	Forster distance, R_{DA} (Å)	Quenching efficiency (%Q)
i - i	10.85	0.66	21.5	68.3
g - i	9.35	0.66	24.3	72.7
g - g	15.15	0.66	24.7	40.4

Table 5.3 shows the FRET performance and FRET parameters. The quenching efficiency of the sample prepared with loading AC (donor) by gas phase method and acceptor (AF) by ion exchange method is higher than that by i – i (68.3%) and g – g (40.4%) that refers to an increase in the loading of the donor able to increase the quenching efficiency and FRET performance. However, in the case of g-g, the high loading of donor (AC) and acceptor (AF) refers to an occurrence of more aggregation of dye is increased.

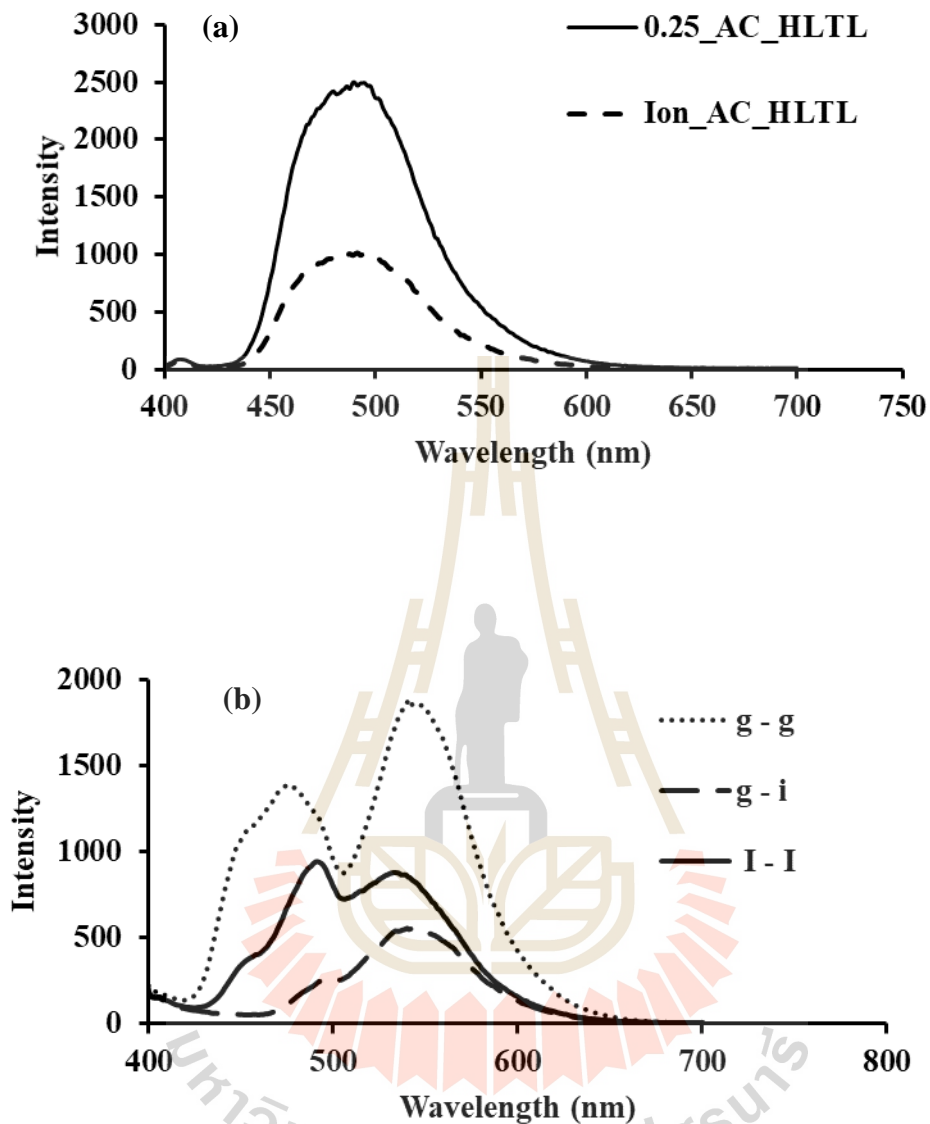


Figure 5.8 a). The emission spectra of AC – H-LTL prepared by the ion exchanged and gas phase method. b) The emission spectra of AC and AF in the system of AC_AF-H-LTL with different sequences of the method for inclusion and that excited at 355 nm for the energy transfer experiment.

All the systems of AC_AF-H-LTL (i - i, g - i and g - g) arise the energy transfer from AC to AF. The system of g - g shows the high intensity emission of AC

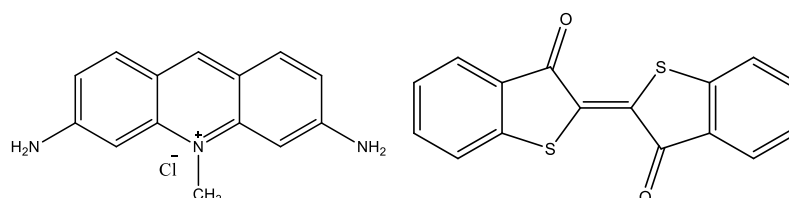
and AF at $\lambda_{em} = 485$ nm and 550 nm, respectively, (Figure 5.8b) referring to the high packing of dye in the channel of zeolite L. However, the high packing of AC by the gas phase method affects the low loading of AF dye in the second step by the cation exchange. That causes to the g - i system giving the emission intensity of AF ($\lambda_{em} = 550$ nm) lower than g – g system.

Table 5.4 Calculated overlap integral, quantum yield, Förster distance and quenching efficiency for the donor–acceptor pairs of AC_AF H-LTL.

Sequence of the loading method AC_AF -H- LTL	Overlap integral (Ω_{DA}) $10^{12} \text{ cm}^{-1} \text{ M}^{-1}$ (nm) ⁴	Quantum yield (Φ_D)	Forster distance, R_{DA} (Å)	Quenching efficiency (%Q)
i - i	8.54	0.66	21.2	62.3
g - i	8.42	0.66	20.8	60.2
g - g	7.86	0.66	19.7	40.4

The more efficient of the energy transfer between donor – acceptor pair becomes from the longer Förster distance of them. In this case, AC_AF H-LTL (i – i) system has a longer Förster distance than AC_AF H-LTL (g – g) but it is close to AC_AF H-LTL (g – i) that is 21.2, 0.66 and 19.7, respectively, and the quenching efficiency is 62.3, 60.4 and 40.4, respectively.

5.4.1.3 Acriflavine (AF) – Thioindigo (Thio) Zeolite L system (AF_Thio-LTL)



Scheme 5.3 AF and Thio molecules.

For development the antenna material, the luminescence might be cover blue to red region that is variety for application of antenna material effectively. Thus, this system develops from green (AF) to red (Thio) luminescence. The absorption and emission spectra of AF and Thio in aqueous solution are shown in Figure 5.9. A large area (grey region) of overlapping emission spectra of donor (AF) and absorption spectra of acceptor (Thio) tends to high quenching efficiency of the energy transfer from a donor (AF) to an acceptor (Thio).

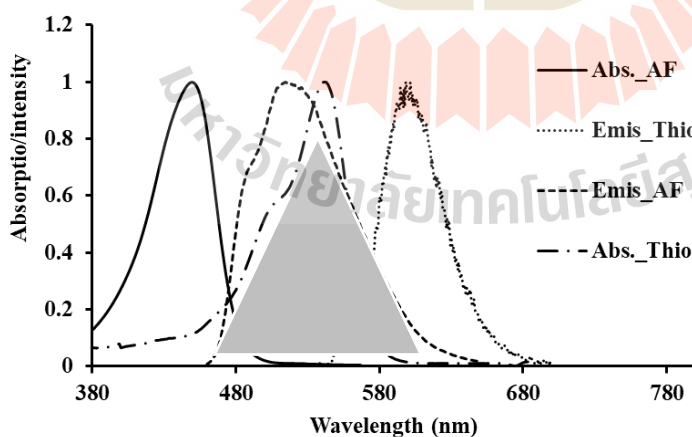


Figure 5.9 Energy transfer experiment, absorption and emission spectra of Ac and hemi dissolved in aqueous solution.

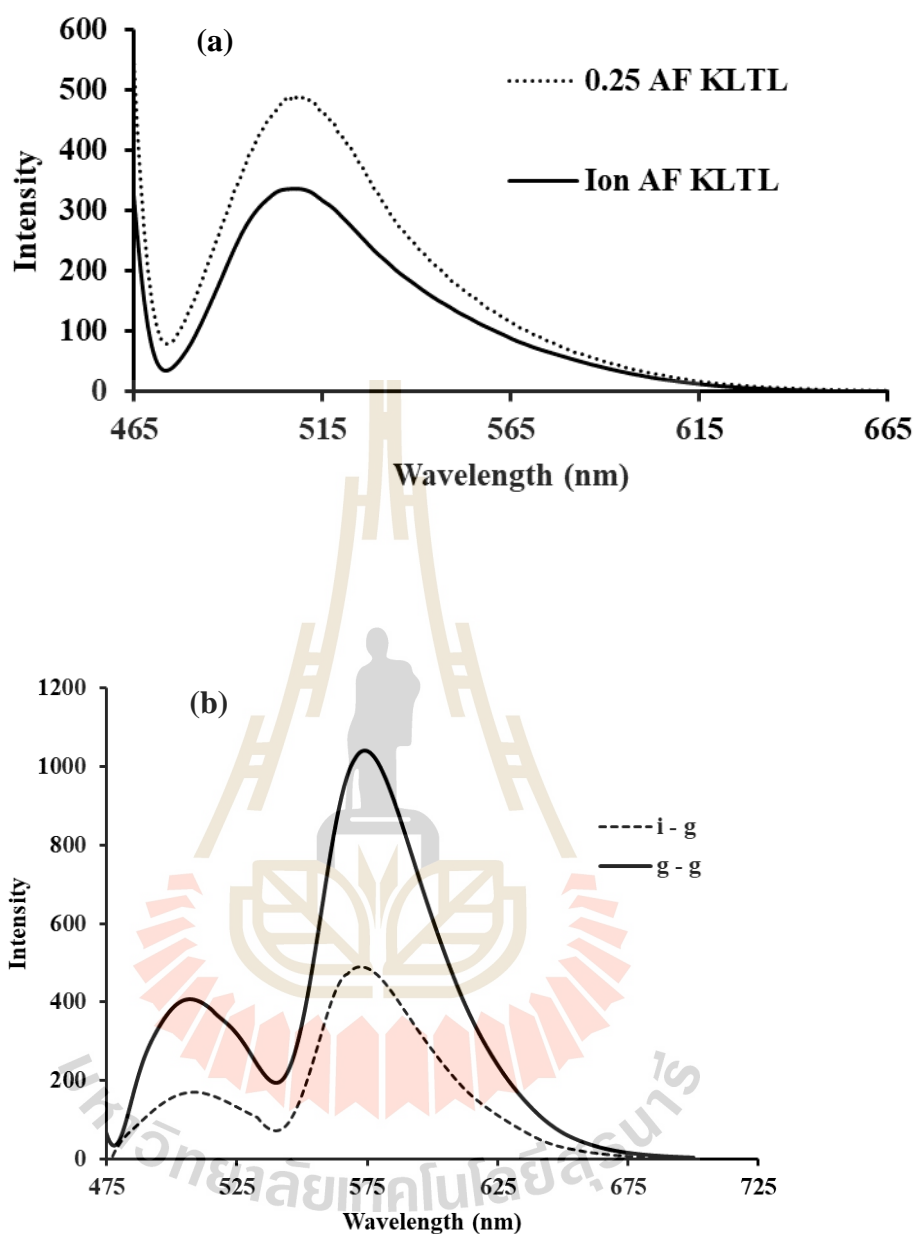


Figure 5.10 a). The emission spectra of AF- K-LTL prepare by the ion exchanged and gas phase method. b) The emission spectra of AF and Thio in the system of AF_Thio-KH-LTL with different sequences of the method for inclusion and that excited at 465 nm for the energy transfer experiment.

The emission spectra of AF loaded on K-LTL with the cation exchange and gas phase method are at $\lambda_{em} = 525$ nm (Figure 5.10a). Due to a neutral dye of Thio, the gas phase method is used only for loading, the two system of AF_Thio-K-LTL, (**i - g**) and (**g - g**), are achieved. Figure 5.10b illustrates the emission spectra of these two systems (**i-g** and **g-g**). The emission spectra of Thio was observed at $\lambda_{em}=585$ nm with an excitation of AF at $\lambda_{ex} = 475$ nm. This refers to the transfer of energy from AF to Thio continuously. The quenching efficiency and other parameters are shown in Table 5.5. For the **i - g** system, the quenching efficiency (52.6%) and Förster distance (20.7) are higher than **g - g** system. A large molecule of Thio dye, normally is hard to be inserted onto zeolite L. Thus, a high temperature is needed for inclusion that causes to destroy the donor (AF) which is inserted before with the first step.

Table 5.5 Calculated overlap integral, quantum yield, Förster distance and quenching efficiency for the donor–acceptor pairs of AF_Thio_K-LTL.

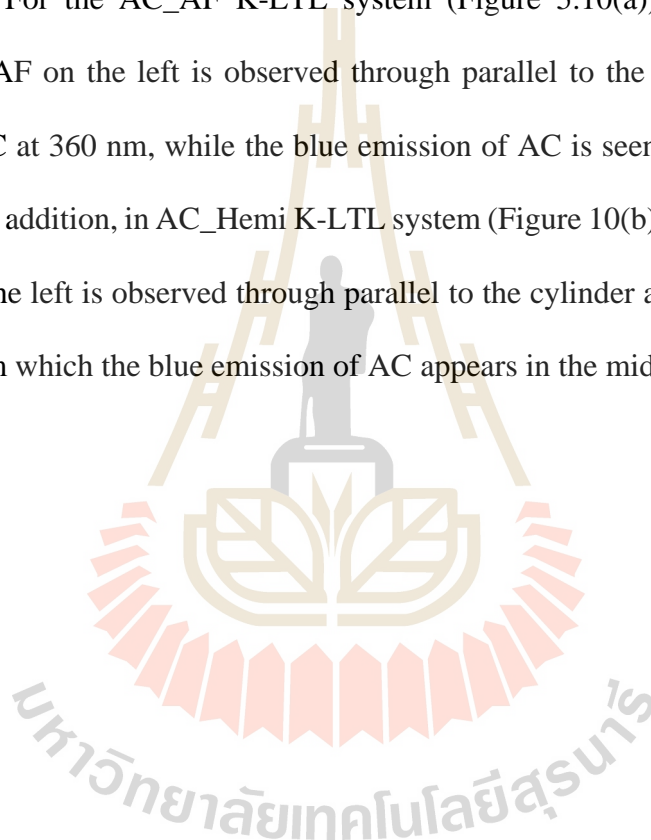
Sequence of the loading method	Overlap integral (Ω_{DA}) $10^{12} \text{ cm}^{-1} \text{ M}^{-1} (\text{nm})^4$	Quantum yield (Φ_D)	Forster distance, R_{DA} (Å)	Quenching efficiency (%Q)
AF_Thio - K-LTL i - g	8.54	0.83	20.7	52.6
g - g	6.65	0.83	17.8	34.8

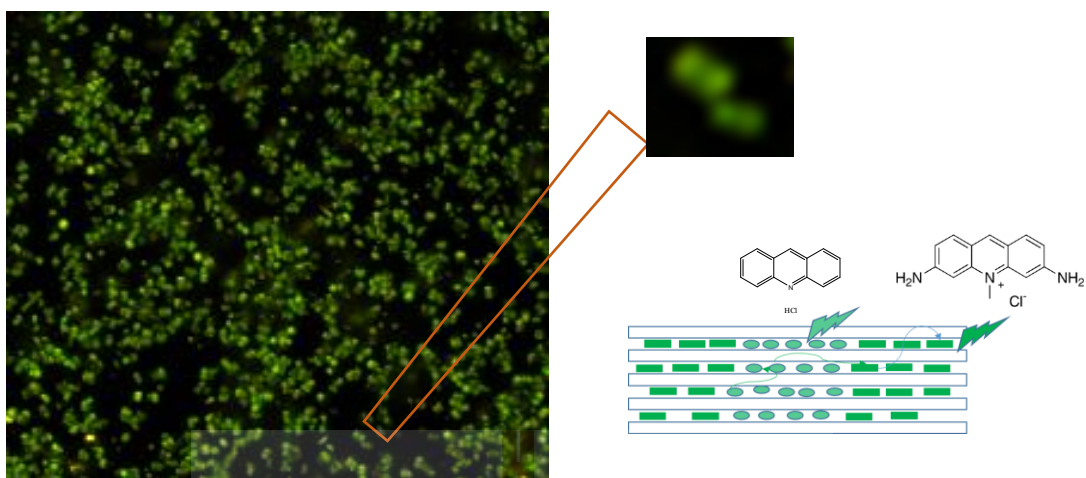
In the case of AF_Thio H-LTL system, we cannot apply the gas phase method to Thio dye inserted onto H LTL zeolite (protonate form) due to the high

temperature be required for insertion causing to degrade and damage the dye resulting in the loss of the luminescence properties of the system.

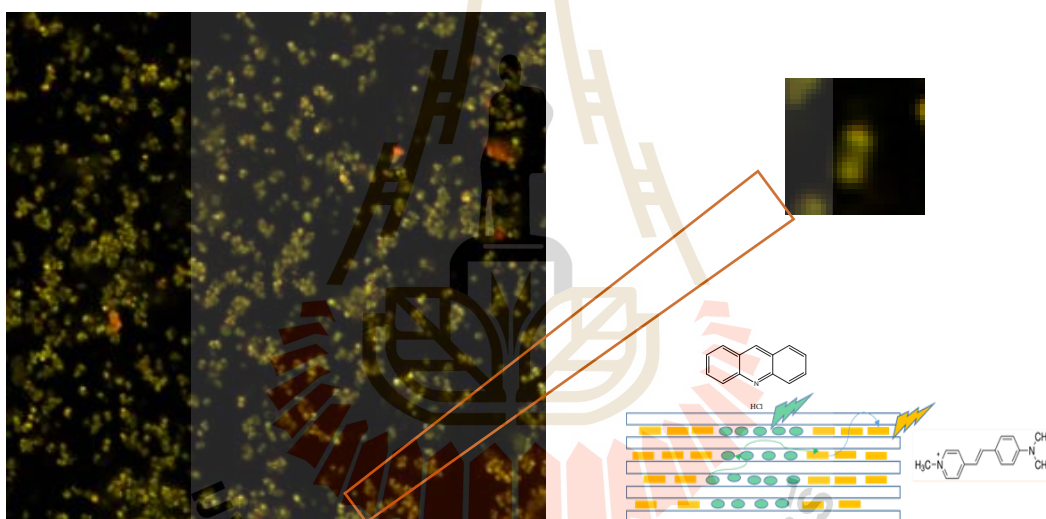
5.4.2 The energy transfer with confocal microscope

The confocal microscope observed the crystals in a microscope equipped with appropriate filters and using an immersion lens gives the pictures in Figure 5.11. For the AC_AF K-LTL system (Figure 5.10(a)), the yellow - green emission of AF on the left is observed through parallel to the cylinder axis with an excitation AC at 360 nm, while the blue emission of AC is seen in the middle part of the crystal. In addition, in AC_Hemi K-LTL system (Figure 10(b)), the orange emission of Hemi on the left is observed through parallel to the cylinder axis with an excitation AC at 360 nm which the blue emission of AC appears in the middle part of the crystal.





a. AC_AF K-LTL system



b. AC_Hemi K-LTL system

Figure 5.11 Schematic representation of a crystal with donors (Blue) at the middle and acceptors (green and yellow) in the both end sides, immersion with microscopy images a) AC_AF K-LTL system and b) AC_Hemi K-LTL system

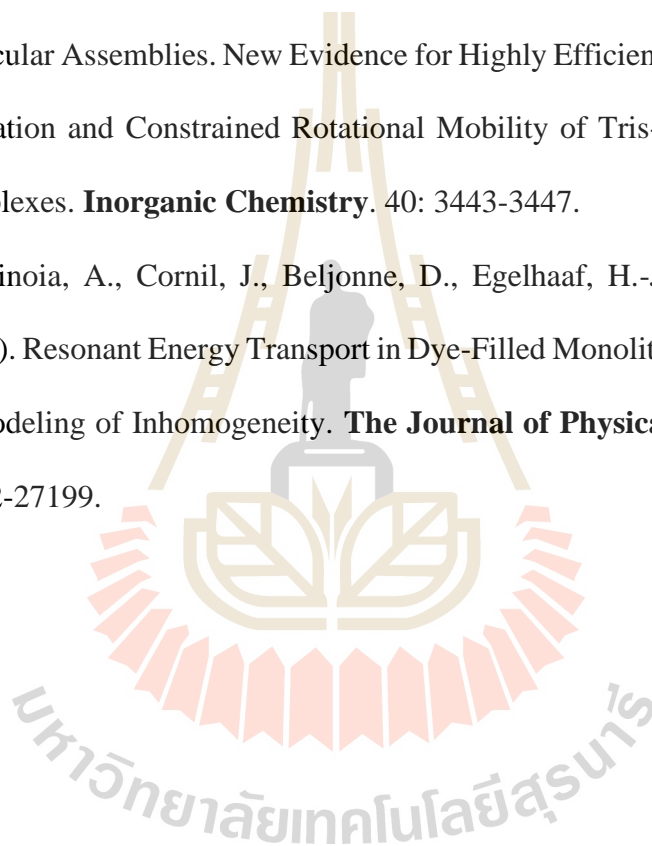
5.5 Conclusion

A variety of antenna systems with light harvesting properties and effective energy transfer were demonstrated on different materials. The sequence of the used method of two dyes insertion onto K-LTL and H-LTL zeolite affect on the energy transfer efficiency. In this study, the sequence of the used method for donor and acceptor is ion exchange and gas phase method, respectively, denoted as (**i – g**), gas phase – ion exchange method (**g-i**) and gas phase – gas phase method (**g - g**). For the systems composed of pair of cationic dyes are AC_Hemi LTL and AC_AF LTL. The quenching efficiency of AC_Hemi K-LTL system for (**i – g**), (**g – i**) and (**g – g**) is 65.9%, 45.9% and 58.7% ,respectively, and those of AC_AF K-LTL is 68.3% (**i – i**), 72.7% (**i – g**) and 40.4% (**g – g**). While the system of two different types of dye as cationic (AF) and neutral (Thio) dye, AF_Thio K-LTL, has quenching efficiency 53.6% (**i – g**) and 34.8% (**g – g**). Unfortunately, protonated form of zeolite L (H-LTL) for this system is unsuitable due to high temperature required for insertion of dye including an existence of Bronsted acidic site of zeolite framework causing to degradation of dye molecule that affects luminescent properties. However, the sequencing method for inclusion dye onto zeolite L that improve efficiency energy transfer and opportunities for developing new photonic devices.

5.6 References

- Calzaferri, G. (2012). Nanochannels: hosts for the supramolecular organization of molecules and complexes. **Langmuir**. 28: 6216-6231.
- Cucinotta, F., Guenet, A., Bizzarri, C., Mróz, W., Botta, C., Milián-Medina, B., De Cola, L. (2014). Energy Transfer at the Zeolite L Boundaries: Towards Photo- and Electroresponsive Materials. **ChemPlusChem**. 79: 45-57.
- Gfeller, N., and Calzaferri, G. (1997). Energy Migration in Dye-Loaded Hexagonal Microporous Crystals. **The Journal of Physical Chemistry B**. 101: 1396-1408.
- Insuwan, W., Jungsuttiwong, S., and Rangsrivatananon, K. (2015). Host-guest composite materials of dyes loaded zeolite LTL for antenna applications. **Journal of Luminescence**. 161: 31-36.
- Kubota, Y., and Steiner, R.F. (1977). Fluorescence decay and quantum yield characteristics of acridine orange and proflavine bound to DNA. **Biophysical Chemistry**. 6: 279-289.
- Lakowicz, R. (2006). Energy Transfer. In J. R. Lakowicz (Ed.), *Principles of Fluorescence Spectroscopy* (pp. 443-475). Boston, MA: Springer US.
- Minkowski, C., Pansu, R., Takano, M., and Calzaferri, G. (2006). Energy Collection, Transport, and Trapping by a Supramolecular Organization of Dyes in Hexagonal Zeolite Nanocrystals. **Advanced Functional Materials**. 16: 273-285.
- Pauchard, M., Devaux, A., and Calzaferri, G. (2000). Dye-Loaded Zeolite L Sandwiches as Artificial Antenna Systems for Light Transport. **Chemistry – A European Journal**. 6: 3456-3470.

- Ryder, A., Power, S., and Glynn, T. (2003). Evaluation of Acridine in Nafion as a Fluorescence-Lifetime-Based pH Sensor (Vol. 57).
- Saha, J., Dey, D., Roy, A.D., Bhattacharjee, D., and Hussain, S.A. (2016). Multi step FRET among three laser dyes Pyrene, Acriflavine and Rhodamine B. **Journal of Luminescence**. 172: 168-174.
- Szulbinski, W.S., Ma'nue, D.J., and Kincaid, J.R. (2001). Zeolite-Entrapped Organized Molecular Assemblies. New Evidence for Highly Efficient Adjacent Cage Dyad Formation and Constrained Rotational Mobility of Tris-Ligated Polypyridine Complexes. **Inorganic Chemistry**. 40: 3443-3447.
- Viani, L., Minoia, A., Cornil, J., Beljonne, D., Egelhaaf, H.-J., and Gierschner, J. (2016). Resonant Energy Transport in Dye-Filled Monolithic Crystals of Zeolite L: Modeling of Inhomogeneity. **The Journal of Physical Chemistry C**. 120: 27192-27199.



CHAPTER VI

CONCLUSIONS

Zeolite L can be synthesized with different morphologies such as cylindrical, round, ice hockey and clam shape with a size in micrometer to nanometer which can be applied in various functions. The dye-zeolite L composites were prepared with cationic dyes such as AC, AF, Hemi and Th. The adsorption isotherms of those dyes are fitted well to Langmuir isotherm and the thermodynamic parameters are summarized in table 6.1 and 6.2

Table 6.1 Thermodynamic parameters for adsorption of dyes on K-LTL.

Sample	temp (K)	ΔG° (kJ/mol)	ΔH° (kJ/mol)
Acridine	303	-28.82	21.15
	313	-30.31	
	323	-32.11	
Acriflavine	303	-28.26	32.79
	313	-30.61	
	323	-33.75	

Table 6.1 Thermodynamic parameters for adsorption of dyes on K-LTL (Continued).

Sample	temp (K)	ΔG° (kJ/mol)	ΔH° (kJ/mol)
Hemicyanine	303	-27.65	29.47
	313	-29.42	
	323	-31.43	
Thionine	303	-27.98	31.06
	313	-29.79	
	323	-31.88	

Table 6.2 Thermodynamic parameters for adsorption of dyes on H-LTL

Sample	temp (K)	ΔG° (kJ/mol)	ΔH° (kJ/mol)
Acridine	303	-27.58	21.15
	313	-30.11	
	323	-32.58	
Acriflavine	303	-29.01	32.79
	313	-30.62	
	323	-32.09	

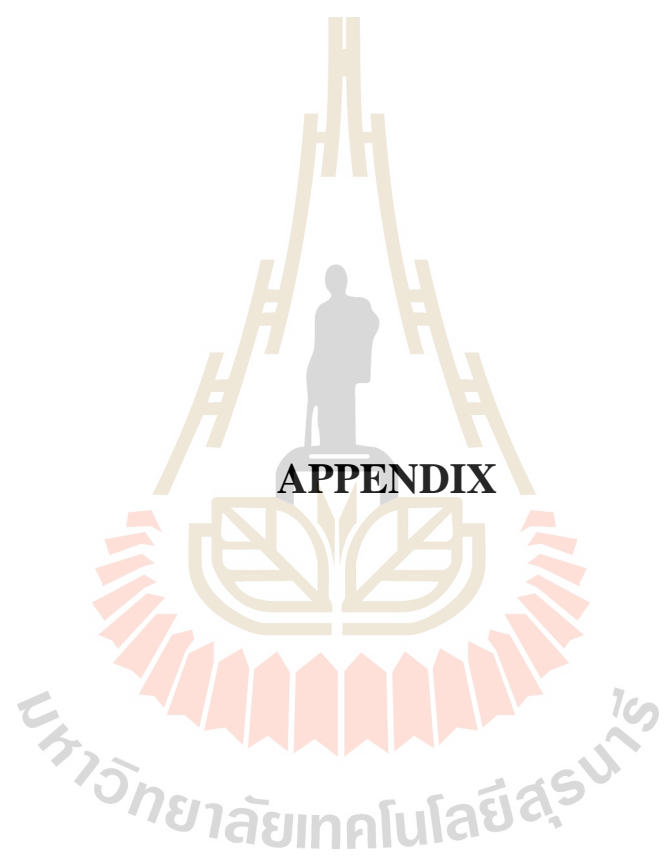
Table 6.2 Thermodynamic parameters for adsorption of dyes on H-LTL (Continued).

Sample	temp (K)	ΔG° (kJ/mol)	ΔH° (kJ/mol)
Hemicyanine	303	-28.23	
	313	-29.72	29.47
	323	-31.28	
Thionine	303	-27.10	
	313	-29.78	31.06
	323	-32.03	

All of cationic dyes show the thermodynamic parameters with negative values of ΔG° (28-32 kJ/mol) and the positive values of ΔH° (21 – 32 kJ/mol) that refer to the higher adsorption capacity observed and the adsorption process is endothermic, respectively. For dye – zeolite L composite, the cationic dyes are normally used for inclusion by cation exchange method which has a limit for dyes incorporated on the channel. To improve this, the gas phase method (thermal diffusion) was employed for the dye-zeolite composite prepared with cationic and neutral dyes such as AC, AF, Hemi, Thio and Th. In addition, the different occupation probabilities ($p = 0.10, 0.25, 0.50$ and 1.00) were used to prepare dye_K-LTL and dye_H-LTL zeolite by the gas phase method. The samples show the high amount of the dye intercalated in the channel of zeolite and the dye aggregation arises as the high loading ($p = 0.50$ and 0.10) that causes to a self – absorption and a reduction of luminescence properties. However, in the case of zeolite H-LTL the gas phase method is unsuitable for some dye such as Thio

due to the protonated form able to degrade with high temperature. The high luminescence property and avoidance of the aggregation of the dye molecule appear at the occupation probability (p) of 0.25 that shows a good result. Consequently, at $p = 0.25$ was applied in the gas phase method for the study of fluorescence resonance energy transfer (FRET).

For the FRET of donor_acceptor-zeolite L, the system is AC_Hemi-LTL, AC_AF-LTL and AF_Thio-LTL, In this study, the sequence of the used method for donor and acceptor is ion exchange and gas phase method, denoted as (**i – g**), gas phase – ion exchange method (**g-i**), gas phase – gas phase method (**g - g**) and cation exchange - cation exchange (**i – i**). The results show that all the systems have a high quenching in the K-LTL zeolite and each system has a high quenching efficiency, which is AC(g)_AF(i) KLTL (72.2%), AC(i)_Hemi(g) (65.9%) and AF(i)_Thio(g) (52.6%). This result shows a high efficiency that can be applied and improved for antenna material and optical devices.



APPENDIX

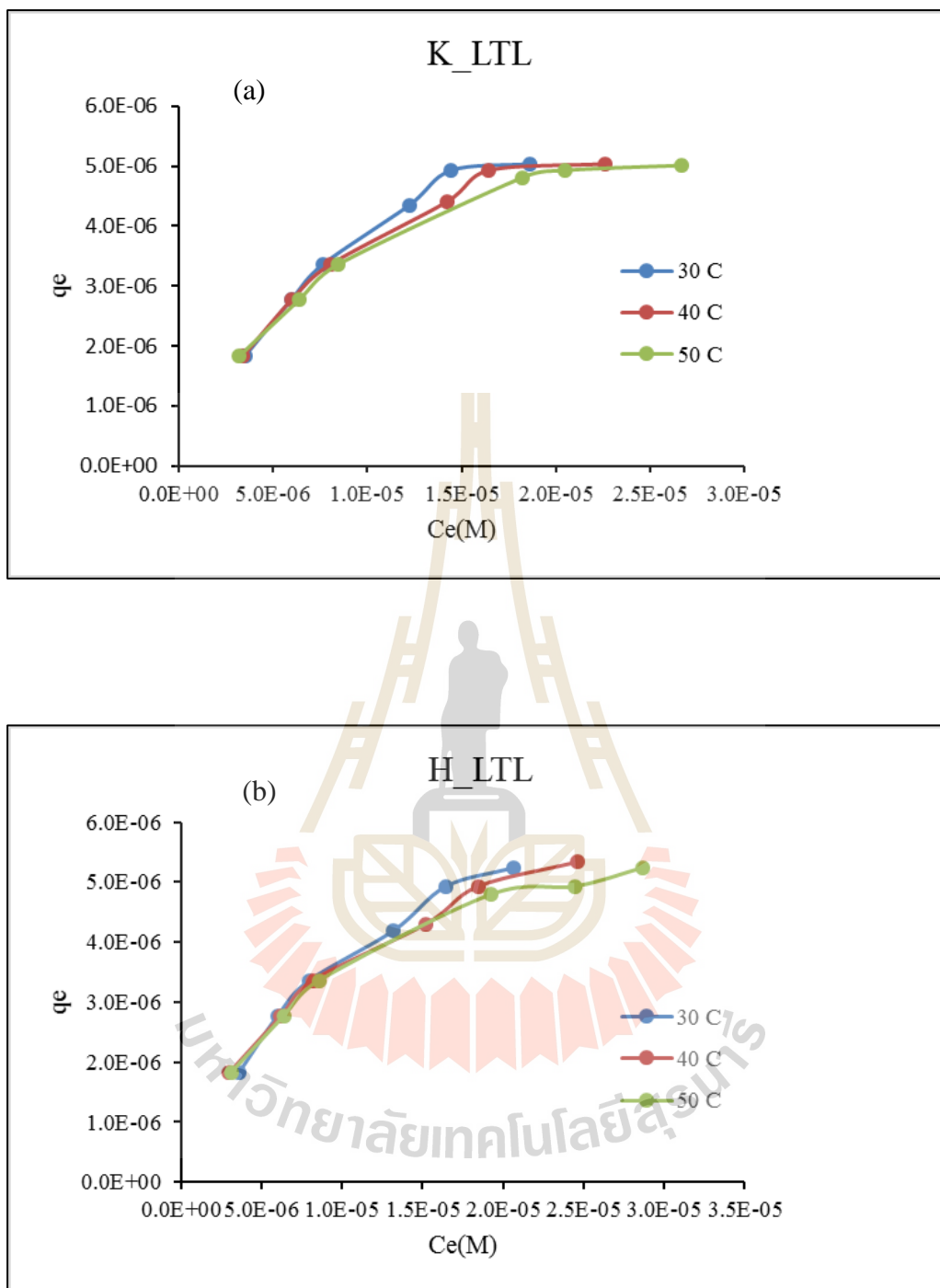


Figure A1 Adsorption isotherms of AF on K-LTL(a) and H-LTL(b) at 303, 313 and 323 K.

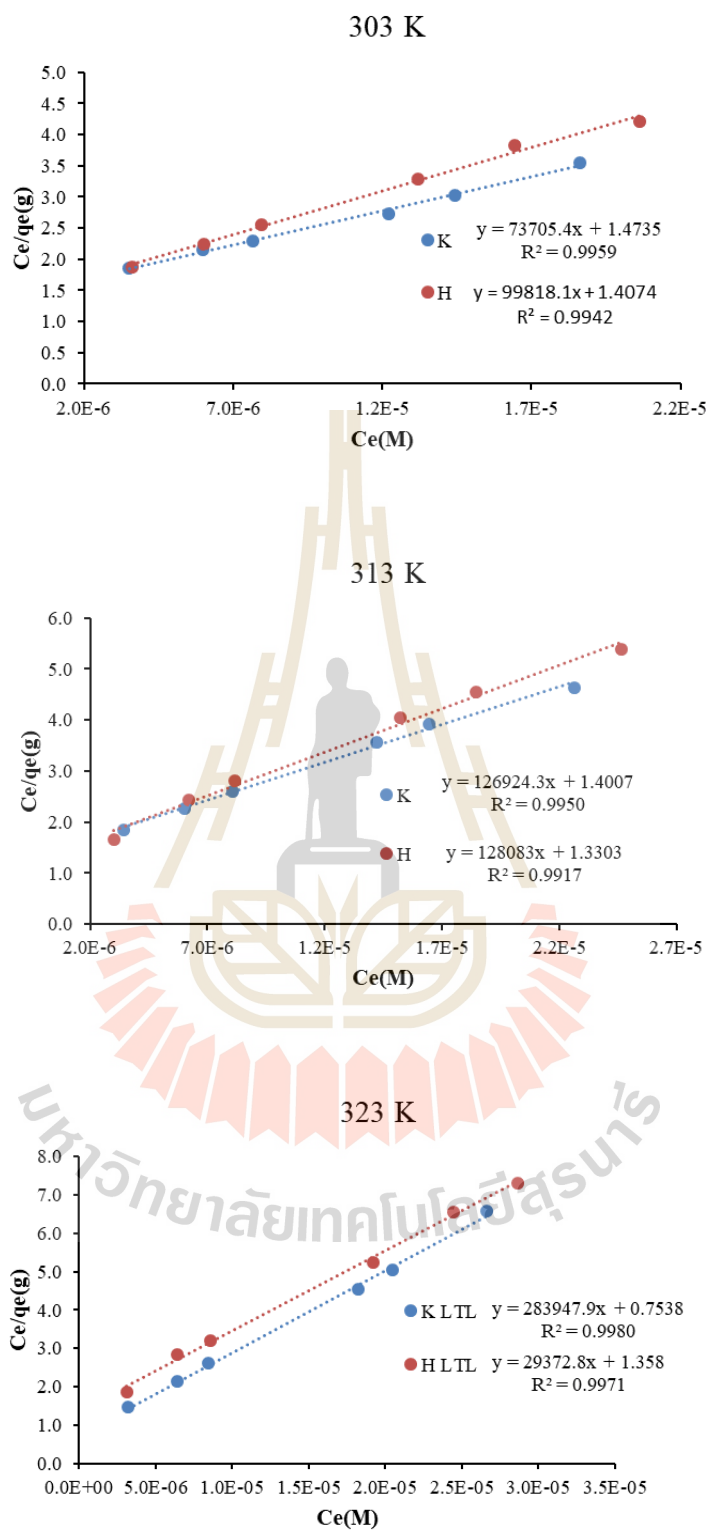


Figure A2 Linear plot of Langmuir isotherm of AF on K-LTL and H-LTL at 303, 313 and 323 K.

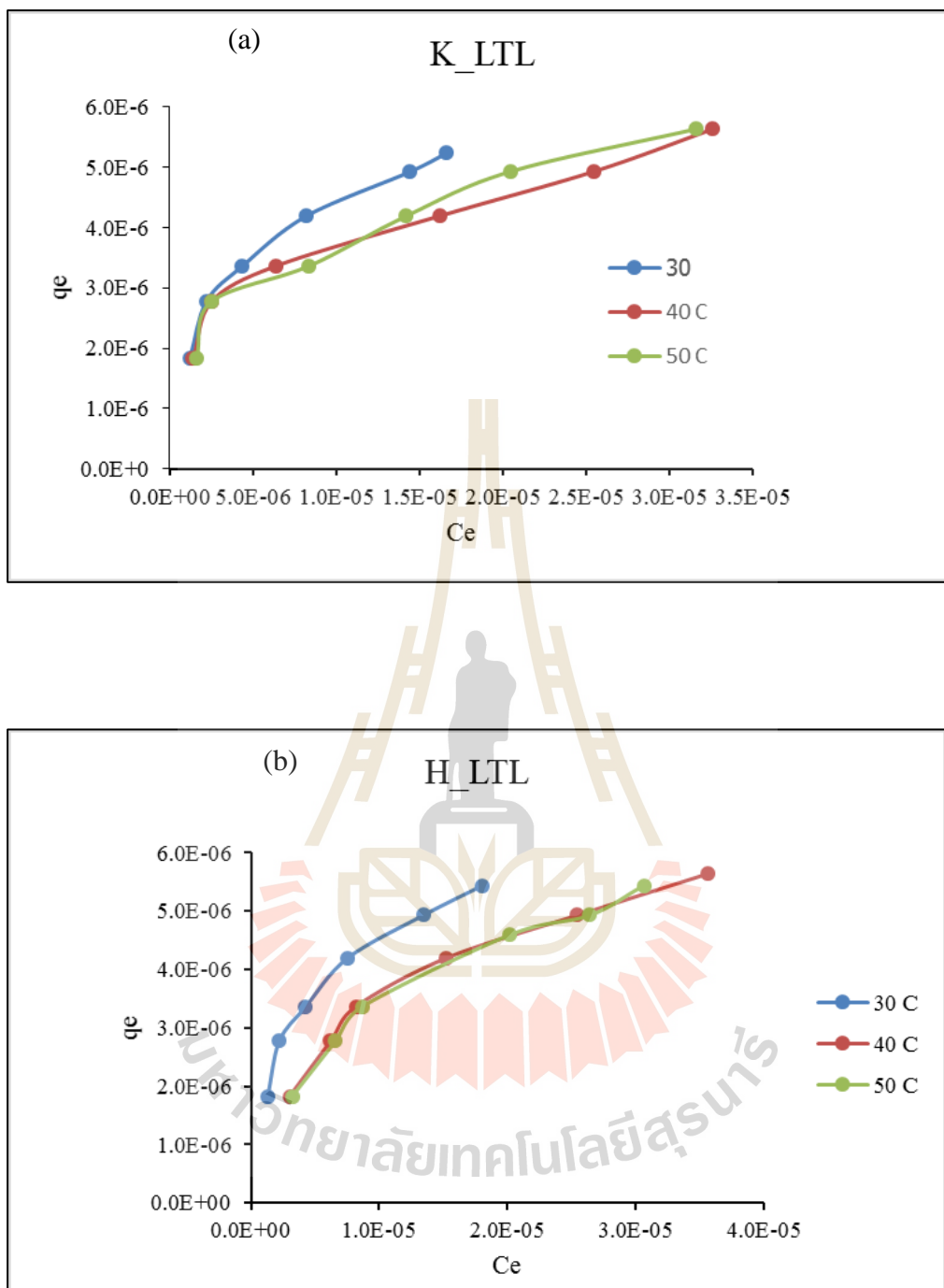


Figure A3 Adsorption isotherms of Hemi on K-LTL(a) and H-LTL(b) at 303, 313 and 323 K.

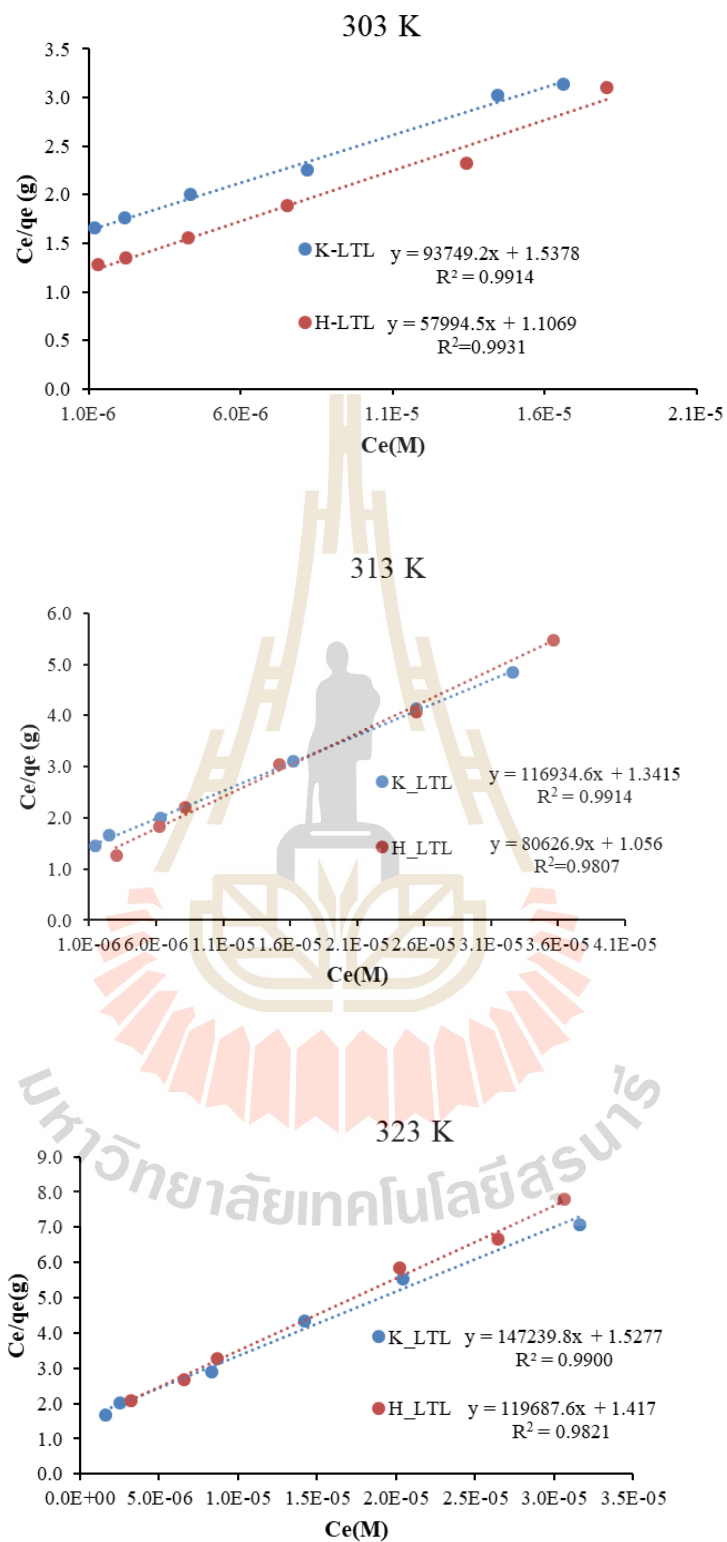


Figure A4 Linear plot of Langmuir isotherm of Hemi on K-LTL and H-LTL at 303, 313 and 323 K.

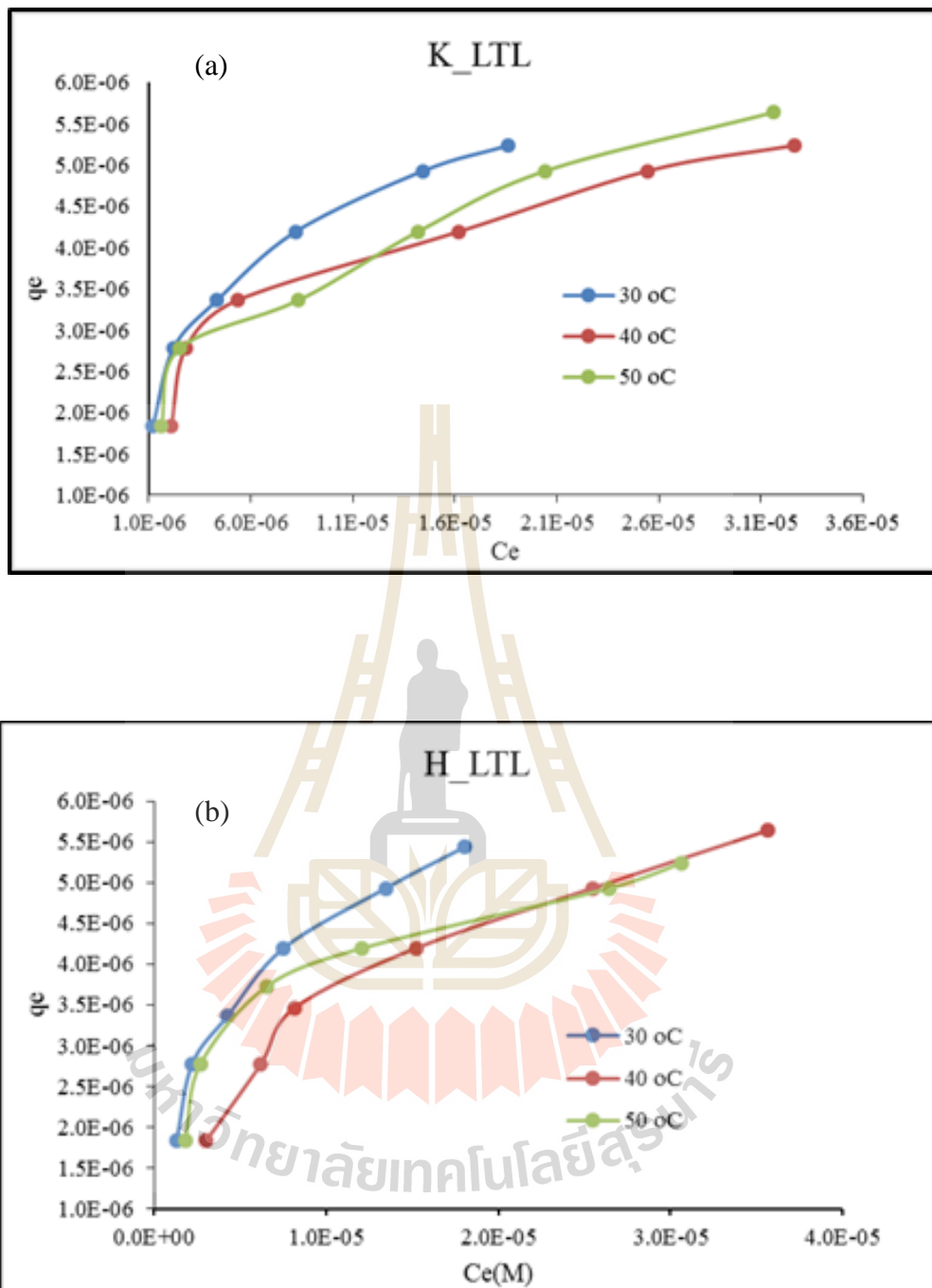


Figure A5 Adsorption isotherms of Th on K-LTL(a) and H-LTL(b) at 303, 313 and 323 K

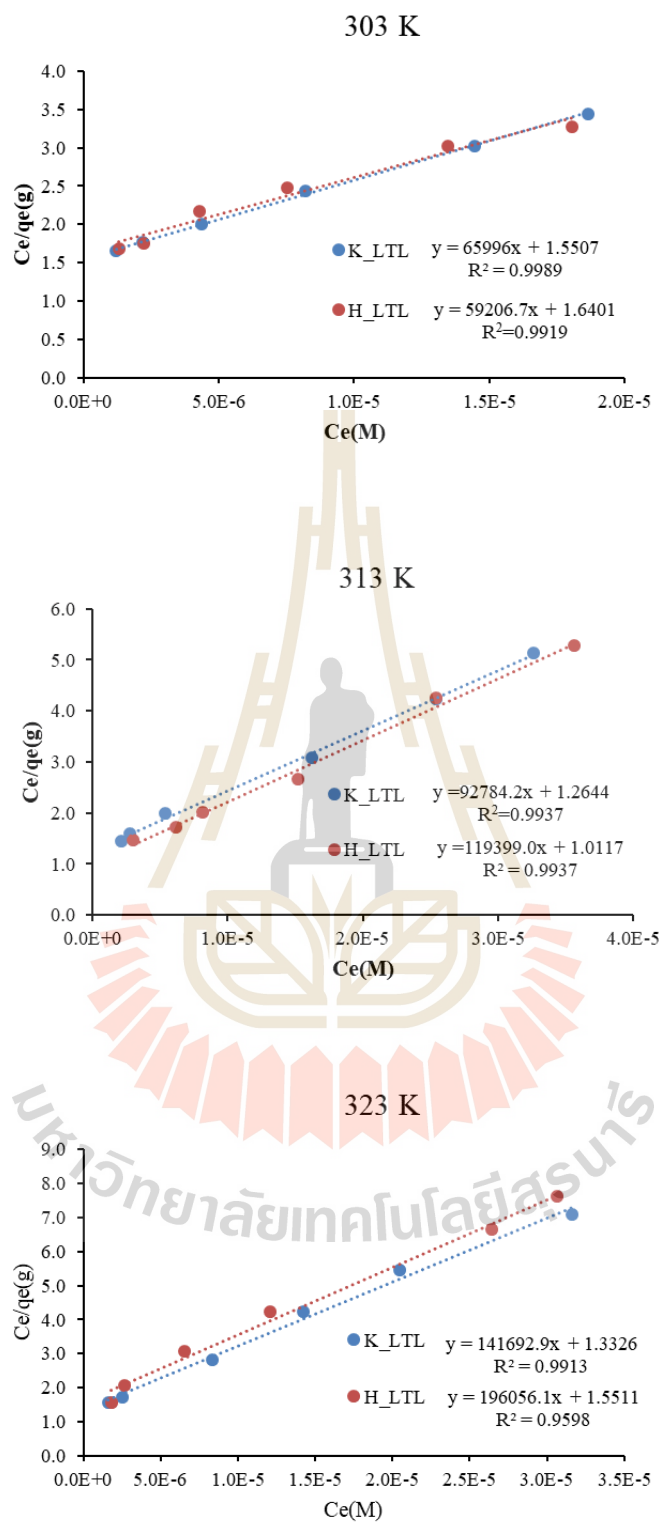


Figure A6 Linear plot of Langmuir isotherm of Thmi on K-LTL and H-LTL at 303, 313 and 323 K.

CURRICULUM VITAE

Name Suriya Duangmanee

Date of Birth July 7, 1984

Place of Birth Srisaket, Thailand

Education:

2006 B.Sc. in Chemistry, Ubon Ratchathani University, Thailand

Relevant Experience:

2007 - 2012 Technician, TOYO INK (THAILAND) CO., LTD. Bangchan
Industrial Estate, Kannayao, Bangkok, Thailand

2013 – 2018 Teaching assistance, School of Chemistry, Institute of science,
Suranaree University of Technology, Nakhon Ratchasima.

2016 – 2018 Local contact BL2.2, Synchrotron Light Research Institute,
Nakhon Ratchasima, THAILAND

Presentation:

2019 Poster presentation “Fluorescence Enhancement of
Hemicyanine Dyes by Encapsulating into Nanosized of Zeolite
L” The Pure and Applied Chemistry International Conference
(PACCON). BITEC Bangna, Bangkok, Thailand.